An Improved Methodological Approach for Analyzing the Biogeochemical Cycling of Phosphorus in Calcareous and Organic Matter-rich Floodplain Aquifers

Dissertation

der Mathematisch-Naturwissenschaftlichen Fakultät
der Eberhard Karls Universität Tübingen
zur Erlangung des Grades eines
Doktors der Naturwissenschaften
(Dr. rer. nat.)

vorgelegt von
Wen Shao, M.Sc
aus Shandong, China

Tübingen
2024

Gedruckt mit Genehmigung der Mathematisch-Naturwissenschaftlichen Fakultät der Eberhard Karls Universität Tübingen.

Tag der mündlichen Qualifikation:	12.11.2024
Dekan:	Prof. Dr. Thilo Stehle
1. Berichterstatterin:	Prof. Dr. Yvonne Oelmann
2. Berichterstatter:	PD. Dr. Harald Neidhardt
3. Berichterstatterin:	PD. Dr. Elisabeth Eiche

Table of contents

Acknowledgments

First and foremost, I would like to thank my two supervisors, PD. Dr. Harald Neidhardt and Prof. Dr. Yvonne Oelmann, for providing me with this promising research topic. I am deeply grateful to Dr. Neidhardt for his generous investment of time in guiding my research and for his invaluable support in both my scientific work and career development. I am deeply grateful to Prof. Dr. Oelmann for consistently discussing the overall concepts and research direction of my PhD research with me, and for skillfully guiding me step by step to arrive at my own conclusions. Special thanks to PD. Dr. Elisabeth Eiche for reviewing this dissertation.

I extend my appreciation to my parents, obviously, their guidance and education have been instrumental in my personal development.

I extend my appreciation to our technicians in the laboratory, Sabine Flaiz and Rita Mögenburg. They are professional, patient and very considerate. I extend my appreciation to Carsten Leven-Pfister for technical support in sampling campaign and constructive suggestions on my research. I extend my appreciation to Simon Martin, Stefan Klingler and Marc Jantz for technical support in sampling campaign.

I extend my appreciation to my colleagues and friends, they are Zuonan Cao, Rongmei Guo, Christiane Nagel, Yao Li, Jialin Liu, Camilo Maliqueo Murga, Haikuo Zhang, Ling Hu, Simon Hauenstein, Arnim Kessler, Zhe Wang, Wen Guo, Yi Zhang, Kai Liu, Daniel Schoeckle, Haojun Zhuo, Heiner Schall, Jens Grammer, Pegah Khosravani, Marc Schwientek, Diana Fiedler and all the other Hiwis. I extend my appreciation to Associated Prof. Kang Hu, PhD and Prof. Gang Liu, PhD for their suggestion and instruction on my PhD study during my visit.

This study was financially supported by China Scholarship Council (CSC-University of Tübingen PhD programme) and the German Research Foundation (DFG reference number: NE 1852/7-1, Project number: 491020408), and the Collaborative Research Centre CAMPOS (DFG CRC 1253) for general support.

List of Figures

List of Tables

Abbreviations

PO_4	inorganic phosphorus/phosphate
P_{org}	organic phosphorus
PO_4-P	phosphate as phosphorus
Phytate-P	phytate as phosphorus
TDP	total dissolved phosphorus
DOC	dissolved organic carbon
Eh	redox potential
IC	inorganic carbon
OC	organic carbon
TC	total carbon
TN	total nitrogen
TS	total sulfur
TP	total phosphorus
CDB	citrate-dithionite-bicarbonate
VSMOW	Vienna Standard Mean Ocean Water
$\delta^{18}O_{PO4}$	the oxygen isotope in phosphate
α	Fractionation factors

Statement of personal contribution

The present dissertation is based on two unpublished manuscripts, which are named below.

Shao, W., Oelmann, Y., Li, Y., Leven, C., Neidhardt, H. The biogeochemistry of phosphorus in calcareous and organic matter-rich floodplain aquifers. Submitted to Science of the Total Environment. Under review.

Contributions: I contributed 30% scientific ideas, 80% data generation, 50% analysis and interpretation, 60% paper writing.

Scientific ideas: Wen Shao, Harald Neidhardt, Yvonne Oelmann

Data generation: Wen Shao, Harald Neidhardt, Yao Li

Analysis and interpretation: Wen Shao, Harald Neidhardt, Yvonne Oelmann

Paper writing: Wen Shao, Harald Neidhardt, Yvonne Oelmann, Carsten Leven

Shao, W., Neidhardt, H., Oelmann, Y. Modification of methods for the analysis of phosphorus pools in groundwater system and interpretation of the results in sequential extraction isotope fractionation. In preparation for submission.

Contributions: I contributed 30% scientific ideas, 90% data generation, 70% analysis and interpretation, 80% paper writing.

Scientific ideas: Wen Shao, Harald Neidhardt, Yvonne Oelmann

Data generation: Wen Shao

Analysis and interpretation: Wen Shao, Harald Neidhardt, Yvonne Oelmann

Paper writing: Wen Shao, Harald Neidhardt, Yvonne Oelmann

Declaration of Academic Integrity in Using AI: I have used only ChatGPT for checking and revising grammar. I have used generative AI tools solely as an aid, and my own creative input predominates in the present work.

Abstract

Groundwater systems can im/mobilize phosphorus (P) and are an important source of P inputs to surface water bodies. Research on P pools and cycle in groundwater systems are therefore important for understanding a broader biogeochemical cycling of P. This thesis firstly identifies a methodology adapted to the groundwater environment for analyzing P pools. Secondly, the modified sequential extraction scheme was applied to analyze P cycling in the Ammer floodplain aquifer in Germany, addressing how total dissolved P (TDP) becomes enriched in the groundwater of a pristine calcareous aquifer. Thirdly, this thesis further explored the potential limitations and challenges of applying combination of stable oxygen isotope analysis of PO_4 ($\delta^{18}O_{PO4}$) with sequential extraction as analytical tool. The results showed that the extraction scheme derived from soil systems (Scheme A) performed better that the extraction scheme derived from marine systems (Scheme B). The expected surface-adsorbed inorganic P (PO_4) pools by Scheme A and expected labile PO_4 pool by Scheme B accounted for 49% to 89% vs 0% to 67% of the total extractable PO_4 in tested synthetic minerals, and the extraction of organic P (P_{org}) by both methods were consistent with their effect on PO_4 extraction. The understanding on roles of NaOH and CDB steps from extraction schemes were further enhanced, and the interpretation of their corresponding P pools in groundwater system has been corrected: NaOH-P should be interpreted alongside sediment mineral composition analysis to represent strongly surface-adsorbed P on Fe- and Al-minerals, moderately labile P_{org}, and relatively fragile structurally bound Fe-P; CDB-P should be interpreted alongside simultaneous measurements of Fe, Mn, and Ca to represent relatively strong structurally bound Fe-P, non-extractable surface-adsorbed P on Fe-minerals, and Ca-associated P. In the Ammer floodplain aquifer, TDP concentrations varied considerably from below the detection limit to 0.61 mg L^{-1} and were significantly associated with reducing redox conditions, dissolved organic carbon (DOC) and NH_4^+ concentrations, suggesting that the *in-situ* mineralization of organic matter (OM) was one of the main P-mobilizing processes. A pronounced proportion of surface-adsorbed PO_4 and P_{org} ($NaHCO_3$- and NaOH-extractable) in addition to PO_4 that was structurally incorporated into Ca-minerals (HCl-extractable) were found in sediments, and Kd values of surface-adsorbed P suggested that P_{org} was found to be preferentially adsorbed over PO_4 in aquifer material. The results suggest Ca-minerals and OM both represent the main P sinks in calcareous aquifer, while the mobilization of P via microbial mineralization of OM represents a comparatively fast process, and degradable OM and electron acceptors are both abundant in the calcareous aquifer of the Ammer floodplain.

As a result, high concentrations of PO_4 have subsequently accumulated in groundwater over time. The results of $\delta^{18}O_{PO4}$ value in sequential extraction P pools indicated variability in the $\delta^{18}O_{PO4}$ values across the different chemical extraction steps, for example, it implied that NaOH preferentially extracts isotopically heavier PO_4 than other P pools within the same mineral, may therefore result in lighter $\delta^{18}O_{PO4}$ value obtained in subsequent extraction steps. And I also observed the $\delta^{18}O_{PO4}$ value in specific P pool of the mixture may vary from the $\delta^{18}O_{PO4}$ value in P pool of corresponding single sample, when this P pool in the mixture is specifically contributed by corresponding single mineral therein. The variation of isotopic values in mixture might be attributed to two possibilities, i) preferentially extracted P between different combination of mineral types might be based on the isotope-related prioritization during chemical extraction which calls further study; ii) re-adsorption and re-precipitation of PO_4 occurred during the extraction, which especially for the sample consists of Fe- and Ca-mineral. I suggest the differences in $\delta^{18}O_{PO4}$ value among subsequently extracted P pools may be not necessarily due to pools were affected by the different P sources but rather to fractionation caused by the extraction schemes. However, due to lack of parameters regarding the properties of mineral and limited literatures, this observation calls for further research. This thesis further explores the research gaps in the study of P cycling in groundwater systems through methodological discussions involving synthesis, labeling experiments, and their applications to groundwater and aquifer sediments.

Zusammenfassung

Grundwassersysteme können Phosphor (P) im/mobilisieren und sind eine wichtige Quelle für den P-Eintrag in Oberflächengewässer. Die Erforschung der P-Pools und des P-Kreislaufs in Grundwassersystemen ist daher wichtig für das Verständnis eines breiteren biogeochemischen P-Kreislaufs. In dieser Arbeit wird zunächst eine an die Grundwasserumgebung angepasste Methodik zur Analyse der P-Pools entwickelt. Zweitens wurde das modifizierte sequentielle Extraktionsschema angewandt, um den P-Kreislauf im Grundwasserleiter der Ammer-Aue in Deutschland zu analysieren, wobei untersucht wurde, wie der gesamte gelöste P (TDP) im Grundwasser eines ursprünglichen kalkhaltigen Grundwasserleiters angereichert wird. Drittens wurden in dieser Arbeit die potenziellen Grenzen und Herausforderungen bei der Anwendung der Kombination von stabiler Sauerstoffisotopenanalyse von PO_4 ($\delta^{18}O_{PO4}$) mit sequentieller Extraktion als Analysewerkzeug weiter untersucht. Die Ergebnisse zeigten, dass das von Bodensystemen abgeleitete Extraktionsschema (Schema A) besser abschnitt als das von Meeressystemen abgeleitete Extraktionsschema (Schema B). Die erwarteten oberflächenadsorbierten anorganischen P (PO_4)-Pools nach Schema A und die erwarteten labilen PO_4-Pools nach Schema B machten 49 % bis 89 % gegenüber 0 % bis 67 % des gesamten extrahierbaren PO_4 in den getesteten synthetischen Mineralien aus, und die Extraktion von organischem P (P_{org}) nach beiden Methoden stand im Einklang mit ihrer Wirkung auf die PO_4-Extraktion. Das Verständnis der Rolle der NaOH- und CDB-Schritte aus den Extraktionsschemata wurde weiter verbessert und die Interpretation der entsprechenden P-Pools im Grundwassersystem wurde korrigiert: NaOH-P sollte zusammen mit der Analyse der Mineralzusammensetzung des Sediments interpretiert werden, um stark an der Oberfläche adsorbiertes P auf Fe- und Al-Mineralen, mäßig labiles P_{org} und relativ zerbrechliches, strukturell gebundenes Fe-P zu repräsentieren; CDB-P sollte zusammen mit gleichzeitigen Messungen von Fe, Mn und Ca interpretiert werden, um relativ starkes, strukturell gebundenes Fe-P, nicht extrahierbares, an der Oberfläche adsorbiertes P auf Fe-Mineralen und Ca-assoziiertes P zu repräsentieren. Im Grundwasserleiter der Ammer-Aue schwankten die TDP-Konzentrationen beträchtlich von unter der Nachweisgrenze bis zu 0,61 mg L^{-1} und standen in signifikantem Zusammenhang mit reduzierenden Redoxbedingungen, gelöstem organischem Kohlenstoff (DOC) und NH_4^+-Konzentrationen, was darauf schließen lässt, dass die In-situ-Mineralisierung von organischem Material (OM) einer der wichtigsten P-mobilisierenden Prozesse war. Ein ausgeprägter Anteil von an der Oberfläche adsorbiertem PO_4 und P_{org} ($NaHCO_3$- und NaOH-extrahierbar) sowie PO_4,

das strukturell in Ca-Mineralien eingebaut war (HCl-extrahierbar), wurde in den Sedimenten gefunden, und die Kd-Werte des an der Oberfläche adsorbierten P deuteten darauf hin, dass P_{org} in Aquifermaterial bevorzugt gegenüber PO_4 adsorbiert wurde. Die Ergebnisse deuten darauf hin, dass sowohl Ca-Mineralien als auch OM die wichtigsten P-Senken im kalkhaltigen Grundwasserleiter darstellen, während die Mobilisierung von P durch mikrobielle Mineralisierung von OM einen vergleichsweise schnellen Prozess darstellt und sowohl abbaubares OM als auch Elektronenakzeptoren im kalkhaltigen Grundwasserleiter der Ammeraue reichlich vorhanden sind. Infolgedessen haben sich im Laufe der Zeit hohe Konzentrationen von PO_4 im Grundwasser angesammelt. Die Ergebnisse der $\delta^{18}O_{PO4}$-Werte in den P-Pools der sequentiellen Extraktion deuten auf eine Variabilität der $\delta^{18}O_{PO4}$-Werte in den verschiedenen chemischen Extraktionsschritten hin, z. B. darauf, dass NaOH vorzugsweise isotopisch schwereres PO_4 extrahiert als andere P-Pools innerhalb desselben Minerals, was zu einem helleren $\delta^{18}O_{PO4}$-Werte in den nachfolgenden Extraktionsschritten führen kann. Ich habe auch beobachtet, dass der $\delta^{18}O_{PO4}$-Werte in einem bestimmten P-Pool des Gemischs von dem $\delta^{18}O_{PO4}$-Werte im P-Pool der entsprechenden Einzelprobe abweichen kann, wenn dieser P-Pool im Gemisch spezifisch von dem entsprechenden Einzelmineral darin stammt. Die Variation der Isotopenwerte in der Mischung könnte auf zwei Möglichkeiten zurückzuführen sein, i) bevorzugt extrahiertes P zwischen verschiedenen Kombinationen von Mineralien könnte auf der isotopenbezogenen Priorisierung während der chemischen Extraktion beruhen, was weitere Untersuchungen erfordert; ii) Wiederadsorption und Wiederausfällung von PO_4 während der Extraktion, was insbesondere für die Probe, die aus Fe- und Ca-Mineralen besteht, gilt. Ich vermute, dass die Unterschiede im $\delta^{18}O_{PO4}$-Werte zwischen den anschließend extrahierten P-Pools nicht unbedingt auf die Beeinflussung der Pools durch die verschiedenen P-Quellen zurückzuführen sind, sondern eher auf eine durch die Extraktionsverfahren verursachte Fraktionierung. Aufgrund des Mangels an Parametern für die Eigenschaften des Minerals und der begrenzten Literatur ist diese Beobachtung jedoch Gegenstand weiterer Untersuchungen. In dieser Arbeit werden die Forschungslücken bei der Untersuchung des P-Zyklus in Grundwassersystemen durch methodische Diskussionen über die Synthese, Kennzeichnungsexperimente und ihre Anwendung auf Grundwasser und Aquifersedimente weiter erforscht.

1 Introduction

1.1 Phosphorus in groundwater systems

The phosphorus (P) is one of the key nutrient elements in the ecosystems, playing a fundamental role in various biological processes. P presents in ecosystems in two primary forms: inorganic P (i.e. phosphate, PO_4) and organic P (P_{org}). PO_4 commonly exists in the dissolved form of HPO_4^{2-} or $H_2PO_4^-$ (depending on the environmental pH) or in mineral structures. P_{org} is the organic compound includes PO_4 in the structure, such as ATP, RNA, DNA, and organic esters. (Childers et al., 2011; Davies et al., 2014; Iheagwara et al., 2013). Given that P is a limiting resource for agriculture obtained from mines and its usage has been developed over the past two centuries, it is possible that economically extractable mineral P resources will become scarce in the future (Burkholder and Glibert, 2013; Childers et al., 2011; Cordell et al., 2009; Davies et al., 2014; Elser and Bennett, 2011). Human activities and natural processes can redistribute P, leading to uneven temporal and spatial distribution in the environment. This can result in excessive accumulation in aquatic environments, causing stoichiometric imbalance in terms of trophic interactions that causes eutrophication (Burkholder and Glibert, 2013; Chapin, 1996; Cordell et al., 2009; Elser and Bennett, 2011; Gilliam, 1995). The nutrient P has been the least abundant among the macronutrients that required in large quantities by primary producers, and it often serves as the limiting factor in freshwater systems. (Burkholder and Glibert, 2013; Hecky and Kilham, 1988). When excess P enters the water body, it promotes the growth of primary producers, which in turn trigger a series of negative effects, resulting in decreased dissolved oxygen and increased carbon dioxide concentrations, along with the decay of excessive algal and plant matter. (Burkholder and Glibert, 2013). The recognition of the importance of P management in non-urban areas first started with efforts to manage lakes (Gilliam, 1995; Seo and Canale, 1996) and improve soil tillage practices (Chapin, 1996; Hooda et al., 2001; Zaccheo et al., 1997). As the understanding of P management has advanced, the transport and transformation of P within groundwater systems has gained increasing attention from researchers, emerging as a critical component in the broader biogeochemical cycling of P (McGinley et al., 2016; Montangero et al., 2007; Neidhardt et al., 2018; Schilling et al., 2018). Numerous studies have identified groundwater, particularly in floodplain aquifers, as a significant source of P inputs to water bodies (Lewandowski et al., 2015; Meinikmann et al., 2015; Nisbeth et al., 2019).

On a global scale, groundwater security is more relevant to human activities than ever before, and increasingly pressing climate change issues add urgency to groundwater research (Jutebring Sterte et al., 2022; Neidhardt and Shao, 2023; Tao et al., 2020). In Europe and America, the challenges are mainly water stress and groundwater contamination (Espindola et al., 2020; Sprenger et al., 2017). In Sub-Saharan Africa, the challenges are vast underexploited shallow aquifers and inadequate infrastructure create uncertainty in the context of climate change (Danert et al., 2020; Duker et al., 2020). In Asia-Pacific region, where is the world's largest groundwater extraction area, multiple challenges are emerging such as groundwater depletion, land subsidence, groundwater pollution (Abdolvand et al., 2015; Hofmann et al., 2010). Enrichment and cycling of P in groundwater systems is one of the concerns on the ecosystem safety (Childers et al., 2011). The enriched P in groundwater can be caused by anthropogenic inputs, such as irrigation, sewage disposal and fertilizer application (Cao et al., 2024; McGinley et al., 2016; Mellander et al., 2013; Robertson et al., 2019; Spiteri et al., 2007). In the meantime, research has gradually shifted from focusing solely on surface-bound processes (such as erosion and surface runoff) to recognizing the important of belowground P transport (Weihrauch and Weber, 2020). As large amounts of geogenic P were stored in the aquifer material during geologic time, geogenic P inputs gaining increased attention (Kazmierczak et al., 2021; Y. Li et al., 2023; M. Liu et al., 2023; Z. Liu et al., 2023; Neidhardt et al., 2018; Zhang et al., 2023). Given the growing ecological and environmental challenges of our era, diverse P inputs from different geological units to groundwater have prompted a reevaluation of P cycling in groundwater systems, encouraging a broader, more diverse perspective.

The challenge of studying P cycling in groundwater systems lies not only in the diverse and often difficult-to-detect sources of P but also in the complex interactions between the aqueous and solid phases, particularly under varying redox conditions. The varying redox conditions can be attributed to water table fluctuation, driven by rainfall event and agricultural irrigation (Cao et al., 2024; Kazmierczak et al., 2020; Li et al., 2022; Schilling et al., 2018), as well as enhanced reducing conditions resulting from the presence of external or internal carbon sources (Neidhardt et al., 2018; Tao et al., 2020). For example, when redox conditions shift to more oxic, dissolved P in groundwater will precipitate with Fe(III)-(hydr)oxides as it moves through the aquifer. Conversely, when redox conditions become more anoxic, reducing groundwater can lead to the reductive dissolution of weakly crystalline Fe(III)-(hydr)oxides, releasing structurally bound P back into the dissolved phase. Thus, P species can change as it is immobilized and mobilized within

the groundwater system. A deeper understanding of P species in terms of preference of im/mobilization is important for studying P cycling in groundwater systems. Furthermore, the challenges are exacerbated when calcareous aquifers are involved, as these aquifers are capable to hold large amounts of P but have a limited capacity to retain it under changing environmental conditions (Bingham et al., 2020; Flower et al., 2022; Liao et al., 2019; Robertson et al., 2019). The study on the risk of P release from pristine calcareous aquifers is a current research gap. Therefore, I emphasize the importance of analyzing potential P sources and assessing whether the increase of groundwater P content could become a long-term phenomenon. In order to be able to categorize P species in these aquifer materials to assess their capacity to retain and/or release of P, chemical sequential extraction scheme and phosphorus-bound stable oxygen isotope technique have been developed, providing us with different perspective for studying the P cycle. These two approaches and the research gaps in their application to groundwater system investigations are described separately in the following sections.

1.2 The study of phosphorus cycling by chemical sequential extraction analysis

It has been recognized that different P pools are of different significance in terms of ecological meaning (Wang et al., 2013). Operationally defined extraction schemes with the purpose of identifying different P pools were gradually modified and generalized for research in the 20th century, which is mainly derived from soil and marine science (Hedley et al., 1982b; Ruttenberg, 1992; Wang et al., 2013; Williams et al., 1967). In soil systems, the proportion of P in various forms changes as soil develops, and external P can be added to the system as fertilizer, accordingly related extraction schemes are characterized by focusing on the intensity of soil weathering and the bioavailability of P to plants (Hedley et al., 1982a; Walker and Syers, 1976; Williams et al., 1967). For example, NaOH extractable P increases as soil becomes more weathered, indicating that P becomes geochemically fixed to iron and aluminum oxides (Cross and Schlesinger, 1995). Therefore, this operationally defined extraction scheme provides a valuable index of the relative importance of biological processes to soil P contents across a soil weathering gradient (Cross and Schlesinger, 1995; Hedley et al., 1982a; Tiessen et al., 1984). In marine systems, P is stored in sediments within the water column and could be buried as authigenic P minerals after its release, accordingly its extraction schemes are characterized by an understanding of burial and diagenesis, with the purpose of identifying the various solid-phase P reservoirs of the sediments (Hylén et al., 2021;

Ruttenberg, 1992). For example, acetate buffer extractable P increases indicating continued precipitation of authigenic P minerals during early diagenesis (Yuan et al., 2019).

The sequence of extractions applied is designed on the principle of continuously using increasingly vigorous solutions on the samples, i.e. a more powerful subsequent extraction solution could further remove P after previous extraction solutions had already extract as much as possible (Barrow, 2021; Wang et al., 2013). Following this approach, the underlying principle involves using alkaline and acidic reagents to extract surface-adsorbed P or release P by dissolving the target fraction. The process can be further refined to extract loosely surface-adsorbed P, strongly surface-adsorbed P, authigenic structurally bound P and detrital fractions. Salt solutions, such as $NaHCO_3$ or $MgCl_2$, are typically used for loosely surface-adsorbed P, and followed by stronger reagents like NaOH and/or citrate-dithionite-bicarbonate (CDB) to remove Al-, Fe- and Mn-(oxyhydr)oxides associated P (Joshi et al., 2015; Neidhardt et al., 2021; Tao et al., 2020; Yang et al., 2019). Strong acid reagents like HCl is used for detrital fractions (Joshi et al., 2015; Neidhardt et al., 2021; C. Wang et al., 2013; Yuan et al., 2019). However, the extraction schemes provide P information based only on the suitability of specific chemical reagents for specific extraction objectives, the effectiveness of these reagents may vary depending on the application scenario (Klotzbücher et al., 2019). A key research gap is the study of extraction schemes for aquifer sediments in groundwater systems. Comparing with soil and marine environments, aquifer sediments are subject to conditions of water flow or water level changes, so P storage phases may undergo constant changes (e.g., mineral dissolution and precipitation) (Bingham et al., 2020; Kazmierczak et al., 2020; Li et al., 2022; Lisboa et al., 2024; McGinley et al., 2016; Tao et al., 2020). Therefore, research regarding how different extraction schemes yield P pool information in groundwater systems is needed to identify the most effective methods for groundwater systems.

1.3 The study of phosphorus cycling by phosphorus-bound stable oxygen isotope technique

The initial motivation for using phosphorus-bound stable oxygen isotope technique in P cycling study was due to lack of inherent tracers as P only has a single stable isotope (Blake et al., 2005; Davies et al., 2014; McLaughlin et al., 2004). Alternatively, oxygen has sufficient stable isotopes in the environment, and PO_4 is the most basic unite in P

cycling (Chang and Blake, 2015; O'Neil et al., 2003). The oxygen isotope ratios in PO_4 ($\delta^{18}O_{PO4}$) can be used for tracking P on two principles: i) P-O bounds in PO_4 are resistant to inorganic hydrolysis under normal natural conditions (equilibration times ca. 10^4 years at 20 °C); ii) P-O bounds in PO_4 break only as a result of enzyme-mediated biochemical reactions (Blake et al., 1997; Chang and Blake, 2015; Cohn, 1958; Longinelli and Nuti, 1973; O'Neil et al., 2003). The processes controlling $\delta^{18}O_{PO4}$ during biogeochemical cycling of P mainly consist of three approaches, i) intracellular metabolism of P; ii) extracellular hydrolysis of organic P compounds; iii) uptake of extracellular P (Fig. 1.1) (Davies et al., 2014). Isotope fractionation in P cycling study mainly involves kinetic fractionation and thermodynamic equilibrium fractionation, the former refers to a process that preferentially selects one isotope to a faster reaction rate or incomplete reactions, while the latter refers to a process which has time to exchange isotopes in order to achieve the lowest energy system (Davies et al., 2014).

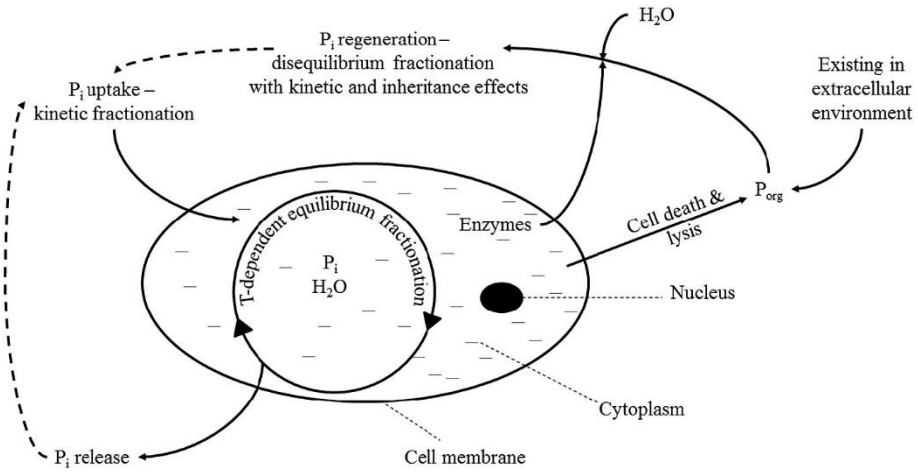

Fig. 1.1. Schematic diagram describing the major isotope effects that can occur within the intracellular or extracellular environment due to metabolic processes. P_{org} = organic P compounds; P_i = dissolved inorganic phosphate ion; H_2O = water molecule, T = temperature. Figure is from Davies et al (2014). Printed with permission by Elsevier B.V.

In order to be determined, environmental samples need to be purified to remove oxygen-containing substances except PO_4 and eventually converted into a precursor (in this study, Ag_3PO_4) to determine the isotope by mass spectrometer. After continuous refinement and modification, the most widely used methods were identified eventually as Ag_3PO_4 (Kornexl et al., 1999; Vennemann et al., 2002; Z. Xu et al., 2018). As the Ag_3PO_4 purification and measurement protocol becomes more sophisticated, it represents a novel and potentially powerful stable isotope tracer for biogeochemical

research, more and more studies have attempted to apply it to the study of P cycling in natural ecosystems (Gebus-Czupyt and Wach, 2022; Ishida et al., 2024; Jin et al., 2023; McLaughlin et al., 2004).

The application of phosphorus-bound stable oxygen isotope method first developed in paleoclimatological and paleoenvironmental studies in 20th century, and subsequently extended to analysis of aqueous, soil and sediment P pool in 21st century (Blake et al., 1997, 1998, 2005; Longinelli and Nuti, 1973; Tudge, 1960; Joshi et al., 2016; McLaughlin et al., 2004; Tamburini et al., 2010). For example, Tamburini et al. (2010) used this approach in soils, indicating the potential of this isotopic tracer to understand P dynamics in soil systems. Joshi et al. (2015) and Yuan et al. (2019) determined $\delta^{18}O_{PO4}$ values in operationally defined P pools of marine and freshwater sediments. With this approach, they were able to assess $\delta^{18}O_{PO4}$ values in different P pools such as exchangeable P, Fe-(hydr)oxides associated P, or P in authigenic an detrital Ca-carbonates and apatite. By comparing $\delta^{18}O_{PO4}$ values in these pools to the theoretical isotopic equilibrium values (equation V), they were able to draw conclusions regarding biotic and abiotic PO_4 cycling processes, sources of dissolved PO_4 in the aqueous phase, and active sinks (Liang and Blake, 2007). However, as the technique is increasingly used to interpret $\delta^{18}O_{PO4}$ values of P pools to conclude P sources as well as P cycle between different pools, new research gaps have emerged in this research field. It's already known that extraction scheme and purification procedure do not change the original $\delta^{18}O_{PO4}$ values in sample but whether specific extraction step preferentially extraction different PO_4 isotopes is unknown (Jiang et al., 2017; Lei et al., 2020). It has been reported in the soil samples, the $\delta^{18}O_{PO4}$ values obtained during single and sequential extraction methods were different, and with same sample, NaOH-P single extractant yielded heaviest $\delta^{18}O_{PO4}$ value (Jiang et al., 2017). The $\delta^{18}O_{PO4}$ values were also reported to have large differences among P pools by using the Hedley extraction scheme and the SEDEX extraction scheme (Lei et al., 2020). Therefore, once abiotic causes, i.e., the chemical extraction method itself, can cause deviations in isotope values for different P pools, interpreting the P cycle through this technology then needs to be treated with more caution.

In order to make up this research gap, the $\delta^{18}O_{PO4}$ values of specific P pool in single mineral and mixture of minerals should be investigated separately, to reveal the variation of extraction results in isotope ratio during chemical extraction scheme. Therefore, I investigated the $\delta^{18}O_{PO4}$ values of different P pools in synthesized minerals that are representative in groundwater systems as well as natural aquifer samples to evaluate

the performance of combined approach of sequential extraction and phosphorus-bound stable oxygen isotope technique.

1.4 Thesis Structure

In order to gain a deeper understanding of P cycling in groundwater systems, this thesis identifies a methodology adapted to the groundwater environment and applies it to analyzing P cycling in the Ammer floodplain aquifer in Germany, addressing how P becomes enriched in the groundwater of a pristine calcareous aquifer. Furthermore, the emerging combined analytical method of a sequential extraction scheme and phosphorus-bound stable oxygen isotope technique was evaluated, and I highlight potential risks for future studies. My dissertation consists of the following chapters:

In Chapter 2, I tested two stepwise extraction schemes for analyzing P pools that were developed from previous researches. I used synthetic mineral samples that represent typical sediment compositions in groundwater system and natural aquifer sediments from three regions: the Ammer floodplain in Germany, the Hetao floodplain in China and the Red River floodplain in Vietnam. The research questions are, Q1: how effectively P incorporated into representative minerals in groundwater systems can be selectively extracted by the two extraction schemes; Q2: which tested extraction scheme is more suitable for groundwater systems? I explore the reasons for the differences in the extraction results and suggest ideas for future applications to groundwater systems.

In Chapter 3, I investigate the reasons of P enrichment in groundwater within a calcareous aquifer at the Ammer floodplain, Germany. I conducted groundwater sampling, collecting data from 65 groundwater wells as well as collecting a 12 m-long drill core to study aquifer material. The research questions are, Q3: what are the sources that are responsible for elevated P in the groundwater of calcareous floodplain aquifers; Q4: how can elevated PO_4 concentrations in a calcareous aquifer system prevail? I conclude possible sources of elevated P in groundwater and explore the competing processes between P immobilization and mobilization in calcareous and OM-rich floodplain aquifers.

In Chapter 4, I assess the applicability of the combined analytical method of sequential extraction and phosphorus-bound stable oxygen isotope techniques. This is achieved by further analyzing the $\delta^{18}O_{PO4}$ results of each mineral in its corresponding extracted P pool through isotope labeling experiments on the synthetic samples from Chapter 2. The

research questions are, Q5: are the $\delta^{18}O_{PO4}$ values in each P pool of a given single mineral related to the extraction scheme under abiotic condition; Q6: how is the variation of $\delta^{18}O_{PO4}$ values in P pools when these minerals are mixed? I observed previously unreported isotopic value differences and made reasonable speculations about the phenomenon. Moreover, I made outlook regarding the research gap in this field.

In Chapter 5, I summarize how the main research questions of this thesis are addressed, highlighting the major outcomes in terms of P pool analytical methods and P cycling research in groundwater system. I also outline the potential risks in the future application of the sequential extraction and phosphorus-bound stable oxygen isotope technique combined method and how should we use the $\delta^{18}O_{PO4}$ value in P pools to explain P cycling in the environment.

2 Testing a suitable approach for analyzing phosphorus pools in groundwater systems

2.1 Introduction

Operationally defined chemical sequential extractions were widely used to interpret certain phosphorus (P) fractions or pools in soil and sediments with the aim to identify geochemical and biological process that occur in the study area (Hupfer et al., 2009; Ruttenberg, 1992). The extraction schemes are designed to differentiate between surface-adsorbed P and P associated with minerals and organic matter, originating mainly from research in soils and marine environments (Hedley et al., 1982a; Ruttenberg, 1992). The shortcomings of sequential extractions are that the mechanisms behind individual extraction steps are not referred to a specific mineral source nor its binding strength to minerals (Klotzbücher et al., 2019). Although controversial, operationally defined chemical P extractions do help to interpret certain processes involved in P cycling. Recently these extraction schemes have been adapted for groundwater studies, where biogeochemical processes influence the fate of P by sorption and precipitation of secondary minerals, dissolution of P-hosting minerals, as well as enzymatic turnover by microorganisms (Liu et al., 2023; Neidhardt et al., 2021).

The P pool composition of aquifer materials are the key factor to reveal the enrichment and biogeochemical cycling of P in groundwater. The forms of P include inorganic phosphate (PO_4) and organic P (P_{org}) that are present in different P pools. The P pools and processes that control PO_4 exchange between the solid phase (i.e. aquifer material) and the aqueous phase (i.e. groundwater) over time were illustrated in Fig. 2.1. However, the interpretation of P pools from soil and marine science may not be suitable for estimating groundwater systems, due to the fact that these schemes only provide approximate values based on the suitability of specific chemical reagents for particular extraction objectives. The typical mineral phases in groundwater systems include Fe-mineral like ferrihydrite, hematite, siderite, goethite, Ca-mineral like carbonates and hydroxyapatite, Mn-mineral like pyrolusite, clay particles like montmorillonite and mica, and quartz (Guo et al., 2007; Kimura et al., 2021; Stolze et al., 2019). One of the main feature against soil and marine systems is that the groundwater systems have variable redox conditions and P storage phase that may undergo dissolution and precipitation reactions (Bingham et al., 2020; Kazmierczak et al., 2020; Li et al., 2022; Lisboa et al., 2024; McGinley et al., 2016; Tao et al., 2020). Another feature of groundwater systems

are that dominant P sinks are often related to Fe-(hydr)oxides and calcium-carbonate minerals (Li et al., 2023; Tao et al., 2020). The application scenarios in groundwater systems require further study of appropriate sequential extraction schemes rather than direct use of ready-made soil, lake or marine sediment extraction schemes. For example, an order of $NaHCO_3$-CDB-NaOH was used for investigating P pools in lake sediments (Yuan et al., 2019) whereas a method where NaOH preceded CDB was used for characterizing aquifer sediments (Neidhardt et al., 2021). An order of $MgCl_2$-CDB-acetate buffer-HCl was used without involving a NaOH treatment in a bay sediment study (Joshi et al., 2015), while an order of NaHCO3-NaOH-HCl was used without involving CDB treatment in a soil study (Joshi et al., 2016). Another potential sink for PO4 in reducing groundwater systems is vivianite (Rothe et al. 2016), which is usually not considered in sequential extraction schemes. Currently, there is very little literature on suitable extraction schemes for groundwater systems. Therefore, this study tested the impact of different extraction schemes to develop a suitable sequential extraction scheme for groundwater systems. The overarching questions were: (i) How effectively P incorporated into representative minerals in groundwater systems can be selectively extracted by the two extraction schemes; (ii) Which tested extraction scheme is more suitable for groundwater systems?

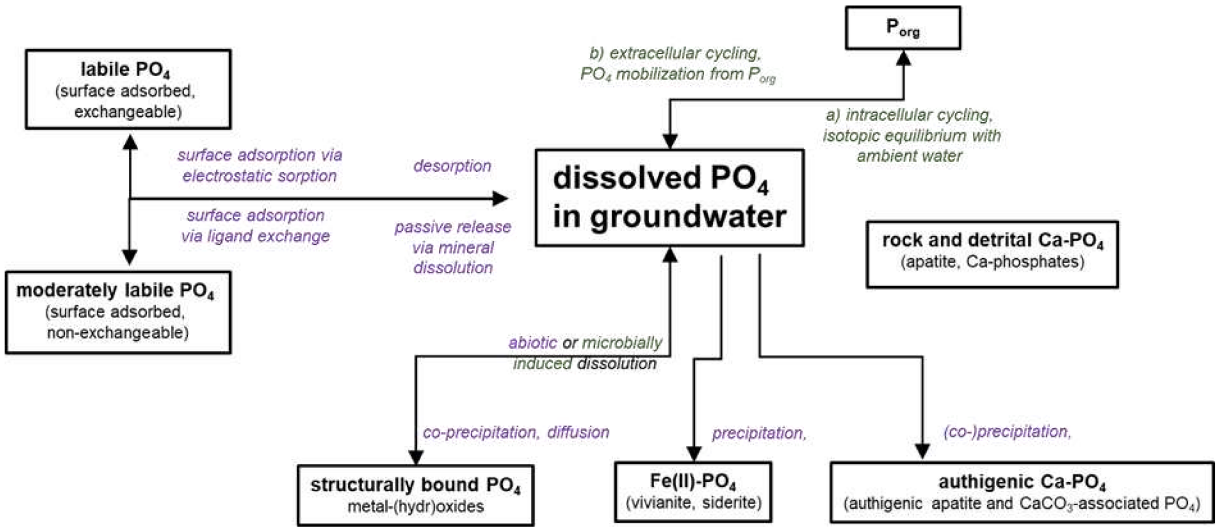

Fig. 2.1 Pools and processes that control PO_4 concentrations in groundwater systems. Biotic (in green) and abiotic (in purple) processes. Fig. from DFG project report NE 1852/7-1.

2.2 Materials and Methods

2.2.1 Synthesis of mineral samples

The synthetic P-free minerals involved ferrihydrite, hematite, siderite, pyrolusite and montmorillonite. In the following, they are referred to Fe1, Fe2, Fe3, Mn1 and Cy1 as abbreviations, respectively. Fe1 was synthesized by slowly neutralizing 0.2M $Fe(NO_3)_3$ solution with 1M KOH solution, magnetic stirrer overnight, repeated 5 times ultrasonic batch (10min) followed by centrifugation to remove impurities and finally freeze dried (Christ lyo cube, apply to the subsequent freezing operations) (Schwertmann and Cornell, 2008). Fe2 was synthesized by adding a 0.2M $Fe(NO_3)_3$ solution to a 90 °C 1M KOH solution, adjusting the pH to 8-8.5, and keeping it in an oven at 90 °C for 48 hours. The solution underwent five cycles of 10-minute ultrasonic batches followed by centrifugation to remove impurities, and was finally dried in an oven at 40 °C (Schwertmann and Cornell, 2008). Fe3 was synthesized by slowly adding 500 ml of a boiling Na_2CO_3 solution (5 g) to 500 ml boiling $Fe(NH_4)_2(SO_4)_2$ solution (20 g) under a nitrogen atmosphere. The precipitated ferrous carbonate was then washed five times with boiling ultrapure water and finally freeze-dried (Hallbeck et al., 1993). Mn1 was obtained from CVU Uni-Tübingen (Mangandioxid, CASNr. 1313-13-9). Cy1 was obtained from Sigma-Aldrich (K 30, Merck).

2.2.2 P loading solutions and loading experiments

To evaluate the performance of the two tested extraction schemes on P pools and species, specific P solutions were prepared and applied to mineral samples in two distinct ways: surface adsorption (i.e. outside loading) and co-precipitation (i.e. inside loading). P solutions were prepared by KH_2PO_4 (10 g L^{-1} PO_4-P) and phytate (1 g L^{-1} PO_4-P, $C_6H_{18}O_{24}P_6$ x Na + yH_2O, Merck) separately, representing inorganic P and organic P, respectively. As the method will be further tested by combining $\delta^{18}O_{PO4}$ analysis of operationally defined PO_4 pools with isotopic labeling experiments, KH_2PO_4 solutions were isotopically labeled. Further information can be found in Chapter 4.

Outside loading of P was done by mixing 4 g dried powder of each five P-free mineral samples with 100 ml P solution (KH_2PO_4 or phytate) in a horizontal shaker overnight (Table 1). In the following, the outside loading mineral samples are abbreviated as Fe1(O), Fe2(O), Fe3(O), Mn1(O) and Cy1(O), respectively. All outside labeling

experiments were conducted at room temperature. All samples were dried (freeze-dried or oven dried at 45 °C) and stored in polyethylene bottes.

Inside loading of P was done by incorporating an additional 250 ml of isotopically labeled P solution (KH_2PO_4) into the synthesis processes. Five mineral phases were used for inside loading: ferrihydrite, hematite, siderite, vivianite, hydroxyapatite. In the following, the five inside loading mineral samples are abbreviated as Fe1(I), Fe2(I), Fe3(I), Fe4(I) and Ca1(I), respectively. The synthesis of Fe1(I), Fe2(I) and Fe3(I) was the same as Fe1, Fe2 and Fe3 described before. Fe4(I) was synthesized by adding a 0.5M $FeSO_4$ solution to 250 ml P solution, and then adding 1M KOH solution under a nitrogen atmosphere. The precipitates were washed five times and finally freeze-dried (Eynard et al., 1992). Ca(I) was synthesized by slowly adding a 250 ml P solution to a $Ca(NO_3)_2$ (adjusted to pH 10-12 with NH_4OH) solution. The final product was dried in an oven at 40 °C for 4 hours (Alobeedallah et al., 2011). All samples were dried and stored in polyethylene bottes.

2.2.3 Sample characterization and TP measurement

Original synthetic mineral samples (P-free), outside loading samples and inside loading samples were ground to small powder and analyzed for their composition by using X-ray powder diffractometry (powder XRD, D8 Advance, Bruker), equipped with a Cu anode operating at 40kV/20mA. Additionally, 0.1 g of original, outside and inside loading mineral samples underwent a microwave-assisted aqua regia pressure digestion (method E701, MLS GmbH) and subsequent measurement by ICP-OES (Optima 5300 DV, PerkinElmer, limit of quantification for TDP: 0.002 mg L^{-1}), aiming to get concentrations of dissolved elements (P, Fe, Al, Mn, Ca).

2.2.4 Sequential extraction schemes

The two fractionation schemes that I used in this study are summarized in Table 2.1. Prior to the extraction steps, 0.2 g synthesized mineral samples were mixed with 0.8 g acid-washed quartz sand (VWR) to mimic the composition of natural aquifer materials, as same procedure was conduct in soil sample studies (Klotzbücher et al., 2019; Schwertmann and Cornell, 2008). For mixed samples, 0.1 g of each mineral samples were combined with 0.8 g quartz sand. For all inside loading samples, Fe1(I), Fe2(I), Fe3(I), Fe4(I) and Ca1(I), additional removal of surface-adsorbed PO_4 through repeated

washing with 0.1M NaOH (same procedures as the NaOH step in extraction protocol, Table 2.1) were applied before testing sequential extraction scheme.

Suitable natural samples were available from previous drilling campaigns (Table 2.2). The samples from the Ammer Valley in Germany consist of porous $CaCO_3$ precipitates (Heidgen et al., 2020). The samples from the Red River floodplain in Vietnam exhibit characteristics of surface-adsorbed PO_4 and PO_4 structurally bound in secondary Fe(III)-oxyhydroxides (Neidhardt et al., 2018). In the samples from the Hetao Basin in China, detrital carbonates represent the dominant PO_4 pool (Li et al., 2022). All samples originate from aquifers characterized by high concentrations of dissolved PO_4 in ambient groundwater. The sample material was stored frozen at -20°C under N_2 atmosphere in oxygen-impermeable zip-log bags at our department in Tübingen. The workflow graphic of sequential extraction schemes can be found in Fig. 2.2.

2.2.5 Quality control

Quality controls of the extraction scheme included: (i) tests for carry-over effects by repeated desorption steps with $NaHCO_3$ or other reagents ; (ii) replicate analysis of certified reference material (BCR-684) to compare the sum of extracted PO_4 to the certified reference value of total PO_4; (iii) plausibility checks for all synthesized mineral samples by calculating recovery rates for PO_4, total P, and other elements (sum of total extractable concentrations compared to total concentrations determined by aqua regia pressure digestion); (iv) quantification of major mineral-borne elements dissolved in the various extraction solutions by ICP-OES (Fe, Al, Mn, Ca) to estimate the extent of mineral dissolution.

2.2.6 Statistical analysis

All geochemical results were analyzed with Microsoft Excel 2019 and SPSS statistical software (v. 25). Comparison of surface-adsorbed P with total extracted P and variation of fractionation factors were tested by t-tests. Significant differences were tested by ANOVA with a post-hoc Bonferroni test. The confidence interval for all tests was 95% and p-values ≤ 0.05 were considered statistically significant.

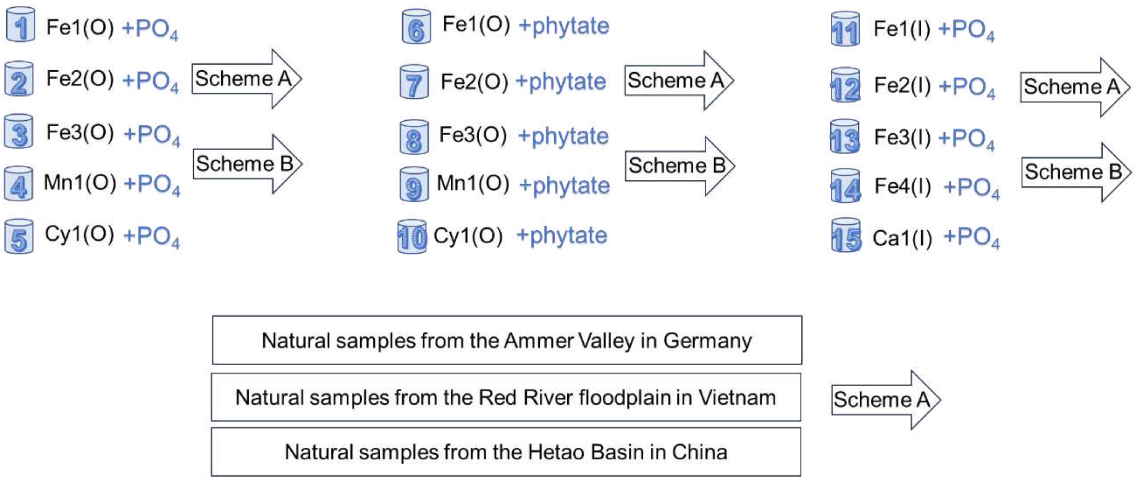

Fig. 2.2 The workflow graphic of sequential extraction schemes. Abbreviations: for original synthetic mineral samples: Fe1: ferrihydrite, Fe2: hematite, Fe3: magnetite with goethite, Mn1: pyrolusite, Cy1: mica; for outside loading samples: Fe1(O): ferrihydrite, Fe2(O): hematite, Fe3(O): magnetite with goethite, Mn1(O): pyrolusite, Cy1(O): mica; for inside loading samples: Fe1(I): ferrihydrite, Fe2(I): hematite, Fe3(I): magnetite with goethite, Fe4(I): decayed vivianite (ferrihydrite), Ca1(I): hydroxyapatite.

Table 2.1 Sequential extraction schemes tested. To avoid carry-over effects and incomplete mineral phase dissolutions, all extraction steps were repeated and additionally extracted with $NaHCO_3$ solution as suggested by Hupfer et al. (2009).

Extraction scheme A (Hedley et al., 1982a; Joshi et al., 2016; Li et al., 2012; Neidhardt et al., 2021; Ruttenberg, 1992)	**Extraction scheme B** (Joshi et al., 2015; Li et al., 2012; Ruttenberg, 1992; Yuan et al., 2019)
1. **Weakly sorbed PO_4** [a] extracted by 30ml 0.5 M $NaHCO_3$ (pH 8.5) solution, shake 30 min;20ml 0.5 M $NaHCO_3$ (pH 8.5) solution, shake 30 min, x 3 times; 10ml Millipore water shake 30 min. Centrifuge and collect solutions mention above with a final total volume of 100ml	1. **Weakly sorbed PO_4** [a] extracted by 30 ml 0.5M $MgCl_2$ (pH 8) solution, shake 30 min;20ml 0.5M $MgCl_2$ (pH 8) solution, shake 30 min, x 3 times; 10ml Millipore water shake 30 min. Centrifuge and collect solutions mention above with a final total volume of 100ml.
2. **Strongly bound PO_4** [b], extracted by 30ml 0.1M NaOH solution, shake 16 h; 20ml 0.1M NaOH solution, shake 30 min, x 3 times; 10ml Millipore water shake 30 min. Centrifuge and collect solutions mention above with a final total volume of 100ml	2. **PO_4 in Fe(II)-minerals** [c] extracted by 45 ml 0.2% 2,2' bipyridine solution at 45 °C, shake 16 h; 20ml 0.2% 2,2' bipyridine solution, shake 2 h, x 2 times; 15ml Millipore water shake 30 min. Centrifuge and collect solutions mention above with a final total volume of 100ml
3. **PO_4 in Fe(II)-minerals** [c] extracted by 45ml 0.2% 2,2' bipyridine solution at 45 °C, shake 16 h; 20ml 0.2% 2,2' bipyridine solution, shake 2 h, x 2 times; 15ml Millipore water shake 30 min. Centrifuge and collect solutions mention above with a final total volume of 100ml	3. **Mn- and Fe-(hydr)oxides associated PO_4** [g] extracted by 45ml CDB mixture [1], shake 16 h; 20ml 0.5M $MgCl_2$ (pH 8) solution, shake 30 min, x 2 times; 15ml Millipore water shake 30 min. Centrifuge and collect solutions mention above with a final total volume of 100ml
4. **PO_4 structurally bound in weakly crystalline Mn- and Fe-(hydr)oxides** [d] extracted by 45ml CDB mixture, shake 16 h; 20ml 0.5 M $NaHCO_3$ (pH 8.5) solution, shake 30 min, x 2 times; 15ml Millipore water shake 30 min. Centrifuge and collect solutions mention above with a final total volume of 100ml.	4. **Al-(oxyhydr)oxide associated PO_4** [g] extracted by 30ml 0.1M NaOH solution, shake 16 h; 20ml 0.1M NaOH solution, shake 30 min, x 3 times; 10ml Millipore water shake 30 min. Centrifuge and collect solutions mention above with a final total volume of 100ml
5. **PO_4 in form of authigenic apatites and $CaCO_3$-associated PO_4** [e] extracted by 45ml 1M acetate buffer solution (pH 4), shake 6 h; 20ml 0.5 M $NaHCO_3$ (pH 8.5) solution, shake 30 min, x 2 times; 15ml Millipore water shake 30 min. Centrifuge and collect solutions mention above with a final total volume of 100ml	5. **PO_4 in form of authigenic apatites and $CaCO_3$-associated PO_4** [e] extracted by 45ml 1M acetate buffer solution (pH 4), shake 6 h; 20ml 0.5 M $NaHCO_3$ (pH 8.5) solution, shake 30 min, x 2 times; 15ml Millipore water shake 30 min. Centrifuge and collect solutions mention above with a final total volume of 100ml.
6. **PO_4 in form of detrital apatite of igneous or metamorphic origin** [f] extracted by 30ml 1M HCl, shake 16 h; 20ml Millipore water shake 30 min. Centrifuge and collect solutions mention above with a final total volume of 50ml.	6. **PO_4 in form of detrital apatite of igneous or metamorphic origin** [f] extracted by 30ml 1M HCl, shake 16 h; 20ml Millipore water shake 30 min. Centrifuge and collect solutions mention above with a final total volume of 50ml.

[a] This pool is easily re-mobilizable and relevant if dissolved PO_4 concentrations are high (Neidhardt et al., 2021).

[b] Also weakly ordered Al-(oxyhydr)oxides could be dissolved by the NaOH solution (Klotzbücher et al., 2019). Although this potential PO_4 pool is expected to be insignificant in aquifers, specific groundwater

materials will be tested by monitoring extractable Al concentrations (Joshi et al., 2015).

[c] Fe(II)-minerals such as vivianite and siderite represent an important potential PO_4 pool in aquifers under Fe(III)-reducing conditions (Li et al., 2012; Schütze et al., 2020).

[d] This is an important pool that can form in groundwater systems with dynamic redox properties and along redox transition zones (Neidhardt et al., 2021).

[e] Comprising carbonate fluorapatite and $CaCO_3$-associated PO_4 which are relevant as a potential PO_4 source in especially Ca-type groundwater systems (Neidhardt et al., 2018)

[f] Note: this step will be carried out at room temperature (as all other steps) to avoid a potential $\delta^{18}O_{PO4}$ value alteration.

[g] Comprising strongly surface bound as well as structurally included PO_4 for this combination of extraction steps

Table 2.2 Overview of natural samples included in the test scheme. The sediment core samples were obtained from the Ammer floodplain, Germany; the Hetao floodplain, China and the red river floodplain, Vietnam. Abbreviations: bls: below land surface.

Origin	Description
Ammer floodplain (Germany)	• core AM20, depth: 12m bls • P_{tot} concentrations ranging from 300 to 1060 mg kg^{-1} • Aquifer material comprising different layers, including $CaCO_3$-rich tufa, organic-rich loamy sand, and silty sand
Hetao floodplain (PR China)	• core K2, depth: 80m bls • P_{tot} concentrations ranging from 200 to 600 mg kg^{-1} • Aquifer comprising alluvial fan and fluvial deposits, groundwater characterized by alkaline pH values
Red River floodplain (Vietnam)	• core RD54, depth: 43.5m bls • P_{tot} concentrations ranging from 50 to 950 mg kg^{-1} • Aquifer material composed of sands with varying redox properties and pronounced change in the Fe-mineralogy

2.3 Results

2.3.1 XRD and P loading results of the synthesized mineral samples

Original, P outside loading and P inside loading samples were all tested by XRD (Fig. 2.3). Fe1, Fe2, Mn1 and Ca1(I) was identified as ferrihydrite [$Fe(III)_2O_3 \cdot nH_2O$], hematite [α-$Fe(III)_2O_3$], pyrolusite [$Mn(IV)O_2$] and hydroxyapatite [$Ca_{10}(PO_4)_6(OH)_2$] as expected. Fe3 was identified as magnetite with goethite [$Fe(II)Fe(III)_2O_4$ with α-Fe(III)O(OH)], Fe4(I) was identified as decayed vivianite (ferrihydrite) [$Fe(II)_3(PO_4)_2 \cdot 8H_2O$ with $Fe(III)_2O_3 \cdot nH_2O$], Cy1 was identified as mica [$AB_{2-3}(X, Si)_4O_{10}(O, F, OH)_2$]. Original, P outside loading and P inside loading samples all underwent with digestion. For estimating P loading, data from the original sample were subtracted as background values. The digestion data for P in the synthesized mineral samples, along with the mass balance check, are presented in Table 2.3 and Table 2.4. For outside loading samples, surface-adsorbed PO_4 followed the order, Fe3(O) > Fe1(O) > Cy1(O) > Fe2(O) > Mn1(O), ranging from 302 to 36511 mg kg^{-1} PO_4-P. Inside loading samples accumulated more PO_4, and absolute majority were removed by preliminary NaOH wash.

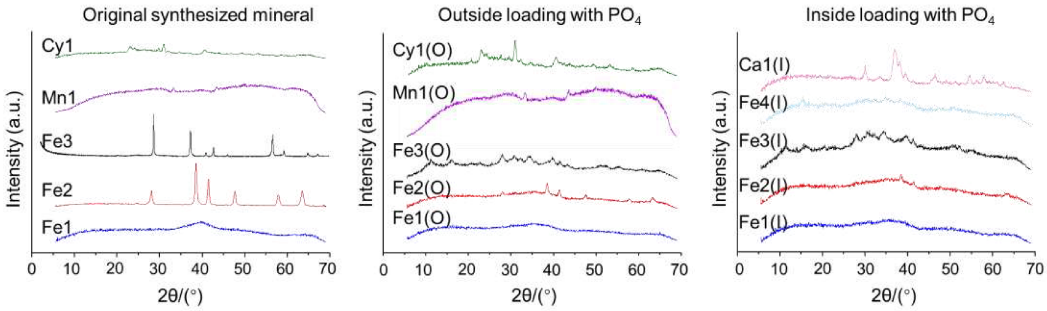

Fig. 2.3 XRD results of original synthetic mineral samples (P free), outside loading samples and inside loading samples. Abbreviations: for original synthetic mineral samples: Fe1: ferrihydrite, Fe2: hematite, Fe3: magnetite with goethite, Mn1: pyrolusite, Cy1: mica; for outside loading samples: Fe1(O): ferrihydrite, Fe2(O): hematite, Fe3(O): magnetite with goethite, Mn1(O): pyrolusite, Cy1(O): mica; for inside loading samples: Fe1(I): ferrihydrite, Fe2(I): hematite, Fe3(I): magnetite with goethite, Fe4(I): decayed vivianite (ferrihydrite), Ca1(I): hydroxyapatite.

Table 2.3 Results of P in the digestion and extraction solutions of all mineral samples in Scheme A and Scheme B. Values with ± standard error (SE) representing replicates (n = 3). E/D represents the ratio of all extracted P / digestion P. Abbreviations: for outside loading samples: Fe1(O): ferrihydrite, Fe2(O): hematite, Fe3(O): magnetite with goethite, Mn1(O): pyrolusite, Cy1(O): mica; for inside loading samples: Fe1(I): ferrihydrite, Fe2(I): hematite, Fe3(I): magnetite with goethite, Fe4(I): decayed vivianite (ferrihydrite), Ca1(I): hydroxyapatite.

Scheme A (mg kg^{-1})	$NaHCO_3$-P	NaOH-P	2,2' bipyridine-P	CDB-P	Acetate buffer-P	HCl-P	Preliminary washed P by 0.1M NaOH	All extracted P	Digestion P	E/D (%)
Fe1(O)	1031 ± 24	14180 ± 469	426 ± 16	11192 ± 245	0	16 ± 2		26846 ± 626	20935 ± 898	128
Fe2(O)	1765 ± 31	625 ± 210	21 ± 4	626 ± 47	0	18 ± 1		3055 ± 207	2812 ± 36	109
Fe3(O)	4921 ± 101	32639 ± 145	117 ± 13	4359 ± 60	0	21 ± 1		42057 ± 103	36511 ± 175	115
Mn1(O)	1 ± 1	15 ± 4	1 ± 1	0	0	15 ± 2		32 ± 2	302 ± 52	11
Cy1(O)	100 ± 4	77 ± 1	11 ± 4	0	2 ± 2	18 ± 3		208 ± 4	8601 ± 486	2
Fe1(I)	17 ± 4	205 ± 102	42 ± 6	1769 ± 62	4 ± 2	18 ± 1	106202 ± 2918	108257 ± 2827	116478 ± 3232	93
Fe2(I)	21	40	29	1624	4	15	69340	71073	112198 ± 703	63
Fe3(I)	17 ± 4	119 ± 5	30 ± 2	696 ± 27	4 ± 1	15 ± 3	62037 ± 719	62917 ± 691	136207 ± 1385	46
Fe4(I)	92	31	30	1146	10	12	68145	69465	114380 ± 397	61
Ca1(I)	4124	6	61	11835	10146	8902	1250	36323	170155 ± 2413	21
Scheme B (mg kg^{-1})	$MgCl_2$-P	2,2' bipyridine-P	CDB-P	NaOH-P	Acetate buffer-P	HCl-P	preliminary washed P by 0.1M NaOH	All extracted P	Digestion P	E/D (%)
Fe1(O)	117 ± 17	494 ± 78	28224 ± 786	4 ± 3	16 ± 1	23 ± 4		28877 ± 727	20935 ± 898	138
Fe2(O)	451 ± 51	1619 ± 289	1359 ± 43	3 ± 2	6 ± 3	36 ± 15		3474 ± 353	2812 ± 36	124
Fe3(O)	1391 ± 102	2890 ± 148	19866 ± 1096	17 ± 6	15 ± 2	25 ± 7		24204 ± 1340	36511 ± 175	66
Mn1(O)	785 ± 17	145 ± 17	154 ± 17	8 ± 17	23 ± 17	16 ± 17		1131 ± 185	302 ± 52	375
Cy1(O)	7470 ± 240	4047 ± 474	500 ± 28	114 ± 3	10 ± 2	111 ±4		12252 ± 618	8601 ± 486	142
Fe1(I)	7 ± 4	3 ± 2	1525 ± 65	0	5 ± 3	11 ± 2	106202 ±	107752 ±	116478 ± 3232	93
Fe2(I)	6	4	1051	0	13	12	69340	70426	112198 ± 703	63
Fe3(I)	2	4	715	2	7	15	62037 ± 719	62783	136207 ± 1385	46
Fe4(I)	0	2 ± 2	1096 ± 43	1 ± 1	27 ± 10	17 ± 3	68145	69287	114380 ± 397	61
Ca1(I)	71	192	17272	7	105506	38382	1250	162679	170155 ± 2413	96

Table 2.4 Results of Fe, Mn, Ca, Al in the digestion and extraction solutions of tested mineral samples in Scheme A and Scheme B (mean value). E/D represents the ratio of all extracted element / digestion P. Abbreviations: for outside loading samples: Fe1(O): ferrihydrite, Fe2(O): hematite, Fe3(O): magnetite with goethite, Mn1(O): pyrolusite, Cy1(O): mica; for inside loading samples: Fe1(I): ferrihydrite, Fe2(I): hematite, Fe3(I): magnetite with goethite, Fe4(I): decayed vivianite (ferrihydrite), Ca1(I): hydroxyapatite.

Scheme A	$NaHCO_3$	NaOH	2,2' bipyridine	CDB	Acetate buffer	HCl	All extracted	Digestion	E/D(%)
Fe (mg kg^{-1})									
Fe1(O)	103	0	3	681976	0	6	682087	544748	125
Fe2(O)	145	0	7	740217	230	1447	742046	638519	116
Fe3(O)	426	1	7	635146	544	830	636953	512465	124
Fe1(I)	67	0	0	248564	0	0	248631	287027	87
Fe2(I)	46	0	0	206348	0	0	206394	324868	64
Fe3(I)	101	2	0	166511	0	0	166613	348679	48
Fe4(I)	39	0	1	239794	0	0	239834	341438	70
Mn (mg kg^{-1})									
Mn1(O)	10	0	33	1223	348232	10674	360173	586830	61
Ca (mg kg^{-1})									
Ca1(I)	1	1840	1978	21307	5154	27245	57526	350053	16
Al (mg kg^{-1})									
Cy1(O)	0	3110	0	35	91	602	3838	40907	9

Table 2.4 continued. Results of Fe, Mn, Ca, Al in the digestion and extraction solutions of tested mineral samples in Scheme A and Scheme B (mean value). E/D represents the ratio of all extracted element / digestion P. Abbreviations: for outside loading samples: Fe1(O): ferrihydrite, Fe2(O): hematite, Fe3(O): magnetite with goethite, Mn1(O): pyrolusite, Cy1(O): mica; for inside loading samples: Fe1(I): ferrihydrite, Fe2(I): hematite, Fe3(I): magnetite with goethite, Fe4(I): decayed vivianite (ferrihydrite), Ca1(I): hydroxyapatite.

Scheme B	$MgCl_2$	2,2' bipyridine	CDB	NaOH	Acetate buffer	HCl	All extracted	Digestion	E/D(%)
Fe (mg kg^{-1})									
Fe1(O)	0	22	621782	0	172	43	622019	544748	114
Fe2(O)	0	1	706381	0	583	23042	730007	638519	114
Fe3(O)	0	319	182572	4	363	9860	193118	512465	38
Fe1(I)	0	8	257387	0	443	963	258801	287027	90
Fe2(I)	0	2	216448	0	232	760	217443	324868	67
Fe3(I)	0	13	176773	0	164	58	177009	348679	51
Fe4(I)	0	341	222623	0	0	604	223568	341438	65
Mn (mg kg^{-1})									
Mn1(O)	3	8	49031	4	12	87746	136804	586830	23
Ca (mg kg^{-1})									
Ca1(O)	9558	3509	24045	2265	222342	77957	339676	350053	97
Al (mg kg^{-1})									
Cy1(O)	0	0	590	466	516	4461	6032	40907	15

2.3.2 Two sequential extraction schemes for outside loading samples

In sequential extraction data, PO_4-P and phytate-P were measured, and for the sake of simplicity, it is abbreviated to PO_4 and phytate when combined with other words (for example, total extractable phytate). For Scheme A, the extracted surface-adsorbed PO_4 in terms of Fe2(O), Fe3(O) and Cy1 (mean value: 78%, 89% and 85% of the total extractable PO_4, respectively) were higher than Fe1(O) and Mn1(mean value: 57% and 49% of the total extractable PO_4, $p < 0.05$, Fig. 2.4 a).

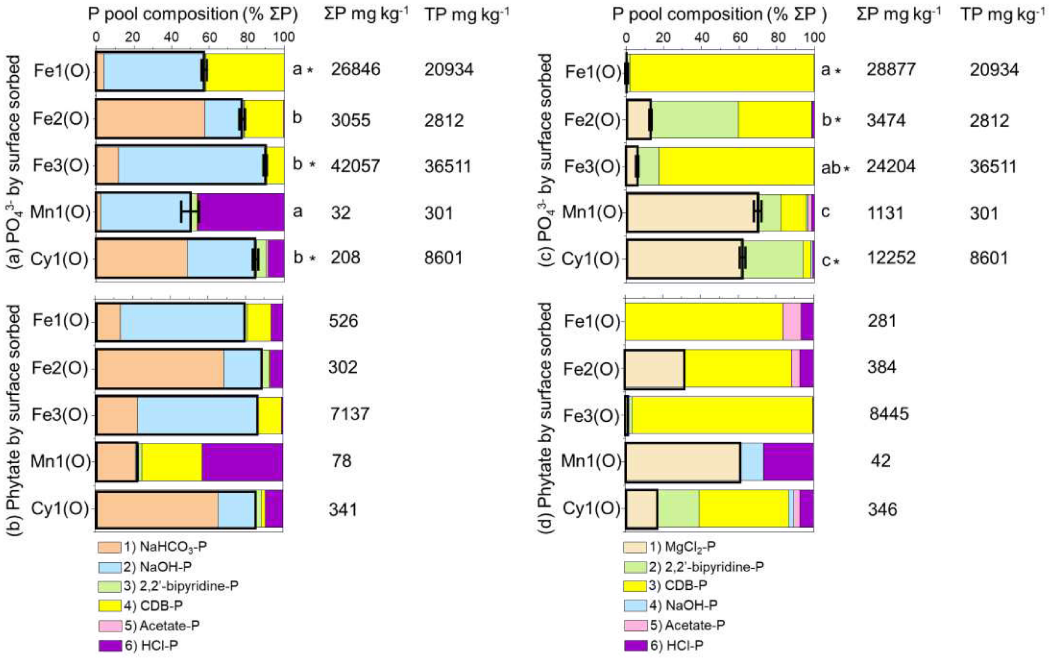

Fig. 2.4 Sequential extraction results for outside loading with PO_4 and phytate by Scheme A (left panel) and Scheme B (right panel). Extraction Scheme A applied to surface-adsorbed PO_4 (a), Extraction Scheme A applied to surface-adsorbed phytate (b), Extraction Scheme B applied to surface-adsorbed PO_4 (c), Extraction Scheme B applied to surface-adsorbed phytate (d). Extraction pools in which expected to observe the respective P loadings are marked with bold frames. TP is obtained by acid digestion. The error bar is employed in case of triplicates. Significant differences between bold frame P pools and total extractable P (ΣP in Figure) are displayed as * ($p < 0.05$). Different letters on the right of the bars indicate significant differences among the Bold frame P pools in different mineral phases ($p < 0.05$). Abbreviations: Fe1(O): ferrihydrite, Fe2(O): hematite, Fe3(O): magnetite with goethite, Mn1(O): pyrolusite, Cy1(O): mica (chlorite).

The surface-adsorbed PO_4 was supposed to be extracted by $NaHCO_3$ and NaOH steps (bold frame in Fig. 2.4 a); However, PO_4 was still found in subsequent extraction steps in the scheme. Especially for Fe1(O), Fe3(O) and Cy1, surface-adsorbed PO_4 was not completely extracted, resulting in a remainder of 43%, 10% and 15% of the surface-adsorbed PO_4, respectively. Extracted surface-adsorbed phytate in Mn1 was the lowest (mean value: 23% of the total extractable phytate) as compared with Fe1(O), Fe2(O),

Fe3(O) and Cy1 (mean value: 80%, 89%, 86% and 85% of the total extractable phytate, respectively, Fig. 2.4 b). For Scheme B, $MgCl_2$ was designed to remove labile PO_4 from the surface, which was also highlighted in the bold frame in Fig. 2.4 c. However, the majority samples were not completely extracted, the extracted PO_4 in terms of Fe1(O), Fe2(O) and Fe3(O) (mean value: 0%, 13% and 6% of the total extractable PO_4, respectively) were lower than that of Mn1 and Cy1 (mean value: 67% and 61% of the total extractable PO_4, $p < 0.05$, Fig. 2.4 c). Surface-adsorbed phytate extracted by $MgCl_2$ accounted for 0%, 32%, 1%, 61% and 17% of the total extractable phytate in terms of Fe1(O), Fe2(O), Fe3(O), Mn1 and Cy1, respectively (Fig. 1 d). In scheme B, 2,2'-bipyridine showed low selectivity and performed inadequately, resulting in unexpectedly extractable PO_4 in Fe2(O), Cy1(O) (Fig. 2.4 c,d). Almost no NaOH extractable-P (both PO_4 and phytate) was observed due to the NaOH step followed by the CDB step (Fig. 2.4 c,d).

2.3.3 Two sequential extraction schemes for inside loading samples

The prior NaOH wash step had removed the majority of PO_4, i.e. preserved inside loading PO_4 were smaller as compared to intended inside loading (Table 2.3). The CDB-extractable PO_4 in Fe1(I), Fe2(I), Fe3(I) and Fe4(I) accounted for 86%, 94%, 79% and 87% of the total extractable PO_4 by Scheme A and 98%, 97%, 96% and 96% of the total extractable PO_4 by Scheme B, respectively (Fig. 2.5). For both Scheme A & B, CDB extracted almost all PO_4 from Fe-(hydr)oxides. Notably, a large amount of PO_4 was extracted from hydroxyapatite in CDB step in Scheme A and Scheme B, with contents of 11835 and 17272 mg kg^{-1}, respectively. In contrast, the CDB-extracted PO_4 contents were 1769, 1624, 696, and 1146 mg kg^{-1} by Scheme A and 1525, 1051, 715 and 1096 mg kg^{-1} by method B in terms of Fe1(I), Fe2(I), Fe3(I) and Fe4(I), respectively (Fig. 2.5 a,b & Table 2.3).

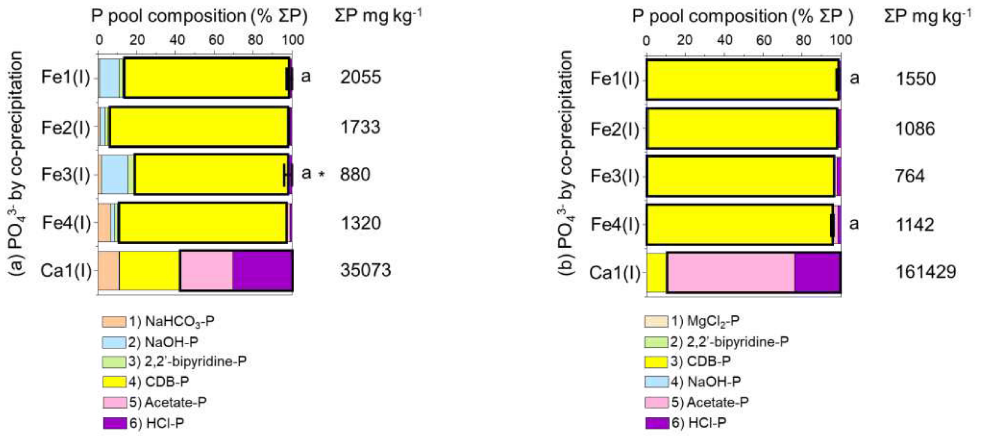

Fig. 2.5 Sequential extraction results for inside loading with PO_4 by Scheme A (left panel) and Scheme B (right panel). Extraction Scheme A applied to co-precipitated PO_4 (a), Extraction Scheme B applied to co-precipitated PO_4 (b). For the co-precipitation minerals, they were synthesized and followed by the removal of surface-adsorbed PO_4 by repeated washing with 0.1M NaOH. Extraction pools in which expected to observe the respective P loadings are marked with bold frames. The error bar is employed in case of triplicates. Significant differences between bold frame P pools and total extractable P (ΣP in Figure) are displayed as * ($p < 0.05$). Letters on the right of the bars indicate significant differences among the Bold frame P pools in different mineral phases ($p < 0.05$). Abbreviations: Fe1(I): ferrihydrite, Fe2(I): hematite, Fe3(I): magnetite with goethite, Fe4(I): decayed vivianite (ferrihydrite), Ca1(I): hydroxyapatite.

2.3.4 The application of Scheme A on natural samples

After comparing the results from the groundwater system-featured synthetic minerals by using two extraction schemes, the extraction Scheme A was chosen for testing natural samples, the reason will be explained in the discussion section. The aquifer samples from three regions yielded distinct P pool characteristics. The aquifer sediments from the Ammer floodplain yielded abundant P Pools, each of $NaHCO_3$-P, NaOH-P, CDB-P and HCl-P pool accounted for a certain percentage of the total P. The aquifer sediments from the Red River floodplain mainly consist of NaOH-P, CDB-P and HCl-P. Significantly high amounts of CDB extractable Fe were found, ranging from 6072 to 67960 mg kg^{-1}. The CDB extractable Ca were found very low, less than 429 mg kg^{-1}. The aquifer sediments from the Hetao floodplain mainly consist of HCl-P. 2,2'-bipyridine extractable-P could reflect the feature of aquifer materials but only account for a very small proportion, accounted for 0 to 4 % of the total extractable P. The acetate buffer extractable-P accounted for 5.5% of the total extractable P in top soil, make less sense in terms of aquifer sediments in our study cases.

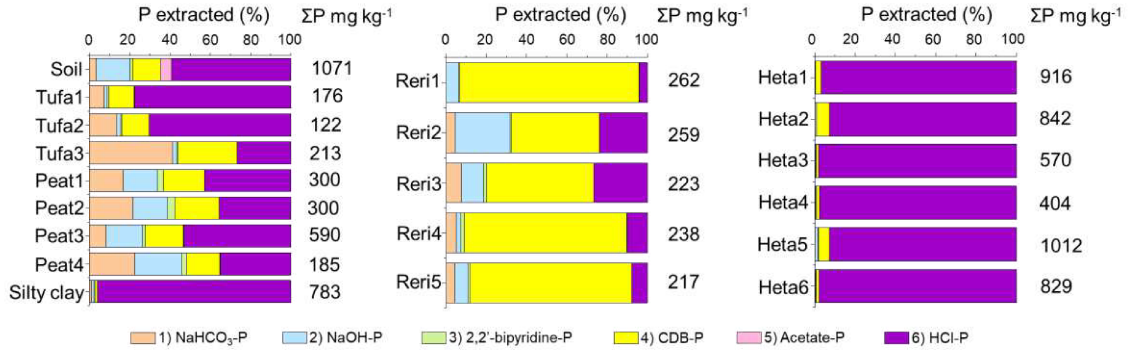

Fig. 2.6 Overview of obtained sequential extraction results for natural samples obtained by Scheme A. The left panel represent nine samples obtained from a calcareous aquifer system at the Ammer floodplain near Tübingen, Germany (Heidgen et al., 2020), sample with name soil belongs to top soil layer and sample with name silty clay belongs to aquitard. The middle panel shows results for five samples obtained from a porous sandy aquifer in the Red River floodplain, Vietnam (Neidhardt et al., 2021). The right panel includes six samples from the Hetao floodplain, PR China, which represent a porous aquifer comprised of primary Ca-P minerals (Li et al., 2022).

Table 2.5 The CDB-extractable elements (P, Al, Fe, Mn, Mg, Ca) in natural samples.

		Elements in CDB step (mg kg^{-1})					
Sample	Name	P	Al	Fe	Mn	Mg	Ca
The Ammer floodplain	Soil	150	391	4765	219	252	3750
	Tufa1	22	79	47	1	111	7949
	Tufa2	17	17	38	0	72	3204
	Tufa3	62	0	0	0	103	4484
	Peat1	61	30	2	0	412	8162
	Peat2	66	0	45	0	249	9490
	Peat3	10	233	664	37	262	2405
	Peat4	112	80	27	1	350	10965
	Silty clay	30	9	0	0	427	7391
The Red River floodplain	Reri1	233	2824	67960	90	67	64
	Reri2	112	225	7771	49	9	30
	Reri3	118	242	6072	32	14	80
	Reri4	192	789	11841	443	53	429
	Reri5	174	617	9271	270	36	111
The Hetao floodplain	Heta1	27	183	4840	138	141	1507
	Heta2	52	435	2043	178	210	2704
	Heta3	7	101	2433	47	30	648
	Heta4	6	71	2442	19	13	276
	Heta5	54	480	2986	275	206	2387
	Heta6	12	132	1133	66	43	790

Table 2.6 Comparison of the advantages and disadvantages of Scheme A and B. + indicates good performance under this criterion; - + indicates not good performance under this criterion; +, - + indicates good performance in some cases under this criterion

Criteria	Scheme A	Scheme B
Removal effect of surface-adsorbed PO_4 in Fe- and Mn-(hydr)oxides, mica	+, -	-
Remove effect of surface-adsorbed phytate in Fe- and Mn-(hydr)oxides, mica	+, -	-
Selectively extract the PO_4 on the surface of Fe-(hydr)oxides	+, -	-
Selectively extract the PO_4 co-precipitation with Fe-(hydr)oxides	+	-
Vulnerability to Ca-mineral interference	-	-
Selectively extract authigenic P in aquifer sediments	-	-

2.4 Discussion

2.4.1 Comparison of the two tested extraction scheme on synthetic mineral samples

In the outside loading experiment, digestion and sequential extraction results showed that Fe-(hydr)oxides were loaded with significant amounts of PO_4, and their adsorption advantage manifests the importance of Fe-minerals in P cycling in groundwater systems. From the point of view of adsorption efficiency, the adsorption results of PO_4 are influenced by its contents, protonation state of PO_4 in aqueous solution and the surface characteristics of the adsorbents involved (Németh et al., 1998; Zhou et al., 2005). The bold frame in Scheme A showed significantly higher recovery of surface-adsorbed PO_4 pools than Scheme B, especially for Fe-(hydr)oxides and mica (Fig. 2.4). Firstly, this can be attributed to the NaOH step, as the strongly surface-adsorbed P is mainly accomplished by ligand bonding, and the sorption of PO_4 is decreased with increasing pH in NaOH step due to competition with OH^- (Ajmal et al., 2018; Zhou et al., 2005). Because OH^- ions would bound with metallic oxides and then the ligand of OH^- in the aqueous solution would be replaced by PO_4 that was bound with metallic oxides. (Bai et al., 2017; Du et al., 2016; Németh et al., 1998; Zhou et al., 2005). It explains that the application of NaOH solution removed a significant amount of surface-adsorbed PO_4 (Fig. 2.4 a,b). Secondly, the adsorption & desorption of PO_4 on oxides are not only related to pH conditions but also to the anion species and oxides surface (Anderson and Malotky, 1979; Huang, 1975). Considering the similar pH conditions of the $NaHCO_3$ step in Scheme A (pH 8.8) and $MgCl_2$ step in Scheme B (pH 8.0), it implied that HCO_3^-, which

is also an anion, is better able than Cl^- to compete with PO_4 for adsorption on the tested mineral surfaces (Flower et al., 2022; Millero et al., 2001).

Most importantly, the extraction sequence of conducting step NaOH before CDB in Scheme A showed more information regarding P pools than that of Scheme B. By Scheme A, it is possible to distinguish between the surface adsorbed and inside coprecipitated P pools in Fe-minerals. The results in Scheme B showed no detection of P in the NaOH step in all Fe (hydr)oxides in both outside and inside loading (Table 2.3). This is attributed to two reasons. First, the CDB step can dissolve Fe(III)-(hydr)oxides, which are a key P sink in groundwater systems, and therefore, it is not suitable to be placed in an earlier sequence. This applies to explain outside loading group conducted by Scheme B. Second, in the context of a groundwater system study, CDB is a stronger extractant than NaOH. It is reasonable to conduct CDB step first as CDB is weaker extractant than NaOH in soil and marine context (Lei et al., 2020; Yuan et al., 2019). But in groundwater system, Fe(III)-(hydr)oxides are important potential sinks for PO_4 (and P_{org}) in most aquifers, and the way that how PO_4 incorporates with Fe(III)-(hydr)oxides is critical as it further influences the judgment of ecosystem risk (Guo et al., 2023; Y. Li et al., 2023; M. Liu et al., 2023; Neidhardt et al., 2018; Zhang et al., 2023). Therefore, I conclude that NaOH step should neither be excluded in groundwater system study as it represents a significant portion of strongly surface-adsorbed P nor be placed after CDB step as it leads to this fraction being extracted, losing important information regarding Fe(III)-(hydr)oxides associated P .

For surface-adsorbed phytate, Scheme A had a higher recovery than Scheme B in case of ferrihydrite, hematite, magnetite with goethite and mica, suggesting that Scheme A is more suitable for reflecting surface-adsorbed P_{org} compositions. The sorption of phytate occurs through its PO_4 groups, and it has six negatively charged PO_4 groups at physiological pH (~ 6–7) (Emanuelli et al., 2014; García-López et al., 2024). Thus, influencing the adsorption behavior of phytate on mineral surfaces is through two aspects, i.e., the separation of PO_4 groups from mineral surface and all the number of PO_4 groups attached to the mineral surface in specific cases is consumed. As already discussed above, it suggests that specific forms of ligand exchange and pH might be attributed to the reason that Scheme A performed better phytate recovery than Scheme B. Another potential reason could be the addition of $MgCl_2$ to the extraction system which allows Mg ions to form precipitates with phytate (Cheryan et al., 1983). The information of surface-adsorbed organic P is important for aquifer studies because organic P does not only

contribute PO_4 to aqueous environment but also act as a sink to immobilize PO_4 (M. Liu et al., 2023; Tao et al., 2023, 2020).

In the inside loading experiment, a large amount of PO_4 was incorporated with minerals during the synthesis and was washed by NaOH step from extraction scheme prior to the chemical sequential extraction. The extraction results showed that Fe-associated P was predominantly released during the CDB step in both schemes. Scheme A and Scheme B extracted roughly similar amounts of P in ferrihydrite, hematite, magnetite with goethite, and vivianite. These results indicate that the use of CDB for extracting internal P, defined by its resistance to NaOH extraction, has been proven to be highly efficient (Barrow, 2021; Tao et al., 2020). Notably, a notable loss of Fe from inside loading minerals in pretreated NaOH wash step was observed, along with significant amounts of PO_4 in the wash solution, where no dissolution occurred in corresponding outside loading samples (Table 2.4). These findings can be attributed to i) that NaOH was able to partially dissolve some of the Fe-minerals that formed by co-precipitation with PO_4; ii) that surface adsorbed Fe^{3+} and/or Fe^{2+} was released along with PO_4 from mineral surfaces through the extraction step. The reason for this may be that coprecipitation of PO_4 alters the structure of Fe (hydr)oxides, decreases the crystallinity of the resulting Fe(III) precipitate by binding to crystal growth sites; by contrast, the PO_4 adsorption onto pre-formed Fe-oxides does not impact its structure (Kraal et al., 2019; Waychunas et al., 1993). For example, it was reported that coprecipitation of PO_4 markedly enhanced Fe (hydr)oxides dissolution rate and rendered Fe (hydr)oxides more reactive towards sulfide compared to pure Fe (hydr)oxides (Kraal et al., 2022, 2019). Therefore, the interpretation of the NaOH extractable P pool needs to be treated more carefully, as the P fraction can be derived from both structural bound and surface-adsorbed P.

An accurate and reliable chemical extraction scheme can help analyze the different forms of P and determine the P composition of aquifer materials. Surface-adsorbed P originates from dissolved P in the aqueous phase, which becomes immobilized on the sediment surface. It can then exchange with groundwater and be utilized by biological activities. Therefore, it serves as an important sink in the P cycling through groundwater systems (Kazmierczak et al., 2020; Neidhardt et al., 2019). The initial P solution concentration and the adsorption environment were the same in each outside loading experiments, the difference in the total amount of PO_4 adsorbed by different minerals was mainly influenced by the surface properties of the adsorbent. In sum, the results showed Scheme A is more suitable than Scheme B as it provided sufficient information about PO_4 and P_{org} from the surface adsorption perspective.

2.4.2 Extraction scheme limitation and the performances on natural aquifer material.

However, the limitations of Scheme A also cannot be ignored. Notably, surface-adsorbed PO_4 cannot be completely extracted by NaOH from various minerals (in our test: ferrihydrite, hematite, magnetite with goethite, pyrolusite, mica), and even within iron (hydr)oxides, the proportion of PO_4 that can be removed by NaOH is different, thereby confirming a certain lack of selectivity of the method, which is consistent with the observations by Klotzbücher et al. (2019). For Fe(III)-(hydr)oxides, the PO_4 adsorption to surface iron ions were reported via inner-sphere complexation, i.e. PO_4 ions are bound with Fe by ligand exchange (Antelo et al., 2010; Spicher et al., 2023). While this adsorption capacity is impact by comparable isoelectric points of specific substance and corresponding pH condition, that is, the greater the difference between these two values, the greater the degree of desorption of PO_4 it exhibits (Spicher et al., 2023; Urdiales et al., 2020; Wang et al., 2015). The different proportion of NaOH extractable PO_4 on Fe1(O), Fe2(O) and Fe3(O) might be attributed to this reason. The rest portion of surface-adsorbed PO_4 was extracted by the CDB solution for Fe1(O), Fe2(O) and Fe3(O). From the comparison of ΣP and TP in Fig. 2.4 a and Fe contents in subsequent extraction solutions in Table 2.4, minerals Fe1(O), Fe2(O) and Fe3(O) had been dissolved in CDB step, suggesting there is a portion of surface-adsorbed PO_4 which is not liberated unless the mineral phase is completely dissolved. In this study, this is referred to as non-extractable surface-adsorbed PO_4, meaning that a portion of surface-adsorbed PO_4 is not liberated unless the mineral phase is completely dissolved. It was previously reported the PO_4 sorption on the passive aluminum surface is a largely irreversible process, it was presumed due to an ongoing surface transformation (Németh et al., 1998). The same phenomenon has also been observed in an experiment that loading PO_4 on the surface of synthetic ferrihydrite, goethite and magnetite (Ajmal et al., 2018). Although the study draw conclusion that the PO_4 sorption was reversible and could be desorbed in alkaline environments, it was more from a perspective of wastewater treatment. Considering the desorption efficiencies were 75%, 85%, and 82% for ferrihydrite, goethite and magnetite using 1 mol L^{-1} NaOH, from a chemical extraction point of view, this also corroborates the presence of non-extractable PO_4 on the surface. The same phenomenon was observed regarding phytate on the surface of poorly crystalline Fe oxides such as ferrihydrite (Chen and Arai, 2019). In short, the CDB solution was intended to release coprecipitated PO_4 in Fe(III)-(hydr)oxides (Hupfer et al., 1995; Ruttenberg et al., 2009). However, the presence of non-extractable surface-adsorbed PO_4 can lead to an overestimation of the structurally bound P pool. This "contamination" cannot be ignored,

especially when surface adsorption is dominant. Further studies are needed to answer the question of the strength of this fraction of PO_4 bound to the Fe(III)-(hydr)oxides surface. Interpretation of non-extractable surface-adsorbed PO_4 in terms of isotopic fractionation will be discussed in a later section.

For Mn1(O) and Cy1(O), their total extractable PO_4 were significantly less than total surface-adsorbed PO_4 that indicated by digestion data (Table 2.3). At meantime, the recovery of Mn ions in Mn1(O) and Al ions in Cy1(O) suggests that their mineral structures were largely undissolved (Table 2.4). It implies a portion of surface-adsorbed PO_4 still remained on the mineral and it is also referred to as non-extractable surface-adsorbed PO_4. i.e. there is a lack of extractant to liberate this P fraction without destroying mineral structure. However, due to the minimal adsorption of PO_4 and the mineral phase remaining largely undissolved throughout the extraction scheme, the risk of misclassification caused by the presence of non-extractable surface-adsorbed PO_4 is significantly reduced in the cases of Mn1(O) and Cy1(O).

Inexpertly, CDB did not only extract PO_4 from Fe1(I), Fe2(I), Fe3(I) and Fe4(I), but also extract PO_4 from Ca1(I). A portion of PO_4 was extracted by CDB from hydroxyapatite in both Scheme A and B. This is unexpected and could result in considerable Ca-associated PO_4 wrongly interpreted as Fe(III)-associated PO_4. With the information provided by Table 2.3 and Table 2.4 it can be calculated that the Ca/P molar ratio were 1.4 and 1.1 in the CDB step of Scheme A and Scheme B, respectively. Crystal hydroxyapatite [$Ca_{10}(PO_4)_6(OH)_2$] has a Ca/P molar ratio of 1.67, other calcium orthophosphates have a Ca/P molar ratio 0.5 – 1.5, for example, Dicalcium phosphate dihydrate [$CaHPO_4 \cdot 2H_2O$] has Ca/P molar ratio of 1.0, α-Tricalcium phosphate [α-$Ca_3(PO_4)_2$] has Ca/P molar ratio of 1.5 (Dorozhkin, 2011; Pastero et al., 2017). It suggests the synthetic hydroxyapatite contains some amorphous calcium phosphates. There are fewer studies reported that CDB extracted PO_4 from hydroxyapatite, however, there were relevant reports that a substantial amount of calcium-bound P was solubilized by the CDB reagent in $CaCO_3$ case, for which the strongly chelating citrate ion was responsible (C. Wang et al., 2013; Williams et al., 1971, 1976). Therefore, I suggest to be more conservative in the interpretation of the CDB-extractable P for calcareous samples. The comparison of the advantages and disadvantages of two schemes was summarized in Table 2.6. Considering (i) the low efficient of $MgCl_2$ as extractant on surface-adsorbed P (PO_4 and phytate) mobilization, (ii) that a later placed NaOH leads to underestimation of surface-adsorbed P, especially Fe-associated P, I conclude

Scheme B is not ideal for analyzing P pools in groundwater systems, Scheme A is chosen for further natural sample experiments.

Combined with the background information of natural samples given in Table 2.2, the sequential extraction results provide the following possible interpretations. The $NaHCO_3$ step extracted a large portion of P from a calcareous aquifer in the Ammer floodplain, which corresponds to the significant amount of P on the sediment surface. Based on the outside loading experiments and the widespread presence of organic matter in the study area, the large amount of surface-adsorbed P is likely involving both PO_4 and P_{org} at same time. The NaOH step extracted a substantial amount of P from the calcareous aquifer in the Ammer floodplain and the porous sandy aquifer in the Red River Delta. This suggests that the NaOH-P fraction in the former case might be attributed to the presence of organic matter (Heidgen et al., 2020; Klingler et al., 2020; Spohn, 2024), while in the latter case, it might be attributed to Fe(III)-(hydr)oxides that adsorb significant amounts of PO_4 on their surfaces (Kraal et al., 2022; Neidhardt et al., 2018). The CDB step extracted a large portion of P from both the calcareous aquifer in the Ammer floodplain and the porous sandy aquifer in the Red River floodplain. It has been reported that in the anoxic sandy Holocene aquifers of the Red River floodplain, PO_4 was released into groundwater through microbial degradation of organic carbon and the concomitant reductive dissolution of Fe(III)-(hydr)oxides (Neidhardt et al., 2018). According to this information in Table 2.5, in the Ammer floodplain case, the extracted P can be interpreted as primarily originating from Ca-minerals, as little Fe was detected in the samples, while in the Red River floodplain case, it can be interpreted as coming from Fe-minerals, with the sediments being nearly devoid of Ca. Therefore, it is crucial to emphasize the importance of considering the potential interference of Ca-P when interpreting CDB-P pools. The HCl step were predominated P pools in the Ammer floodplain and porous clay aquifer in the Hetao floodplain. The aquitard composed of silty clay exhibited a markedly different composition of P pools. This additionally demonstrates that the sequential extraction scheme can effectively differentiate the functional sink of P between various sediments within the same geological environment.

The 2,2'-bipyridine and acetate buffer step did not perform well in practice. The reasons of 2,2'-bipyridine step's performance can be attributed to two reasons. First, Fe(II)-associated P may have been extracted in earlier steps. The reference method specifically targeted the extraction of Fe(II)-associated P, utilizing a 2,2'-bipyridine solution with KCl to remove surface P, which resulted in the inclusion of surface P pool within the Fe(II)-P pool (Li et al., 2012). In this study, Fe4(I), decayed vivianite, was

dissolved during the preliminary NaOH wash step, as a result, both Scheme A and Scheme B did not show a detectable 2,2'-bipyridine extractable P pool in synthetic sample. Another possible reason is the time constraint, as the original protocol required 150 hours to extract Fe(II)-P, a duration that was impractical to include in the chemical sequential extraction scheme and was therefore shortened in the experimental protocol. However, this is secondary explanation for the lower P extraction observed in the experimental results. Additionally, the use of 2,2'-bipyridine introduces the complication of the extracted solution turning a light red color, while this color interference can be degraded by using acid, it remains a notable interference (Wang et al., 2021). Authigenic P is the most important long-term P sink in most marine sediments (März et al., 2018; Ruttenberg, 1992). It has been reported that in anoxic environments, PO_4 is thus released back to the water column instead of being retained in the sediment where it eventually could be buried as authigenic P minerals, but the overall burial efficiency of P in this environment is low (Hylén et al., 2021). This may explain why the aquifer sediments from the three locations I investigated did not respond to the acetate buffer step in the same way as marine sediments. Based on the above discussion, the sequential extraction scheme was further refined as: $NaHCO_3$ – NaOH – CDB – HCl.

2.5 Conclusion

The extraction Scheme A has been found to be more suitable for analyzing P pools in groundwater systems. The use of stronger extraction solutions and a more rational extraction order provides more accurate information by this extraction scheme, especially when analyzing aquifer minerals where Fe-minerals serve as the primary P sink. NaOH can release surface-adsorbed P without dissolving Fe-minerals, but it may lead to an underestimation of surface P, as some fraction may remain on the surface until the CDB step is conducted. It is also important to note that the NaOH extraction step, when dealing with P co-precipitated with Fe-minerals, is likely to extract both surface-adsorbed and structurally bound PO_4. Similarly, the CDB extraction step does not only target on structurally bound PO_4 but is also able to extract a substantial portion of strongly adsorbed-surface PO_4. This dual extraction capability is crucial for minerals like ferrihydrite, where previous extraction steps might not completely remove all the surface-adsorbed PO_4. One of the most challenging aspects of using the CDB step is interpreting the CDB-P pool in the context of calcareous material, as it may release considerable PO_4 as well and might be wrongly interpreted to Fe(III)-(hydr)oxides associated P. By applying this extraction scheme to natural samples, it was concluded

that 2,2'-bipyridine and acetate buffer have limited effects on aquifer materials of various properties. This finding suggests that these steps may not be necessary for groundwater studies, allowing for a more streamlined and efficient extraction process. Based on these insights, the recommended extraction sequence for future studies of P cycling in groundwater systems is $NaHCO_3$ – NaOH – CDB – HCl. Methodological limitations interfere precise identification of P pools, but this sequence of the extraction scheme suggested relatively accurate identification and quantification of surface-adsorbed and structure-bound P species and is particularly suited to groundwater system studies. In summary, the optimized extraction scheme offers a robust methodology for analyzing P pools in groundwater systems. By carefully considering the properties of the extractants and the sequence of their application, researchers can obtain more precise and reliable data on the distribution and speciation of P in aquifer materials.

3 The biogeochemical cycling of phosphorus in calcareous and organic matter-rich floodplain aquifer

3.1 Introduction

Groundwater has gained attention due to its potential to transport substantial amounts of phosphorus (P) to neighbouring surface water bodies, such as lakes (Kazmierczak et al., 2021; Nisbeth et al., 2019), urban streams (Roy and Bickerton, 2014) and polders (Yu et al., 2018), which is concern regarding the eutrophication of surface waters. Floodplain aquifers, representing crucial water resources for ecosystems and human activities, play a vital role in the im/mobilization and transport of P (Hauer et al., 2016; Sharpley et al., 2013). Elevated total dissolved P (TDP) concentrations in floodplain aquifers have been observed globally e.g., in Iowa and northern Indiana watersheds in the US (Schilling et al., 2018; Trentman et al., 2020), in the Gudenå River Catchment and the Amsterdam area in Europe (Kazmierczak et al., 2021; Yu et al., 2018), in the Bengal Delta Plain and Red River Delta in South and Southeast Asia (Neidhardt et al., 2018), and in the Hetao Plain and Jianghan Plain in China (Li et al., 2022; Tao et al., 2020).

The sources of elevated TDP in groundwater were mainly attributed to i) weathering of P-bearing minerals such as apatite (Bingham et al., 2020; Li et al., 2022), ii) reducing redox conditions and concomitant reductive dissolution of Fe(III)-(hydr)oxides (Li et al., 2022; Neidhardt et al., 2018; Tao et al., 2020), iii) mineralization of organic matter (OM), including sedimentary organic carbon (SOC) and dissolved organic carbon (DOC) which contain P (Li et al., 2022; Z. Liu et al., 2023; Tao et al., 2020). In addition, anthropogenic activities can also cause elevated TDP concentrations in groundwater when their input exceeds the immobilization capacity of an aquifer. For example, animal manure accumulation (Liao et al., 2019), wastewater inputs (Huang et al., 2020), and leaking sewage canals (Robertson et al., 2019) may introduce additional P into underlying aquifers. Furthermore, Robertson et al. (2019), focused on the attenuation of P in groundwater plumes from septic systems, and emphasized the importance of understanding the behaviour of P in calcareous aquifers, which remains largely unknown so far.

The TDP in groundwater usually occurs in form of inorganic orthophosphate (PO_4), which represents the basic molecule in the biogeochemical cycle of P (Davies et al., 2014; Holman et al., 2008). However, P species in global aquifers have not been widely

reported so far. The commonly measured TDP concentrations in groundwater and total P contents in aquifer sediments provide no further information regarding the respective P species, such as different PO_4 and organic P (P_{org}) species. It has already been reported that P_{org} contributes to the geogenic P enrichment in groundwater, primarily consisting of aliphatic compounds and highly unsaturated compounds (Tao et al., 2023). Shinohara et al. (2017) reported P_{org} in sediment particles as a source for dissolved P_{org} in the pore water of a lake sediment. Furthermore, Liu et al. (2023) investigated the enrichment of P in aquifer systems from the perspective of depositional evolution and concluded that the sedimentary facies mainly controlled P_{org}, while paleo-climate controlled both Fe-bond PO_4 and P_{org}. Therefore, detailed knowledge of the present P species is crucial for addressing the fate of P in groundwater systems.

Floodplain aquifers can act as sinks for PO_4 that is transported within groundwater. First, PO_4 can be immobilized via surface adsorption to primary and secondary minerals, OM and other aquifer materials, which is strongly affected by pH and competing oxyanions (Barcala et al., 2023; Flower et al., 2022; Spiteri et al., 2007). Second, PO_4 can be immobilized by the formation of secondary minerals like Ca-P minerals (e.g. hydroxyapatite), Fe(III)-P (e.g. ferrihydrite, strengite) or Fe(II)-P minerals (e.g. vivianite). Under oxic conditions PO_4 can be co-precipitated with newly formed Fe(III)-(hydr)oxides, while under anoxic conditions secondary Fe(II)-minerals can serve as important sinks for PO_4 (Neidhardt et al., 2018; Rothe et al., 2016). Furthermore, when the redox conditions reach SO_4^{2-} reducing conditions, PO_4 might also be immobilized through the co-precipitation with Fe(II)-sulfides as suggested by Li et al. (2021). Third, PO_4 can also be immobilized by uptake and storage by biota, such as microorganisms and aquatic invertebrates (Bean et al., 2015; Trentman et al., 2020).

Floodplain aquifers may also act as sources of PO_4 for groundwater. First, surface-adsorbed PO_4 can be desorbed and re-released into the groundwater by changes in the hydrological flow paths and associated changes in redox conditions (Flower et al., 2022; Sharpley et al., 2013). Specifically, adsorbed and/or occluded PO_4 can be released into ambient groundwater by the reductive dissolution of Fe(III)- and Mn(IV)-(hydr)oxides when redox conditions change from oxidizing to reducing (Li et al., 2022; Y. Li et al., 2023; Neidhardt et al., 2021). Second, non-redox sensitive P-hosting phases like Ca-P minerals are also known to release PO_4 through weathering (Bingham et al., 2020). Third, PO_4 present in OM can be released by microbial mineralization and enriches subsequently in groundwater especially under reducing redox conditions (Z. Liu et al., 2023; Neidhardt et al., 2018). All the processes mentioned above are often closely

intertwined and occur in parallel and are further strongly affected by the mineralogical and geochemical properties of the aquifer. As most floodplain aquifers typically contain high amounts of buried OM and are additionally often covered with thick layers of alluvial loam, anoxic conditions usually occur, which foster the geogenic release of PO_4 into groundwater. However, it remains unclear whether PO_4 mobilization processes can outpace the respective immobilization processes under certain circumstances. The precipitation of secondary minerals may especially be relevant in calcareous aquifers, but so far, our knowledge is limited regarding pristine calcareous systems.

In anoxic calcareous aquifers, TDP concentrations in groundwater were reported to be generally higher and more mobile as compared to oxic and acidic aquifers (Liao et al., 2019; Robertson et al., 2019; Spiteri et al., 2007). This suggests that neutral pH values and reducing conditions may prevail high PO_4 concentrations in groundwater. However, this phenomenon has not been investigated in case of non-contaminated calcareous systems before. Here, I investigated the aquifer of the Ammer floodplain catchment in Southwest Germany. In the Ammer floodplain, a shallow aquifer exists that is formed of secondary calcium-carbonate precipitates ("tufa") with partially high contents of organic matter (peat). Beneath the shallow aquifer, a deeper limestone gravel aquifer is present. The overarching questions were: (i) What are the sources that are responsible for elevated P in the groundwater of calcareous floodplain aquifers? (ii) How can elevated PO_4 concentrations in a calcareous aquifer system prevail? To our best knowledge, this study is the first on groundwater P cycling in a non-contaminated calcareous aquifer.

3.2 Materials and Methods

3.2.1. Study area

The study area is located in the Ammer floodplain in Southwest Germany (Fig. 3.1). The Quaternary floodplain sediments comprise a silty clay alluvial cover at the surface (1 – 2 m below land surface, bls), with a shallow aquifer beneath that was previously described as a tufaceous ("tufa") aquifer (1 – 9 m bls) (Klingler et al., 2020; Martin et al., 2020). In short, the shallow aquifer is calcareous and contains varying proportions of organic matter (mainly in form of peat), which were formed 8400 to 7870 years before present when the system represented a paleo-mire (Heidgen et al., 2020). A low-permeability clay aquitard (1 – 3 m thick) separates the shallow from a deeper gravel aquifer, which represents a channel infill and is embedded in the underlying Triassic bedrock (gypsum-bearing mudstone). The average depth to the underlying bedrock is 14 m. Further information regarding the groundwater properties and the sedimentation history of the

study area in the Ammer catchment is provided elsewhere (Heidgen et al., 2020; Klingler et al., 2020; Martin et al., 2020).

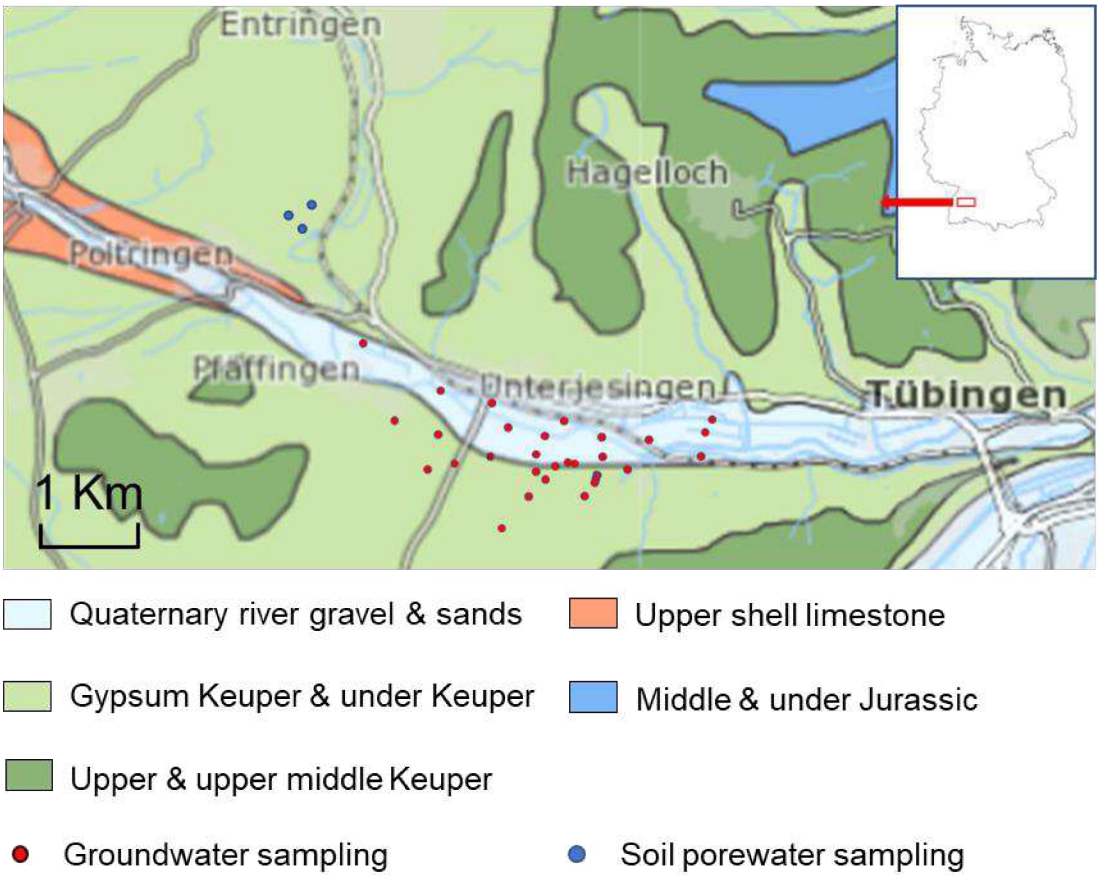

Fig. 3.1 Study area and sampling locations. Groundwater sampling locations represent a shallow groundwater well or a shallow and a deep groundwater well (Map: https://maps.lgrb-bw.de/).

3.2.2. Sampling

Groundwater sampling: The groundwater data used in this study originates from two sampling campaigns, the principal campaign was conducted in November 2019 (sample numbers for the two aquifers: $n_{shallow}$ =36, n_{deep} =20), and a complementary in March 2020 ($n_{shallow}$ = 6, n_{deep} = 3) (Table S3.2). Shallow groundwater samples were collected at depths of 3 to 7 m bls, deep groundwater samples were collected at depths between 7 and 17 m bls. Field parameters were assessed and recorded continuously during the purging of the monitoring wells in 30 seconds intervals using a flow-through cell and a multi-parameter probe (smarTROLL and Aqua TROLL 500, In-Situ), including pH, water temperature, electrical conductivity (EC), oxidation reduction potential (ORP, which was

converted into Eh according to the manufacturer's manual) and dissolved oxygen (O_2) concentration. All monitoring wells were first purged until the water temperature, pH, and EC stabilized before groundwater samples were taken. Samples were then filtered (0.45 µm cellulose acetate filter, Sartorius), and subdivided into two aliquots immediately in the laboratory. One aliquot was acidified (1% v/v with 65% HNO_3; Merck, suprapure) and stored in acid-washed, pre-conditioned PE flasks for further ICP-OES analysis, the other aliquot without acidification was used for UV-vis, IC and TOC measurements. Additionally, to check if TDP is downward transported into the groundwater from the surface, soil porewater samples were collected at 50 cm and 100 cm bls by a lysimeter at a location 2 km away from the closest groundwater well in February 2020, under same hydrologic conditions as the groundwater sampling campaigns (Fig. S1).

Sediment core sampling: In the centre of the Ammer floodplain, a 12 m-long sediment core was collected at the place where highest groundwater TDP concentration was detected by Direct Push probing (Geoprobe 6610 DT with Dual Tube DT325 sampling) in August 2020 (Fig. 3.2 a). The drill cores (51 mm in diameter, 12 m in length) were retrieved and stored in PVC liners. After core retrieval, the sediment cores were logged and split according to lithology and colour variations. At the same time, subsamples for the sequential analysis were collected rapidly from within the core and wrapped with aluminium foil, sealed in sterile and gas-tight polythene bags, filled with ultrapure N_2 gas before closure, and were finally kept at -20 ºC for further analysis.

3.2.3. Chemical analysis

Groundwater analysis: Acidified groundwater samples were measured by ICP-OES (Optima 5300 DV, PerkinElmer, limit of quantification for TDP: 0.002 mg L^{-1}) to get concentrations of dissolved major and trace elements (including P as TDP). Same-day filtered, non-acidified aliquots were analyzed for inorganic orthophosphate with the molybdenum blue method (SPECORD 200 PLUS, limit of quantification for PO_4-P: 0.003 mg L^{-1}), major ion hydrochemistry with ion chromatography (DX-120, Dionex) and dissolved organic carbon (HighTOC, Elementar). In addition to groundwater samples, all lysimeter samples were measured by UV-vis, with several sample undergoing a microwave-assisted aqua regia pressure digestion (method E701, MLS GmbH) prior to ICP-OES analysis.

The groundwater composition was used to calculate the saturation indices for mineral phases that might serve as a sink or source for PO_4 at the field sites using the geochemical modeling program PHREEQC (Vers.3) and the wateq4f database

(Parkhurst and Appelo, 1999). SO_4^{2-}/Cl^- ratios were calculated by their mEq ratio, aimed at mitigating the influence of evaporation (Guo et al., 2016). As a quality control, I calculated also the ion balances for each sample with PHREEQC (Percent error, 100*(Cat-|An|)/(Cat+|An|)), showing good results ranging from -8.2 to 1.5% (Table S3.3).

Aquifer materials: Aquifer materials were separated into two subsets. One set of sediment samples was first dried at room temperature and homogenized with a planetary ball mill (Puluerisette 5, Fritsch GmbH). From each powdered subsample, 0.5 g were used to determine total carbon (TC), total nitrogen (TN) and total sulfur (TS) with an Element Analyzer (vario EL III). The calcium carbonate content was determined by a Calcimeter (Scheibler system, Royal Eijkelkamp B.V.) and the outcome converted into inorganic carbon (IC) contents by equation (I):

$$\frac{a*p*1.204*10^{-3}}{(273+t)*E} = \%CaCO_3 \qquad (I)$$

With *a* standing for CO_2 volume changes (cm^3), *p* for atmospheric pressure in pascal (Pa), *t* for temperature (°C), and *E* for sample weight (g). The differences between TC and IC represents organic carbon (OC). Dominant minerals were assessed from a subset of three representative samples using X-ray powder diffractometry (powder XRD, D8 Advance, Bruker), equipped with a Cu anode operating at 40kV/20mA.

The other sample subset was used freshly thawed, and a five-step sequential extraction scheme was applied to extract different P pools from the aquifer sediment including tufa (n=9), peat (n=8) and silty clay (n=7) as described by Li et al. (2021) and Neidhardt et al. (2019). In brief, 0.5 g dry weight equivalent sediment sample was first extracted with 20 mL of 0.5M $NaHCO_3$ solution for 30 minutes to assess labile P ($NaHCO_3$-extractable P), also referred to as exchangeable P. Secondly, the same samples were extracted with 30 mL 0.1M NaOH for 16 h targeting moderately labile P (NaOH-extractable P), which is considered to represent strongly surface-adsorbed P. Next, 45 mL of a CDB solution was applied for 16 h, comprising a mixture of 0.3M Na_3-citrate and 1M $NaHCO_3$ solution and 1.125 g Na-dithionite to liberate structurally bound P in Fe(III)/Mn(IV)-oxides P (CDB-extractable P). Note that CDB-P is supposed to reflect occluded P in Fe(III)/Mn(IV)-oxides, only as the surface-adsorbed P fraction was already removed. After that, 25 mL of 1M HCl was used to dissolve Ca/Fe(II) minerals (HCl-extractable P) at room temperature for 16 h. The HCl-P pool comprises PO_4 in the form of primary and secondary Ca/Fe (II)-phosphate minerals. Finally, remaining sample material was combusted at 550°C and then extracted with 20 ml 0.5M H_2SO_4 to assess residual P (H_2SO_4-extractable P). Here, H_2SO_4-P is generally considered to contain non-extractable

mineral PO_4 and organic phosphorus in the form of recalcitrant organic carbon compounds. All the extractions were conducted at room temperature (except for the H_2SO_4 fraction) and a subsequent wash step (with corresponding extraction solution or $NaHCO_3$) was applied one to four times to ensure all corresponding P species were collected. All extraction solutions were analyzed by ICP-OES for major and trace elemental compositions, including total phosphorus (TP) concentrations. For the first to the third extraction step, extraction solutions were additionally measured by UV-vis to obtain extractable PO_4 in the specific pools. Extractable P_{org} was calculated as the difference between extractable TP and extractable PO_4 (Neidhardt et al., 2018; Tao et al., 2020). Sediment core Kd values were calculated for tufa and peat samples (collected from 1.0 to 7.3 m bls depth) based on groundwater TDP concentrations and surface-adsorbed P (i.e. $NaHCO_3$- and NaOH-extractable PO_4 and P_{org}) (Limousin et al., 2007; Sheppard et al., 2009). The Kd values were calculated as the ratio of the concentration of surface-adsorbed P in the aquifer sediment matrix (in mg kg^{-1}) to the concentration of dissolved PO_4 (0.60 mg L^{-1}) and P_{org} (0.02 mg L^{-1}) observed in groundwater of the shallow aquifer closest to the drilling site (4.2 m bls depth).

The aquifer samples were first grouped into shallow aquifer and aquitard material, of which the former consists of sand and OM clumps and the latter of silty clay, as designated by finger test (D. P. Franzmeier and P. R. Owens, 2008). Samples of the shallow aquifer were further subdivided into peat (OC content exceeding 10 wt%, TS content over 1 wt%, and calcium carbonate content below 55 wt%), whereas the remaining aquifer samples were classified as tufa. In summary, the samples were classified into three facies: tufa, peat and silty clay.

3.2.4. Statistical analysis

All geochemical results were analyzed with Microsoft Excel 2019 and SPSS statistical software (v. 25). All groundwater and aquifer material data were first tested for normal distribution (Shapiro-Wilk test). Normal distributed data was then tested for significant differences by a paired *t*-test or a one-way ANOVA. Non-normal distributed data were tested for significant differences by non-parametric Kruskal-Wallis one-way ANOVA with a post-hoc test (LSD). In addition, a Spearman's correlation two-tail test was applied to identify significant correlations between different measured variables. The confidence interval for all tests was 95% and p-values ≤ 0.05 were considered statistically significant.

To expand the groundwater dataset, results from both sampling campaigns (November 2019, March 2020, Table S3.2) are merged and depicted in Fig 3.2. For the correlation

analysis, only samples with matching variables were included, resulting in a reduction in sample numbers in some cases. Besides, as the data from the sampling campaign in November 2019 lacked information regarding dissolved PO_4 concentrations, the proportion of PO_4-P to TDP was analyzed using data from the March 2020 sampling campaign ($n_{shallow}$ = 28, n_{deep} = 12).

3.3 Results

3.3.1 Groundwater

Groundwater properties: Groundwater temperatures in the shallow aquifer were significantly higher than in the deep aquifer (median: 12.5°C and 11.6°C, respectively, $p < 0.01$, Fig. 3.2 b). Also, the DOC concentrations were significantly higher in the shallow aquifer than in the deep aquifer (median: 4.5 mg L^{-1} and 1.9 mg L^{-1}, respectively, $p < 0.01$, Fig. 3.2 c). The NH_4^+ concentrations were similar for the two aquifers, with median values around 2.0 mg L^{-1} (Fig. 3.2 d; Table S3.4). The Ca concentrations in both aquifers were consistently high, exceeding 100 mg L^{-1} (Fig. 3.2 e). In both aquifers, Ca^{2+} and Mg^{2+} represented the predominant cations, with HCO_3^- and SO_4^{2-} as dominant anions (Table S3.2 and Table S3.4). The pH of the groundwater did not significantly differ between the shallow and deep aquifer, with values between 6.8 to 7.4, representing a circum-neutral range (Table S3.2). The redox state, as indicated by Eh and DO concentrations, reflected anoxic and reducing conditions for the two aquifers (median values: -29 mV and 0.60 mg L^{-1} in shallow, -11 mV and 0.38 mg L^{-1} in deep, respectively, Table S3.4). In the shallow aquifer, the SO_4^{2-}/Cl^- ratios ranged from 0.3 to 37.2 (median: 3.9), while in the deep aquifer, they ranged from 0.5 to 118 (median: 13.0, Fig. 3.2 f; Table S3.4). Further groundwater properties are presented in tables S1 and S3. Note that most variables did not significantly differ between the two aquifers ($p > 0.05$, Table S3.4).

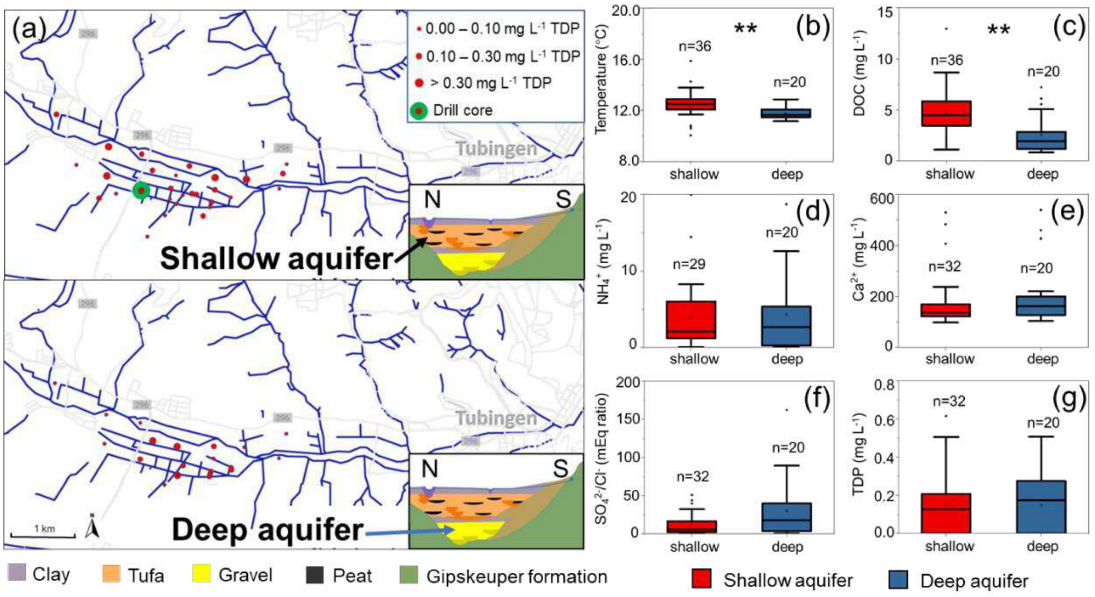

Fig. 3.2 Groundwater TDP spatial distribution pattern and location (a, created with openstreet map); geochemical parameters in shallow and deep aquifers (b-g). Significant differences between the shallow and deep aquifer are displayed as * ($p < 0.05$) or ** ($p < 0.01$). Abbreviations: dissolved organic carbon (DOC), total dissolved phosphorus (TDP).

Groundwater TDP concentrations and relationships with other variables: In both aquifers, TDP concentrations were similar, with median concentrations of 0.13 and 0.17 mg L^{-1} in shallow and deep aquifer, respectively (Table S3.2). The spatial distribution of TDP concentrations in groundwater was highly variable, as reflected by concentrations of up to 0.61 mg L^{-1}, with irregularly distributed "hotspots" within the shallow aquifer (Fig. 3.2 a, upper map). In the deep aquifer, TDP concentrations also varied widely, ranging up to 0.51 mg L^{-1}, with highest concentrations mainly located in the centre of the valley (Fig. 3.2 a, lower map). The proportion of PO_4 to TDP was 103 ± 8 % (n = 28) for the shallow aquifer and 97 ± 4% (n = 12) for the deep aquifer, suggesting that is the PO_4 is the primary P species in groundwater (Table S3.1). Additionally, TDP and PO_4 concentrations remained at very low concentrations in soil porewater (< 0.03 mg L^{-1}, Table S3.6).

Concentrations of TDP generally sharply increased as soon as Eh values dropped below 50 mV, and were negatively correlated with Eh in both aquifers (shallow: $r = -0.55$, $p < 0.01$; deep: $r = -0.72$, $p < 0.01$, Fig. 3.3 a). Furthermore, TDP was positively correlated with DOC (shallow: $r = 0.62$, $p < 0.01$; deep: $r = 0.90$, $p < 0.01$, Fig. 3.3 b), and with NH_4^+ (shallow: $r = 0.48$, $p < 0.05$; deep: $r = 0.90$, $p < 0.01$, Fig. 3.3 c). There were also positive correlations between DOC and NH_4^+ (shallow aquifer: $r = 0.68$, $p < 0.01$; deep aquifer: $r = 0.87$, $p < 0.01$, Table S3.5). A positive correlation between TDP and HCO_3^- was observed in the deep aquifer ($r = 0.85$, $p < 0.01$, Fig. 3.3 d). Furthermore, HCO_3^-

concentrations were positively correlated with NH_4^+ (shallow: r = 0.56, p < 0.01; deep: r = 0.76, p < 0.01) and DOC concentrations in both aquifers (shallow: r = 0.52, p < 0.01; deep: r = 0.84, p < 0.01, Table S3.5).

Saturation indices: Saturation indices indicated that groundwater in the shallow aquifer was under-saturated with regard to amorphous Fe-hydroxides (median: -4.29), vivianite (median: -6.62), siderite (median: -1.48), and hydroxyapatite (median: -0.36). On the other hand, groundwater was supersaturated with regard to goethite (median: +1.15), hematite (median: +4.24), magnetite (median: +3.32), and calcite (median: +0.26). In the deep aquifer, saturation indices values were alike, except for hydroxyapatite, which was in equilibrium (median: -0.02, Table S3.3).

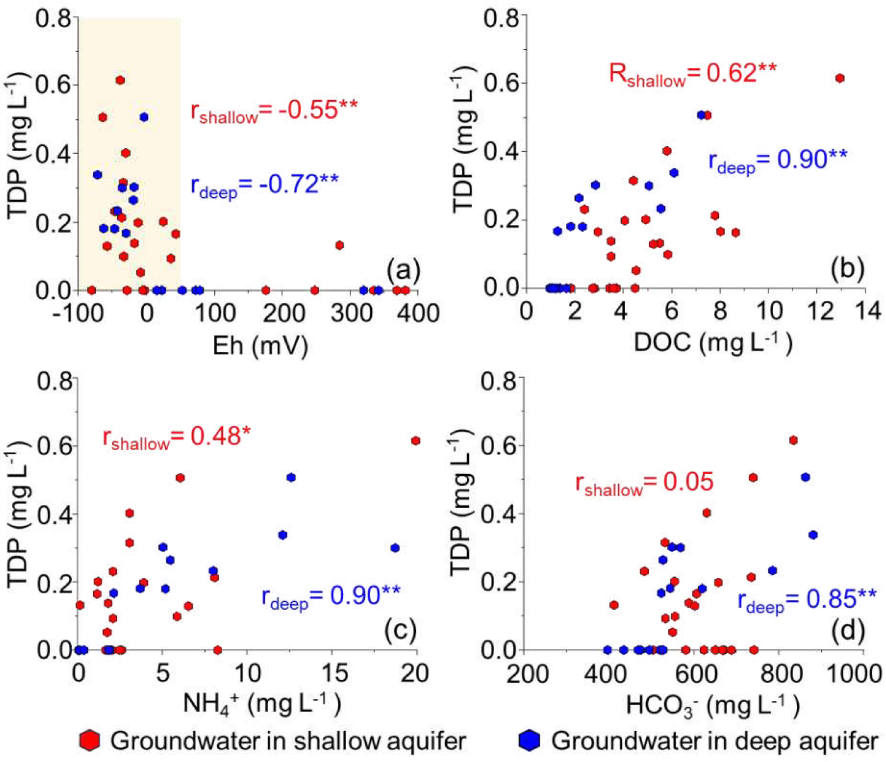

Fig. 3.3 Scatter plots of groundwater parameters: Eh-TDP (a), DOC-TDP (b), NH_4^+-TDP (c) and DOC-NH_4^+ (d). * and ** indicate the level of significance of the spearman correlation with p < 0.05 and p < 0.01, respectively. Abbreviations: redox potential (Eh), dissolved organic carbon (DOC), total dissolved phosphorus (TDP).

3.3.2 Sediment core

General sediment core composition: The sediment core was composed of an approximately 1-m thick clay layer representing the alluvial floodplain loam at top, and an approximately 6-mthick layer of porous tufa and peat material representing the shallow aquifer. Below the tufa and peat layer, an approximately 4 m thick layer of silty clay with some gravel sand occurred, which represented an aquitard and a transition from the shallow aquifer above (Fig. 3.6 a). The OC contents ranged from 48 to 68 g kg^{-1} in the tufa (median: 65 g kg^{-1}) and from 99 to 215 g kg^{-1} in the peat (median: 150 g kg^{-1}, Fig. 3.6 b). The IC contents ranged from 66 to 88 g kg^{-1} in the tufa (median: 76 g kg^{-1}) and from 48 to 68 g kg^{-1} in the peat (median: 65 g kg^{-1}, Fig. 3.6 c). Corresponding to the high amount of IC in the shallow aquifer, the major mineral detectable by XRD in the aquifer material was calcite (Fig. S2). In the silty clay, OC and IC contents were much lower than in the aquifer materials (median: 30 g kg^{-1} and 19 g kg^{-1}, respectively, Fig. 3.4 b,c). Furthermore, TN contents varied within the different facies, with median values of 0.8, 6.9 and 0.7 g kg^{-1} in tufa, peat and silty clay, respectively (Fig. 3.6 d). Similarly, TS contents varied, with median values of 3.1, 11.6 and 8.1 g kg^{-1} in tufa, peat and silty clay, respectively (Fig. 3.6 d). In range of the shallow aquifer, TN and TS were positively correlated with OC ($r = 0.93$, $p < 0.01$ and $r = 0.92$, $p < 0.01$, respectively, Table S3.8) and mainly represented by peat (Fig. 3.6 d).

The TP content generally decreased with depth from the topsoil to the aquifer material, after which it remained stable throughout the aquifer and aquitard layers, except for a peak in the peat at 3.1 m bls (Fig. 3.4 e). In comparison, TP contents in the tufa were significantly lower as compared to the peat and silty clay, with median values of 465, 524 and 692 mg kg^{-1}, respectively. Note that for the shallow aquifer, TP was negatively correlated with IC ($r = -0.51$, $p < 0.05$, Table S3.8). The P_{org} contents in the aquifer sediment varied, with median values of 70, 118 and 161 mg kg^{-1} in tufa, peat and silty clay, respectively (Fig. 3.4 e).

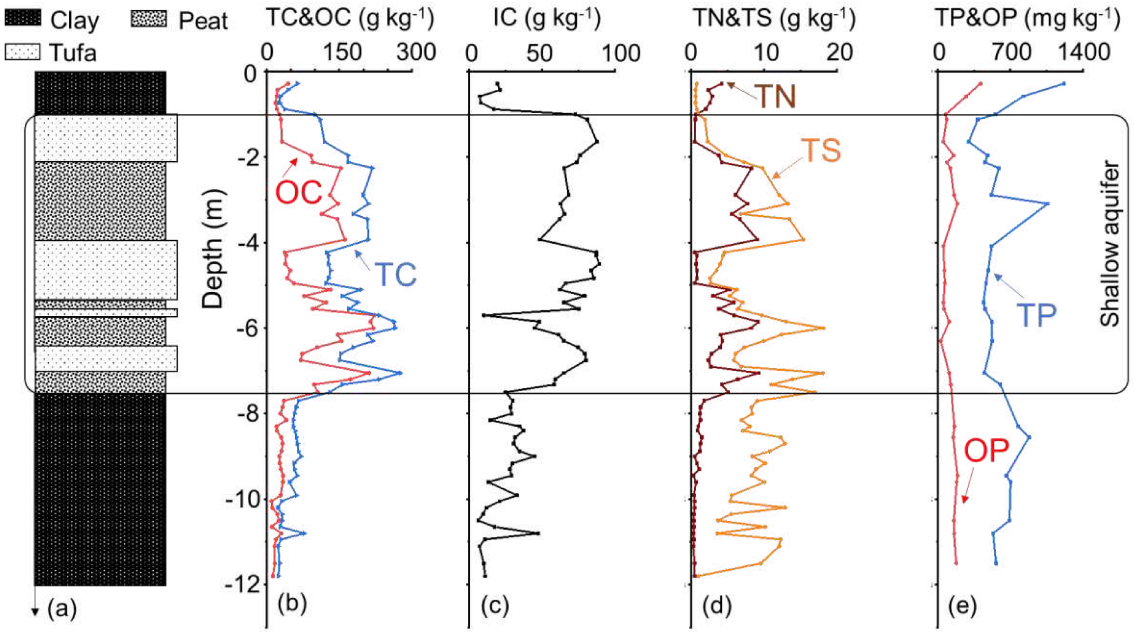

Fig. 3.4 Depth profile of the sediment core of lithologic properties (a), TC&OC (b), IC (c), TN&TS (d) and TP&OP (e). Abbreviations: inorganic carbon (IC), organic carbon (OC), organic phosphorus (OP), total carbon (TC), total nitrogen (TN), total phosphorus (TP), total sulfur (TS).

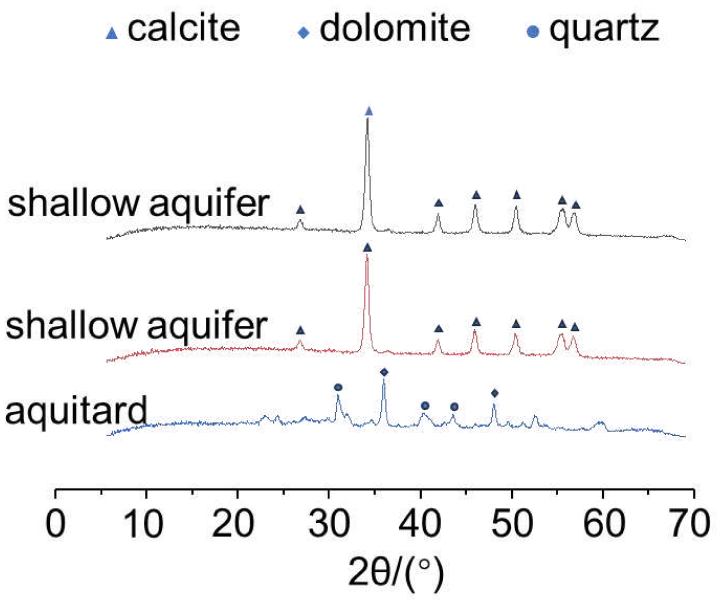

Fig. 3.5. X-ray diffraction (XRD) patterns of the drill core sediments

Composition of P pools: Depth profile of the sediment core of extractable P pools is shown in Fig. 3.6 a. In all three facies, the $NaHCO_3$-extractable P proportion was similar (median: 17%, 17% and 19% of TP for tufa, peat and silty clay, respectively, Fig. 3.6 c). Note that P_{org} accounted for more than half of the $NaHCO_3$-extractable P in the tufa and the peat (median: 60% and 57%, respectively). The proportion of NaOH-extractable P in the peat (median: 16% of TP) significantly exceeded those in the tufa and the silty clay (median: 4% and 6% of TP, respectively), and over half of its was in form of P_{org} (56%, Fig. 3.6 d). For CDB-extractable P, the tufa had higher contents (median: 18%) as compared to peat and silty clay (median: 13% and 9% of TP, respectively, Fig. 3.6 e). The HCl-extractable P was the generally the dominant pool (median: 55%, 44% and 59%, respectively, for tufa, peat and silty clay, Fig. 3.6 f). Finally, the H_2SO_4-extractable P in the peat was significantly higher than in the tufa and silty clay (median: 11 %, 2 % and 5 %, respectively, Fig. 3.6 g).

For the tufa, the median Kd value of surface-adsorbed PO_4 and P_{org} were 88 L kg^{-1} and 3163 L kg^{-1} (Table 3.1). For peat, median Kd value of surface-adsorbed PO_4 and P_{org} were 127 L kg^{-1} and 5677 L kg^{-1} (Table 3.1).

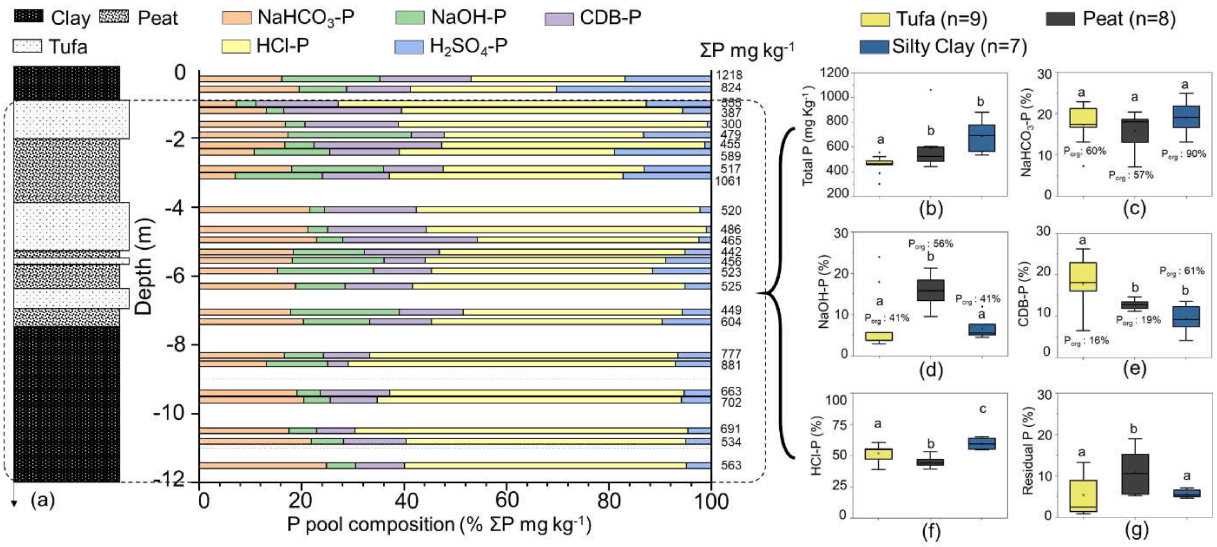

Fig. 3.6 Depth profile of the sediment core of extractable P pools (a), boxplot of extractable P pools: total P (b), $NaHCO_3$-extractable (c), NaOH-extractable (d), CDB-extractable (e), HCl-extractable (f), H_2SO_4-extractable (g). P_{org} in b-g represents the median value of organic P proportion in the corresponding pools. Different letters (a, b, c) above the bars indicate significant differences ($p < 0.05$) among different facies.

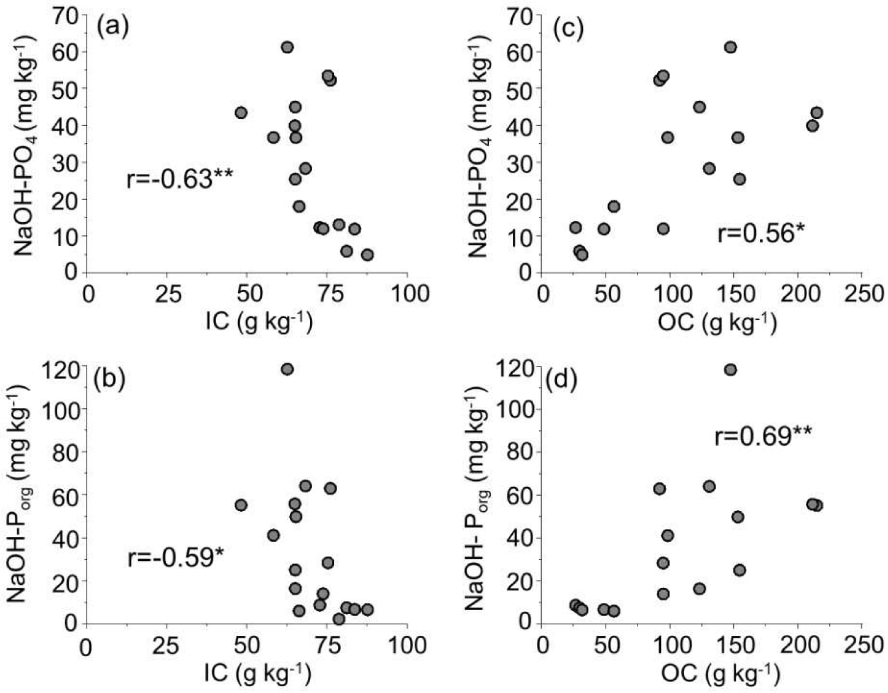

Fig. 3.7 Correlation of aquifer materials parameters: inorganic carbon (IC) – NaOH-PO_4 (a), inorganic carbon (IC) – NaOH-P_{org} (b), organic carbon (OC) – NaOH-PO_4 (c), organic carbon (OC) – NaOH-P_{org} (d). * and ** indicate the level of significance of the spearman correlation with $p < 0.05$ and $p < 0.01$, respectively. Abbreviations: inorganic carbon (IC), organic carbon (OC).

Table 3.1 Sediment core Kd median values for surface-adsorbed PO_4 and P_{org} ($NaHCO_3$ and NaOH extractable) in the study sites. Groundwater well 57a (Table S3.2) was collected at 4.2 m depth, tufa and peat section was collected from 1.0 to 7.3 m depth. Dissolved PO_4 concentration (0.60 mg L^{-1}) and dissolved P_{org} (0.02 mg L^{-1}) in groundwater are used for both tufa (n=9) and peat (n=8) calculation. Significant difference between surface-adsorbed PO_4 and P_{org} is expressed by * ($p < 0.05$) and ** ($p < 0.01$). Significant difference between tufa and peat is expressed by + ($p < 0.05$) and ++ ($p < 0.01$).

Kd values (L kg^{-1})	Tufa (n=9)	Peat (n=8)	p
Surface-adsorbed-PO_4	88	127	+
Surface-adsorbed-P_{org}	3163	5677	
p	**	**	
P in solid phase (mg Kg^{-1})	Tufa (n=9)	Peat (n=8)	p
Surface-adsorbed-PO_4	88	123	
Surface-adsorbed-P_{org}	91	165	
p			

3.4 Discussion

3.4.1 General groundwater properties

The groundwater in the shallow and deep aquifer showed many similarities, including i) circum-neutral pH values and concentrations of major ions (Ca^{2+}, Mg^{2+}, SO_4^{2-} and HCO_3^-); ii) anoxic and reducing redox conditions; and iii) elevated TDP concentrations. Considering the overall groundwater composition, the dominating ions reflected the influence of the local and upstream geology, including: 1) fractured karstified limestone, 2) thin marly clay layers and dolomite, as well as 3) gypsum-rich sedimentary rock (Martin et al., 2020; Stober et al., 2023), which in sum led to the enrichment of Ca^{2+}, SO_4^{2-} and HCO_3^- in groundwater of the Ammer valley. The chemical-physical properties and trace element composition further emphasized the impact of anoxic microbial mineralization of OM on the groundwater, which is also tightly connected to the fate of P as discussed in the following. As our drilling core only covered the shallow aquifer and the underlying clayey aquitard, the following discussions related to the solid phase are focused on the shallow aquifer.

3.4.2 Immobilization of P within the aquifers

Ca-minerals as P sink: According to the sequential extraction outcomes, the largest P pool in the aquifer materials was represented by the HCl-extractable P pool (tufa median: 55% of TP, peat median: 44% of TP). This fraction generally represents Ca- and, potentially, Fe(II) minerals (Li et al., 2022; Neidhardt et al., 2021). In our case, the HCl-extractable pool was nearly exclusively composed of Ca, with only traces of Fe (Table S7). Furthermore, XRD diffractograms (Fig. S2) and high IC contents (Fig. 3.4 c) showed that calcite ($CaCO_3$) represented the principal mineral in the aquifer. This agreed with Martin et al. (2020) and Heidgen et al. (2020), who showed that the shallow aquifer is calcareous and was formed by the precipitation of calcite (tufa facies) in an open mire environment (8400 to 7870 BP). As today's groundwater was found to be consistently supersaturated with regard to calcite (Table S3.3), secondary calcite formation may have also occurred in the present aquifer system. Considering the mineralogical composition of the shallow aquifer and the groundwater chemistry, PO_4 immobilization was linked to the co-precipitation with calcite. For example, Spiteri et al (2007) generally reported for a P plume derived from a leaky septic system that Ca-P mineral precipitation is highly important for the retention of P in the long term. The presence of calcite may also enhance the formation of hydroxyapatite ($Ca_5(PO_4)_3OH$) (Bańkowska-Sobczak, 2021; Flower et al., 2022). For hydroxyapatite, saturation indices indicated partially over- and

partially undersaturation (Table S3.3), i.e. that both precipitation and dissolution might have occurred within the aquifer system. For the sites with its saturation indices in equilibrium, its long-term significance remains open (Flower et al., 2022; Robertson et al., 2019). Also other Ca-minerals may have formed, such as amorphous calcium phosphate, and tricalcium phosphate ($Ca_3(PO_4)_2$) (Geng et al., 2022; Ren et al., 2021). To ultimately identify the Ca-P mineral phases in the aquifer, further mineralogical analysis (e.g., microscopic techniques) are required.

I furthermore observed a substantial proportion of surface-adsorbed PO_4 ($NaHCO_3$- and NaOH-extractable) in our aquifer material (Fig. 3.6 b,c). Here, PO_4 adsorption may have occurred on calcite surfaces via ligand exchange (Bańkowska-Sobczak, 2021; Flower et al., 2022). This is especially relevant for calcareous sediments, where an alkaline environment can enhance the adsorption of PO_4 on calcite (Claveau-Mallet et al., 2020; Ren et al., 2021; Xu et al., 2014). For example, Claveau-Mallet et al (2020) reported that calcareous soil was able to remove P in septic tank effluents, and lower PO_4 concentrations were observed in high-alkalinity wastewater.

As the surface-adsorbed P was generally characterized by a high proportion of P_{org}, calcite, as predominated mineral in the aquifer material may also have acted as an adsorbent for organic P molecules (Sawada et al., 2003; Spohn, 2020). The adsorption of P_{org} molecules on calcite has been generally rarely addressed for aquifers so far, but there is some evidence from sorption experiments that reported that calcite is able to adsorb P_{org} molecules involving ligand exchange, electrostatic interactions, and surface complexation (Sawada et al., 2003; Song et al., 2023).

Despite the important role of calcite and other Ca-minerals as sink for P, the IC contents showed significant negative correlations with TP (Table S3.8), contradicting an expected incorporation of P at a first glance. This suggests that, calcite initially acted as a major PO_4 sink in the past, while currently has already been saturated. In the meantime, for newly released geogenic PO_4 and P_{org}, other constituents of the solid phase gradually became a more important sink, eventually reflected by the high proportion of NaOH-extractable PO_4 and P_{org}. This is further supported by a negatively correlated of NaOH-extractable PO_4 and P_{org} with IC ($r = -0.63$, $p < 0.01$; $r = -0.59$, $p < 0.05$, respectively, Fig. 3.7 b,d). Thus, while Ca-minerals represented an important potential sink for PO_4 within the shallow aquifer, further sinks must be present, especially in regard to P_{org}.

Further mineral phases: A characteristic sorbent for PO_4 and P_{org} in aquifer systems are Fe(III)- and Fe(II)-minerals such as ferrihydrite, goethite, hematite, and siderite (Y. Li

et al., 2023; M. Liu et al., 2023; Neidhardt et al., 2018). While groundwater from two aquifers was mainly supersaturated with regard to more stable Fe(III)- and Fe(II/III)-oxides like goethite, hematite and magnetite (Table S3.3), no Fe-minerals were detectable by XRD (detection limit ~1 wt.%) in the aquifer material (Fig. 3.5). More importantly, the amount of CDB-extractable Fe, which representing Fe(III)-(hydr)oxides, was generally very low (median value of only 34 mg kg^{-1}, Table S3.7). Similarly, HCl-extractable Fe, which representing Fe(II)-carbonates such as siderite, was very low. I therefore concluded that Fe(III)/Fe(II)-oxides did not represent the principal adsorbents for PO_4 and P_{org} in our study system either.

Organic matter as sorbent: Pronounced contents of OC occurred in the shallow aquifer (Fig. 3.4 b), revealing that OM represented the second major compound besides calcite in the sediments. The OM in the tufa was mainly deposited as layers of peat that have formed 8400 to 7870 BP under warm and humid climate (Heidgen et al., 2020; Klingler et al., 2020). In the shallow aquifer, a high proportion of surface-adsorbed P (both $NaHCO_3$- and NaOH-extractable PO_4 and P_{org}) was found in the tufa and the peat samples (Fig.4c,d). Here, the strongly adsorbed proportion (NaOH-extractable) of PO_4 and P_{org} was significantly higher in the peat as compared to the tufa samples. Moreover, NaOH-PO_4 and -P_{org} exhibited significant positive correlations with total OC, TC and TN contents (Fig. 3.7 a,c & Table S3.8). I therefore concluded that OM represented another principal sorbent for P. This agreed with previous observations for surface waters and soils (Spohn, 2020; Wang et al., 2007; Zhang et al., 2022). Additionally, Wang et al. (2007) studied DOC, PO_4 and P_{org} sorption on lake sediment, showing that the order of sorption was as follows: P_{org} > PO_4 > DOC. The Kd values that have been calculated for our aquifer sediments were in line with these observations, showing significantly higher median Kd values for surface-adsorbed P_{org} than PO_4 (Table 3.1). Thus, the absence of dissolved in groundwater suggested a preferential immobilization over PO_4. Previous studies highlighted that NaOH-extractable P_{org} is more accessible to microbial cycling, allowing a subsequent mineralization and release of PO_4 as a by-product (Richardson and Simpson, 2011; Siegenthaler et al., 2022). Potential sources and mobilization mechanisms for P are discussed in the following subchapter. In sum, our results highlight the role of OM as sorbent for PO_4 and especially P_{org}, which calls for further investigations.

3.4.3 Mobilization of P

Organic matter mineralization: To draw conclusions regarding the potential P sources and mobilization processes, the discussion begins with the groundwater data. Here, the

TDP in groundwater (as mainly represented by PO_4) was positively correlated with NH_4^+ and DOC concentrations in both aquifers. Moreover, elevated TDP concentrations were observed mainly under reducing redox conditions (Fig. 3.3 a-c). This suggested that TDP concentrations were mainly influenced by microbial metabolic activities, as TDP, DOC, and NH_4^+ can all be released to groundwater through the *in-situ* mineralization of OM under anaerobic and reducing conditions (Li et al., 2022; Sondergaard et al., 2001; Tao et al., 2020; Yu et al., 2018). High SO_4^{2-} concentrations occurred in groundwater of both aquifers, which are considered to be regularly replenished through the dissolution of gypsum deposits in the adjacent geological units (Martin et al., 2020). For microorganisms in the aquifers, the dissolved SO_4^{2-} represents an important electron acceptor for the degradation of OM in absence of other TEA's (O_2, NO_3^-, Mn(VI), Fe(III)) (Tao et al., 2020). As the aquifers in the Ammer valley are characterized by a low hydraulic transmissivity with a geometric mean on the order of 1.8×10^{-5} m^2/s (Martin et al., 2020), the resulting low groundwater flow velocities allow for a subsequent accumulation of TDP, NH_4^+ and DOC in the aqueous phase. This especially relevant for the shallow aquifer, which is rich in peat layers (Martin et al., 2020), resulting in generally higher DOC concentrations in groundwater of the shallow aquifer.

Thus, DOC, NH_4^+, and PO_4 were released to the groundwater as a by-product of microbial OM mineralization (Jiang et al., 2018; Xu et al., 2022). Another important by-product is HCO_3^- (Chen et al., 2023; J. Xu et al., 2018; Zhang et al., 2023), whose concentrations were positively correlated with NH_4^+ and DOC in both aquifers (Table S3.5). Consequently, the cumulative impact of microbial OM mineralization could be witnessed by the groundwater properties (i.e. low Eh, elevated NH_4^+, HCO_3^-, DOC and PO_4 concentrations). This connection between elevated TDP, NH_4^+, and DOC concentrations and reducing redox conditions has also been observed in other floodplain aquifers (Correa et al., 2020; Z. Liu et al., 2023; Zhang et al., 2023), suggesting that OM mineralization is crucial for P mobilization, especially under reducing redox conditions.

The important role of OM as source of PO_4 in groundwater was also reflected in the composition of the aquifer sediments. As previously highlighted, the OM in the aquifer sediments was also associated with the adsorption of PO_4 and P_{org}. As OM can be subsequently mineralized, PO_4 and P_{org} can be (re-)released into ambient groundwater (M. Liu et al., 2023; Z. Liu et al., 2023; Tao et al., 2020). I therefore considered the OM present in the shallow aquifer to not only represent a sink for PO_4 and P_{org}, but also as a potential source when it is subject to microbial mineralization.

Considering the deep aquifer, the possibility that the DOC in the groundwater was externally derived could not be excluded. According to previous findings by Martin et al (2020), the deeper aquifers' solid phase is composed of gravel, which is dominated by well-rounded limestone clasts alongside a few sandstone and mudstone clasts, displaying no signs of vegetation (i.e., peat) and therefore OM was not likely to present. As such, potential P mobilization processes in the deep aquifer remained open, calling for further investigation.

Ca-mineral mineral weathering: As previously highlighted, the main P pool within the solid phase of our system was represented by Ca-minerals such as calcite. However, groundwater in the shallow aquifer was generally supersaturated with regard to calcite. Therefore, P derived from the dissolution of calcite was not likely the main source for elevated TDP in groundwater. Other Ca-P minerals like hydroxyapatite have been shown to represent important potential sources for dissolved PO_4 in groundwater elsewhere (Bingham et al., 2020). Yet, groundwater in our study area was largely supersaturated with regard to hydroxyapatite, especially when TDP concentrations were increased (Table S3.3). Considering the circum-neutral pH values and saturation indices of Ca-P minerals in both aquifers, the dissolution of Ca-minerals rather unlikely in our system.

Reductive dissolution of Fe(III)-hydroxides: Similarly to other oxyanions such as arsenate, PO_4 can be released during the reductive dissolution of Fe(III)-hydroxides under strongly reducing redox conditions (Neidhardt et al., 2021; Zhang et al., 2023). In our study area, the elevated TDP concentrations were observed mainly under reducing conditions, but there was only little dissolved Fe present in the groundwater (Table S3.2). Moreover, only low concentrations of Fe in CDB-extraction were found in the shallow aquifer (Table S3.7). Thus, Fe(III)-hydroxides was not regarded as a significant source of TDP.

External P sources: High concentrations of TDP could have also been related to external P inputs in addition, or instead of an *in-situ* P release. This could be lateral and/or vertical inputs, generally reflecting transport of TDP within the aquifer (Kazmierczak et al., 2020; Lewandowski et al., 2015; Mellander et al., 2013). For the study area, I excluded the possibility of lateral inputs based on the spatial distribution of TDP in both aquifers; high concentrations occurred in form of isolated hotspots toward the centre of floodplain (Fig. 3.2). If lateral transport of TDP from upstream directions would occur, different patterns (e.g., plumes) would be observable in groundwater.

Furthermore, lysimeter data at depths of 50 and 100 cm bls showed that neither PO_4 nor TDP were visible in porewater (Table S3.6), excluding the possibility of a vertical input of fertilizer-derived P from the surface. Given that the deep aquifer, which was found separated from the shallow aquifer by an impermeable clay-rich layer (Klingler et al., 2020), also showed high TDP concentrations, the possibility of vertical P inputs from shallow aquifer above was excluded. Thus, I consider the dissolved PO_4 in groundwater as derived *in-situ* and as such of a geogenic origin.

Mobilization versus immobilization: Considering the widespread occurrence of elevated PO_4 concentrations in groundwater of the Ammer valley, mobilization mechanisms obviously outpace immobilization reactions. Our findings agree with Liao et al. (2019), Robertson et al. (2019) and Spiteri et al. (2007), who observed high TDP concentrations in anthropogenically contaminated calcareous aquifers. In this study, I argue that PO_4 was not fully immobilized mainly because: (i) co-precipitation with Ca-minerals is a kinetically slow process (Flower et al., 2022; Robertson et al., 2019); (ii) the microbial mineralization of OM including surface-adsorbed P_{org} is generally a fast process especially when degradable OM and electron acceptors (here: SO_4^{2-}) are available (Zheng et al., 2024); (iii) immobilization is additionally reduced through competitive adsorption (e.g., preferential adsorption of P_{org} over PO_4) (Guppy et al., 2005; Z. Liu et al., 2023). In sum, our results suggest that neutral pH values, reducing conditions, and an ample supply with OM as well as electron acceptors may foster the enrichement of PO_4 in groundwater in non-contaminated calcareous and OM-rich systems.

3.5 Conclusion

In line with the initial expectations, I attributed elevated TDP concentrations in form of PO_4 in groundwater of the Ammer valley to the *in-situ* mineralization of OM, which was reflected by the composition of the groundwater and the solid phase. Moreover, I observed a competition between mobilization and immobilization of PO_4 and P_{org} in the calcareous and organic matter-rich aquifer system. Here, Ca-minerals and OM both represent the main P sinks, as reflected by a pronounced proportion of surface-adsorbed PO_4 and P_{org} in addition to PO_4 that was structurally incorporated into Ca-minerals. The surface-adsorbed P is further determined as the most likely active mechanism immobilizing PO_4 and P_{org}. However, the immobilization of PO_4 is slower as compared to its mobilization, which I attribute to slow kinetics of Ca-minerals precipitation reactions and a competition for sorption sites (including preferential adsorption of P_{org} over PO_4).

The mobilization of P via microbial mineralization of OM represents a comparatively fast process, and degradable OM and electron acceptors are both abundant in the shallow aquifer of the Ammer floodplain. As a result, high concentrations of PO_4 have subsequently accumulated in groundwater over time.

Our observations call for further research regarding the (im)mobilization and dynamics related to P_{org} in floodplain aquifers. I further highlight that anoxic, calcareous groundwater systems are characterized by limited or absent self-purification capabilities, rendering them vulnerable to anthropogenic contamination with DOC and PO_4. While this has been studied locally for contamination plumes of leaky septic tanks, our results verify this for pristine calcareous aquifer systems. I therefore emphasize the urgent need to enhance protective measures and intensify monitoring of such systems to prevent long-term environmental damage.

4 Combining of phosphorus pools analysis with phosphorus-bound stable oxygen isotope ratios

4.1 Introduction

Chemical sequential extraction schemes help assess the forms of phosphorus (P) in soil and sediments. However, in order to further understand the dynamics of P between individual P pools, stable oxygen isotope composition of PO_4 ($\delta^{18}O_{PO4}$) technique is required. By combining $\delta^{18}O_{PO4}$ and P pools analysis, microbial cycling as well as abiotic processes that control in concert the fate of PO_4 in groundwater and other environments could be monitored (Davies et al., 2014; Helfenstein et al., 2018; Joshi et al., 2016; Yuan et al., 2019). The analysis of $\delta^{18}O_{PO4}$ in operationally defined P pools emerged as a novel and promising tool. Many studies have successfully investigated the $\delta^{18}O_{PO4}$ values in different P pools within soil and sediments, and discussed possible P sources and pathways in corresponding cases. For instance, the $\delta^{18}O_{PO4}$ values of Al-bound P (NaOH extractable) were found to be generally higher than it in Fe-bound P (CDB extractable) in a study of lake sediments, which was interpreted as indicating a potential terrestrial source (Yuan et al., 2019). The $\delta^{18}O_{PO4}$ values of $NaHCO_3$- and NaOH-P were found to be heavier than other pools in a study of soil samples, and the heavier isotopic composition of the NaOH-P was interpreted due to the transformation of other P pools that have relatively heavier $\delta^{18}O_P$ values of H_2O- or $NaHCO_3$-P (Joshi et al., 2016). The $\delta^{18}O_{PO4}$ values of NaOH-P were found to be higher than $NaHCO_3$- and HCl-P pool in a study of lake sediments, which was attributed to divergent equilibrium conditions (soil temperature and $\delta^{18}O_{H2O}$), different P sources and biological processes (Jin et al., 2023). A study on bay sediments using extraction scheme $MgCl_2$-CDB-actate buffer-HCl found that the Fe-bound P (CDB extractable) were isotopically heavier than other P pools and equilibrium isotopic composition, therefore it was interpreted as the original isotopic compositions were largely unaltered and indicating to other specific P sources (Joshi et al., 2015).

However, it has not yet been reported whether the $\delta^{18}O_{PO4}$ values obtained from the combination of sequential extraction and phosphorus-bound stable oxygen isotope technique are influenced by the specific extraction step. The primary concern is whether the chemical environments created by the extractants influence the isotopic composition of PO_4 to adopt different strategies of binding and release. At the same time, the influences come not only from the chemical extraction step but also from the adsorption and coprecipitation processes. It has been reported that the $\delta^{18}O_{PO4}$ value observed

during immobilization on the surface of ferrihydrite underwent variation, and it is attributed to fractionation associated with the sorption phase rather than the breaking of P-O bonds during the sorption and desorption processes (Jaisi et al., 2010). In groundwater systems, there can be frequent exchange between solid and aqueous phases (immobilization of PO_4 via sorption and precipitation of secondary minerals), the presence of distinct P sources (primary or secondary P-hosting minerals such as apatite or P associated Fe(III)-(hydr)oxides) (Liu et al., 2023; Neidhardt et al., 2021). Therefore, there is a greater need to assess the impact of combining the two analytic methods before the scientific research goes into greater depth. Given the adsorption of PO_4 on the surface not only depends on its contents and protonation states, but also depends on the surface properties of the adsorbents (Németh et al., 1998; Zhou et al., 2005). Therefore, it is necessary to investigate the methodological approach for reliably determining and interpreting $\delta^{18}O_{PO4}$ values from P pools in different synthetic minerals that represent typical aquifer materials in groundwater systems. The overarching questions were: (i) Are the $\delta^{18}O_{PO4}$ values in each P pool of a given single mineral related to the extraction scheme under abiotic condition; (ii) How is the variation of $\delta^{18}O_{PO4}$ values in P pools when these minerals are mixed?

4.2 Materials and Methods

4.2.1 P loading solutions

The ratio of stable isotopes ^{18}O : ^{16}O with in a sample is expressed as $\delta^{18}O$, relative to Vienna Standard Mean Ocean Water (VSMOW), defined as 0 ‰VSMOW (equation II) (Davies et al., 2014).

$$\delta^{18}O_{sample} = 1000 * \left[\frac{(\frac{^{18}O}{^{16}O})_{sample}}{(\frac{^{18}O}{^{16}O})_{standard}} - 1 \right] \text{‰VSMOW} \qquad (II)$$

KH_2PO_4 solutions were isotopically labeled at four different levels relative to the VSMOW value prior to loading experiments. In short, the water enriched in ^{18}O (> 98%, Rotem Industries Ltd.) was mixed with PCl_5 (> 95%, Merck) at 80 °C for preparing H_3PO_4 solution, NaOH and ultrapure water was added to neutralize pH and generate stock solution. 1ml stock solution (around 35 million ‰VSMOW) were used to mix with preliminary prepared KH_2PO_4 solution (10 g L^{-1} PO_4-P) at ratio of 1:900, 1:1200, 1:1500, 1:2000 (v/v), respectively, aiming to spike the solutions ranging from +100 to +250 ‰

VSMOW. The final solutions were still at concentration of 10 g L^{-1} PO_4-P but with different isotopic values. The isotopic labeling scheme of all mineral samples can be found in Table 4.1.

4.2.2 Loading samples and mixtures

Outside and inside loading experiments were described in Chapter 2. In addition, three groups of mixtures were prepared. Same as individual sample experiment, prior to the extraction steps, 0.1 g of each synthetic mineral sample was mixed with 0.8 g acid-washed quartz sand (VWR). They were mixed by i) Fe1(O)+Fe1(I); ii) Fe3(O)+Fe3(I); iii) Fe1(O)+Fe1(I)+Fe4(I)+Ca1(I). In addition, natural aquifer samples were also tested for the purpose of investigating $\delta^{18}O_{PO4}$ values in P pools. Further details of natural samples can be found in Chapter 2.

4.2.3 Purification protocol and measurement of $\delta^{18}O_{PO4}$ values of specific P pools

As outlined in Chapter 2, the extraction solution by Scheme A was employed for this research. Stepwise purification of P in different extraction steps and final precipitation of silver phosphate is shown in Fig. 4.1. This procedure applies to P pools of synthetic mineral samples and natural samples with the latest purification protocol (Adu-Gyamf and Pfahler, 2022). In short, the extractants are first purified in four consecutive steps (A1-A4) followed by an ultimate precipitation step (A5): A1: APM precipitation and dissolution, A2: MAP precipitation and dissolution, A3: Cation removal by resin slurry, A4: AgCl removal, A5: Ag_3PO_4 precipitation. For the acetate buffer and HCl extraction solutions, I applied procedures A1-A5. Due to the presence of acidic reagents in the step A1, all alkaline extraction solutions ($NaHCO_3$, NaOH, CDB) underwent the Magnesium-induced coprecipitation (MagIC) to enriched as particles (Karl and Tien, 1992). As the MagIC method was ineffective for $NaHCO_3$ and CDB extraction solutions, an additional A2 step was incorporated prior to the A1-A5 procedures, as suggested by Adu-Gyamf and Pfahler (2022). The PO_4 enriched precipitates were dissolved to smaller volume solution before applying procedures A1-A5. The samples were then ultimately prepared as Ag_3PO_4 and packed into silver capsules (IVA-analysentechnik). Liquid samples were pipetted into silver capsules and sealed to ensure the mass did not change, which included IAEA-607, IAEA-608 and lab water. The measurement was carried out by thermochemical conversion using a PyroCube and isoprime visION Mass Spectrometer

(TC/EA-IRMS, Elementar). The final $\delta^{18}O$ values were expressed relative to VSMOW value. The Fractionation factor (α) was calculated by equation (III):

$$\alpha = (\delta_p+1000) / (\delta_s+1000) \qquad (III)$$

where *p* is the product ($\delta^{18}O_{PO4}$ value in extraction solution), *s* is the educt ($\delta^{18}O_{PO4}$ value initial labeling solution). In order to calculate the α results of mixtures combining individual minerals, a theoretical $\delta^{18}O_{PO4}$ value was first calculated as the value of the total PO_4 in the sample, it was calculated by the $\delta^{18}O_{PO4}$ value in corresponding individual mineral's initial solutions and the absolute mass of PO_4 obtained from the extraction data by equation (IV):

$$\delta_3 * M_3 = \delta_1 * M_1 + \delta_2 * M_2 \qquad (IV)$$

δ_3 represents the $\delta^{18}O_{PO4}$ value in total P, ‰ VSMOW. M_3 represents the total mass of P, mg. δ_1 *and* δ_2 represent the $\delta^{18}O_{PO4}$ value in P pools, ‰ VSMOW. M_1 and M_2 represents the mass of P in corresponding P pools, mg. The intracellular metabolism of P results in a temperature-dependent thermodynamic equilibrium fractionation of the P-O bonds with ambient H_2O (Blake et al., 1998). The resulting equilibrium value of $\delta^{18}O_{PO4}$ can be calculated for known temperatures and $\delta^{18}O_{water}$ values of ambient (ground)water according to the equation published by Longinelli and Nuti (1973), later revised by Chang and Blake (2015) (equation V):

$$\delta^{18}O_{PO4} = (\delta^{18}O_{H2O} + 10^3)\, e^{\frac{\left[\left(14.43*\frac{10^3}{T}\right)-26.54\right]}{10^3}} - 10^3 \qquad (V)$$

4.2.4 Quality control

Quality controls of $\delta^{18}O_{PO4}$ analysis included: (i) IRMS measurement of original KH_2PO_4 powder and the Ag_3PO_4 derived from KH_2PO_4 by protocol to check potential fractionation; (ii) tests for potential oxygen exchange between PO_4-O of sample and H_2O-O of the respective solutions. This was done by measuring Ag_3PO_4 obtained from standard protocol and a parallel protocol in which all solutions were spiked with $\delta^{18}O_{H2O}$ (+50.0‰ VSMOW); (iii) IRMS measurement of KH_2PO_4 solutions during the MagIC step; (vi) a wider range of reference material (vs. VSMOW) for calibration and quality control, including USGS80 ($\delta^{18}O$ = ~ +13.1 ‰), USGS81 ($\delta^{18}O$ = ~ +35.4 ‰), IAEA-601 ($\delta^{18}O$ = +23.14 ‰), IAEA-607 ($\delta^{18}O$ = +99.02 ‰) and IAEA-608 ($\delta^{18}O$ = +736.4 ‰); (v) oxygen-yield evaluation of Ag_3PO_4 samples by comparing with CO peak area; (vi) conduction of triplicates and their standard error.

4.2.5 Statistical analysis

All geochemical results were analyzed with Microsoft Excel 2019 and SPSS statistical software (v. 25). Comparison of surface-adsorbed P with total extracted P and variation of fractionation factors were tested by t-tests. Significant differences among $\delta^{18}O_{PO4}$ values in P pools were tested by ANOVA with a post-hoc Bonferroni test. Note that the $\delta^{18}O_{PO4}$ values of the initial solution were measured only once rendering a statistical comparison with the $\delta^{18}O_{PO4}$ values of the extraction steps impossible. The confidence interval for all tests was 95% and p-values ≤ 0.05 were considered statistically significant.

Table 4.1 Overview of loading and labeling approaches. Two different labeling approaches, namely outside loading and inside loading, will allow to distinguish between surface-adsorbed and (co-) precipitated PO_4. Labeling level + stand for 1ml stock solution (around 35 million ‰VSMOW) mixed with preliminary prepared KH_2PO_4 solution (10 g L^{-1} PO_4-P) at ratio (v/v) of 1:900 (++++), 1:1200 (+++), 1:1500 (++), 1:2000 (+), respectively. All outside loadings took place at 20°C.

Labeling approach	Details regarding included mineral phases	labeling level
labeling of surface sorbed PO_4 (outside loading)	*metal-(oxyhydr)oxides:*	
	Fe1(O): ferrihydrite (Schwertmann and Cornell 2008);	+
	Fe2(O): hematite (Schwertmann and Cornell 2008);	++
	Mn1(O): pyrolusite (Alfa Aesar)	+
	Fe(II)-minerals:	
	Fe3(O): siderite (Hallbeck et al. 1993)	+
	Clay minerals:	
	Cy1(O): montmorillonite (Sigma Aldrich)	+
labeling PO_4 via (co-) precipitation (inside loading)	*metal-(oxyhydr)oxides:*	
	Fe1(I): ferrihydrite (Schwertmann and Cornell 2008)	++++
	Fe2(I): hematite (Schwertmann and Cornell 2008)	++++
	Fe(II)-minerals:	
	Fe3(I): siderite (Hallbeck et al. 1993);	++++
	Fe4(I): vivianite (Eynard et al. 1992)	+++
	Ca-P mineral phases:	
	Ca1(I): hydroxyapatite (Alobeedallah et al. 2011)	++

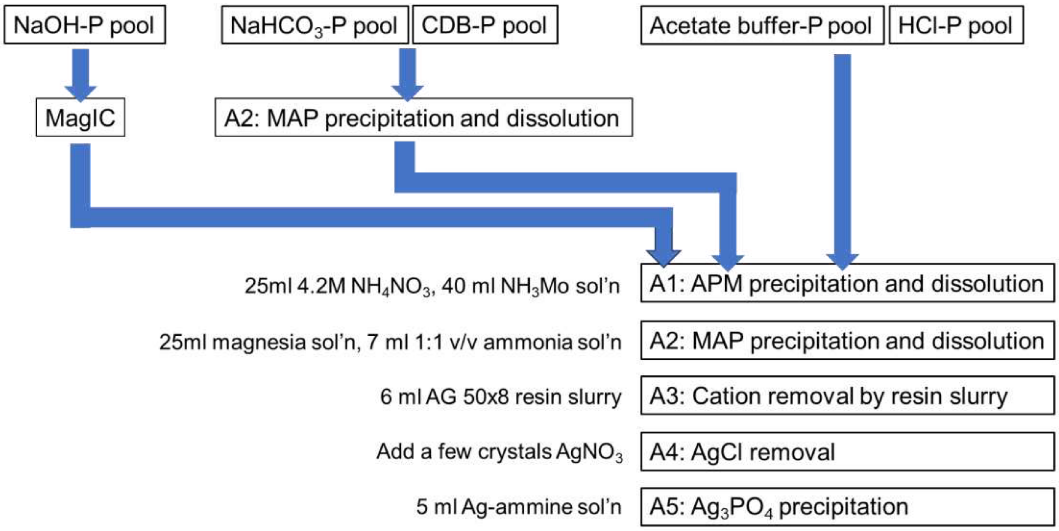

Fig. 4.1 Stepwise purification of P in different extraction steps and final precipitation of silver phosphate.

4.3 Results

4.3.1 Quality controls of $\delta^{18}O_{PO4}$ analysis

The in-house standard KH_2PO_4 yield +12.14 ± 0.16 ‰ (n=3) after it was converted to Ag_3PO_4, was equivalent to its original isotopic value +12.12 ± 0.02 ‰ (n=3, Table 4.2). This suggests that the purification protocol used in the experiment did not result in isotopic fractionation in samples. The KH_2PO_4 yielded +16.70 ± 0.05 ‰ (n=3) when all solutions involved in the experiment got spiked (spiked to isotopic $\delta^{18}O_{H2O}$ value of around +50‰), implying that either there was a weak impact from high range of experimental reagents or there was contamination from labeled $\delta^{18}O_{PO4}$ samples by the same batch operation (Table 4.2). The samples with preliminary MagIC preparation yielded +12.13 ± 0.72 ‰ (n=3), was same as original isotopic value, therefore, no fractionation occurred during this process (Table 4.2). The reference materials USGS80 ($\delta^{18}O$ = 13.38 ± 0.14, n=17), USGS81 ($\delta^{18}O$ = 34.78 ± 0.63, n=13) and IAEA-601 ($\delta^{18}O$ = 23.37 ± 0.45, n=26) showed good stability of the measurement in the sample weight range of 0.2 – 0.6 mg (Fig. S4.1). Liquid reference material IAEA-607 ($\delta^{18}O$ = 105.28 ± 3.01, n=3) and IAEA-608 ($\delta^{18}O$ = 798.69 ± 14.55, n=3) showed relatively good stability of the measurement in the sample weight range of 0.5 – 2.5 mg. Sample weight of USGS80 showed a linear pattern with CO peak area, and the closer the CO peak area and sample weight distribution are to the USUG80 line, the higher the purity of Ag_3PO_4 in analytes. Not all analytes were close distributed to USGU80 line, only the result of CDB-P in Tufa2 close to USGS80 line for natural samples, suggesting that Ag_3PO_4 in these samples were less pure and may have been interfered with impurities or lost some mass through operation.

Table 4.2 Overview of $\delta^{18}O_{PO4}$ values (‰ VSMOW) obtained for artificial sample (prepared from an in-house KH_2PO_4 standard dissolved in laboratory water) for quality control. i.e. KH_2PO_4 as original powder, KH_2PO_4 in standard Ag_3PO_4 protocol, KH_2PO_4 in standard Ag_3PO_4 protocol with all process solutions spiked (spiked to isotopic $\delta^{18}O_{H2O}$ value of around +50‰) and KH_2PO_4 in standard Ag_3PO_4 protocol with preliminary MagIC preparation.

Samples for fractionation quality control	$\delta^{18}O_{PO4}$ values (‰ VSMOW)	amount
KH_2PO_4 as original powder	+12.12 ± 0.02	n=3
Ag_3PO_4 (KH_2PO_4 processed protocol)	+12.14 ± 0.16	n=3
Ag_3PO_4 (KH_2PO_4 processed protocol with all solution spiked, $\delta^{18}O_{H2O}$ value of around +50‰)	+16.70 ± 0.05	n=3
Ag_3PO_4 (KH_2PO_4 processed with MagIC before protocol)	+12.13 ± 0.72	n=3
Lab water involved in experiments	-7.00	n=1

4.3.2 $\delta^{18}O_{PO4}$ results of operationally defined pools

Due to low mass of P (< 0.2 mg) in specific extraction solutions for some samples, the measurement of $\delta^{18}O_{PO4}$ value was only partially successful, the results are shown in Table 4.3, and these data were further converted to α in Fig. 4.2, showing the isotopic change with its corresponding labeling solution.

For $\delta^{18}O_{PO4}$ values in $NaHCO_3$-extractable P pool, Fe3(O) had α with mean value = 0.999, same to the original P source isotopic background, i.e. +119 ‰. Ca1 had α = 0.919, i.e. the PO_4 in this P pool was isotopically lighter O signal than original P source isotopic background. The α of Fe3(O) and Fe3(O)+Fe3(I) were significantly same (mean value: 0.999 and 1.001, $p < 0.05$, Fig. 4.2 a). For $\delta^{18}O_{PO4}$ signal in NaOH-extractable P pool, Fe1(O) had α with mean value = 0.991, which was significantly isotopically lighter than the initial labeling solution ($p < 0.05$). Fe3(O) had a value that was not significantly different from 1.00. Fe1(O)+Fe1(I) had α with mean value = 0.966, Fe3(O)+Fe3(I) had α with mean value = 0.978, indicating there were varying degrees of fractionation that result in isotopically lighter value than its own individual outside loading case. Fe1(O)+Fe1(I)+Fe4+Ca1 had α with mean value = 0.997, note that only Fe1(O) should have contributed to this P pool. For $\delta^{18}O_{PO4}$ value in CDB-extractable P pool, the α of Fe1(O), Fe3(O) and Ca1(I) were found to be 0.924, 0.996 and 0.919, respectively, which were unexpected extracts by the extraction scheme. The α of Fe1(I) and Fe1(O)+Fe1(I)+Fe4+Ca1 were found to be 0.950 and 0.925 respectively. For $\delta^{18}O_{PO4}$ values in acetate buffer extractable-P pool was only observed in Ca1, with α= 0.964. For $\delta^{18}O_{PO4}$ value in HCl extractable-P pool, Ca1 had α with mean value = 0.935, showing greater fractionation occurred than that in acetate buffer. Fe1(O)+Fe1(I)+Fe4+Ca1 had α with mean value = 0.978. Note that in this mixture, the $\delta^{18}O_{PO4}$ values in HCl-P was assumed to be provided by Ca1, whose original P source value was +151‰. The results of natural aquifer materials are shown in Table 4.6, with majority P pools ranging from +6.34 to +12.29‰.

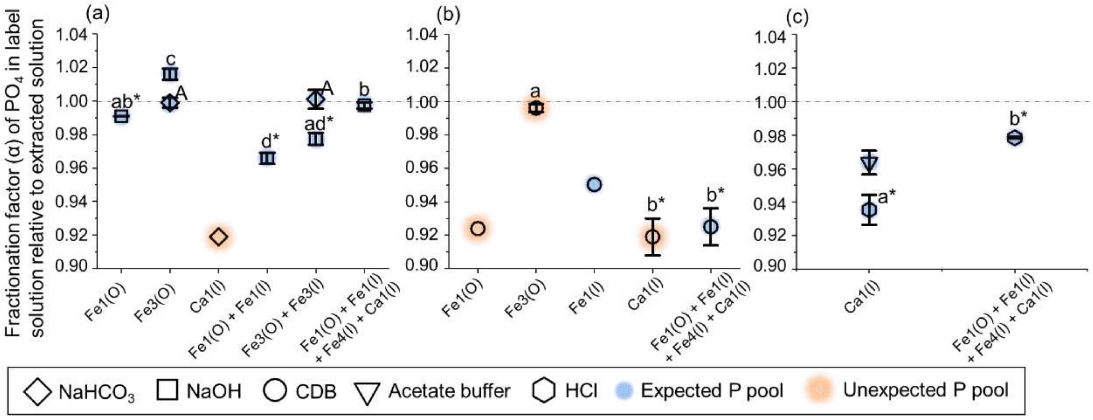

Fig. 4.2 Fractionation factors (α) in sequential extraction steps. α was calculated by: $\alpha = (\delta_p+1000) / (\delta_s+1000)$ where p is the product ($\delta^{18}O_{PO4}$ value in extraction solution), s is the educt ($\delta^{18}O_{PO4}$ value initial labeling solution). α = 1.00 represents there was no fractionation compared with initial solution in outside or inside loading experiments. α > 1.00 represents the $\delta^{18}O_{PO4}$ value obtained from the extraction step was isotopically heavier than that in initial labeling solution. α < 1.00 represents the $\delta^{18}O_{PO4}$ value obtained from the extraction step was isotopically lighter than that in initial labeling solution. The error bar is employed in case of triplicates. Significant differences between α and value 1.00 are displayed as * ($p < 0.05$). Letters indicate significant differences in α value among different samples within the same extraction step ($p < 0.05$). If two extraction steps occur within a subfigure, separate upper- and lower-case letters are used. Abbreviations: Fe1(O) and Fe1(I): ferrihydrite, Fe3(O) and Fe3(I): magnetite with goethite, Fe4(I): decayed vivianite (ferrihydrite), Ca1(I): hydroxyapatite.

Table 4.3 Overview of $\delta^{18}O_{PO4}$ results (‰ VSMOW) of the loading solutions and P pools of mineral samples. For the inside loading samples, they were synthesized and followed by the removal of surface-adsorbed PO_4 by repeated washing with 0.1M NaOH. $^{(CL)}$ represent a calculated value rather than measured value. Different letters on the right of the results indicate significant differences of P pools within same sample ($p < 0.05$). The precipitation did not work out for all extraction steps (n.d.) and for some there were less than three replicates (no standard error (SE) provided). In the latter case, no statistical test was possible and letters were omitted. Fe1: ferrihydrite, Fe2: hematite, Fe3: magnetite with goethite, Fe4: decayed vivianite (ferrihydrite), Ca1: hydroxyapatite. The superscript letters indicate significant differences in $\delta^{18}O_{PO4}$ value among the extraction steps within the same sample ($p < 0.05$).

synthesized samples	$\delta^{18}O_{PO4}$ value in initial labeling solution	$\delta^{18}O_{PO4}$ value in preliminary wash solution by NaOH	$\delta^{18}O_{PO4}$ value in $NaHCO_3$-P pool ‰VSMOW		$\delta^{18}O_{PO4}$ value in NaOH-P pool ‰VSMOW		$\delta^{18}O_{PO4}$ value in CDB-P pool ‰VSMOW		$\delta^{18}O_{PO4}$ value in Acetate buffer-P pool ‰VSMOW		$\delta^{18}O_{PO4}$ value in HCl-P pool ‰VSMOW	
	‰VSMOW	‰VSMOW	Mean	SE	Mean	SE	Mean	SE	Mean	SE	Mean	SE
Fe1(O)	+119		n.d.		+109	0.23	+34					
Fe2(O)	+151		n.d.		n.d.		n.d.					
Fe3(O)	+119		+118 ^{a}	3.28	+137 ^{b}	3.72	+115 ^{a}	2.71				
Mn1(O)	+119											
Cy1(O)	+119											
Fe1(I)	+260	+301					+197					
Fe2(I)	+260	+289					n.d.					
Fe3(I)	+260	+303					n.d.					
Fe4(I)	+193	+243					n.d.					
Ca1(I)	+151		+58				+58 ^{a}	12.53	+109 ^{a}	7.98	+77 ^{a}	9.99
Fe1(O)+Fe1(I)	+129 $^{(CL)}$		n.d.		+91	3.82						
Fe3(O)+Fe3(I)	+122 $^{(CL)}$		+123 ^{a}	6.26	+97 ^{b}	4.01						
Fe1(O)+Fe1(I)+Fe4(I)+Ca1(I)	+142 $^{(CL)}$		n.d.		+140 ^{a}	2.21	+57 ^{b}	12.59	n.d.		+118 ^{a}	0.72

Table 4.4 Calculated $\delta^{18}O_{PO4}$ value (‰ VSMOW) of mineral phase before chemical extraction steps. The isotopic value of each P pools and extracted mass of P at corresponding extraction step is showing by the mean value. Uncon: Other P pools that were not included in the calculation/total amount of extracted P

	loading	Calculated	$NaHCO_3$		NaOH		CDB		acetate		HCl		total amount of extracted P (mg)	Uncon
	‰	‰	‰	mg	‰	mg	‰	mg	‰	mg	‰	mg		
Fe1(O)	+119	+76			+109	2.84	+34	2.24					5.37	5%
Fe3(O)	+119	+132	+118	0.98	+137	6.53	+115	0.87					8.41	0.30%
Ca1(I)	+151	+78	+58	0.82			+58	2.37	+109	2.03	+77	2.29	7.01	0%

Table 4.5 The extracted P and Fe contents of in individual mineral samples and in form of mixture. CaL represents the sum of the halved data obtained from the individual extraction of two or four minerals. Mixture 1: Fe1(O)+Fe1(I); Mixture 2: Fe3(O)+Fe3(I); Mixture 3: Fe1(O)+Fe1(I)+Fe4(I)+Ca1(I). Mixture/CaL (%) represents the ratio between measured data and calculated data. Calculated isotopic signal of mineral phase before chemical extraction steps. Only the ratios relevant to the discussion are shown in the table.

	$NaHCO_3$ step		NaOH step		2,2-bipyridine step		CDB step		Acetate buffer step		HCl step	
	P	Fe	P	Fe	P	Fe	P	Fe	P	Fe	P	Fe
Fe1(O)	1031	103	14180	0	426	3	11192	681976	0	0	16	6
Fe1(I)	17	67	205	0	42	0	1769	248564	4	0	18	0
CaL	524	85	7193	0	234	2	6481	465270	2	0	17	3
Mixture 1	595	20	7907	0	81	0	7211	518056	21	0	41	1900
Mixture/CaL (%)	114		110				111	111				
Fe3(O)	4921	426	32639	1	117	7	4359	681976	0	0	21	6
Fe3(I)	17	101	119	2	30	0	696	166511	4	0	15	0
CaL	2469	264	16379	2	74	4	2528	424244	2	0	18	3
Mixture 2	7142	598	13626	0	133	8	3236	507923	0	0	25	2065
Mixture/CaL (%)	289		83				128					
Fe1(O)	1031	103	14180	0	426	3	11192	681976	0	0	16	6
Fe1(I)	17	67	205	0	42	0	1769	248564	4	0	18	0
Fe4(I)	92	39	31	0	30	1	1146	239794	10	0	12	0
Ca1(I)	4124	0	6	0	61	5	11835	4	10146	0	8902	23
CaL	2632	104	7211	0	280	5	12971	585169	5080	0	4474	15
Mixture 3	1915	20	4190	0	104	0	6762	518056	8150	0	75286	1900
Mixture/CaL (%)	73		58				52		160		1683	

Table 4.6 Overview of observed $\delta^{18}O_{PO4}$ value (‰ VSMOW) in different P pools in natural aquifer materials. Ammer floodplain in Germany (Tufa2, Peat4), Red River floodplain in Vietnam (Reri4), Hetao floodplain in PR China (Heta5). Abbreviations: inorganic carbon (IC), organic carbon (OC).

$\delta^{18}O_{PO4}$ value (‰ VSMOW)	$NaHCO_3$-P	NaOH-P	2,2'-bipyridine-P	CDB-P	Acetate-P	HCl-P
Tufa2 (OC: 3% / IC:9%)		+0.22		+6.34		+7.46
Peat4 (OC: 21% / IC:5%)						+20.85
Reri4 (OC: <0.05% / IC: <0.05%)						+12.29
Heta5 (OC: <1% / IC:<1%)						+8.87

4.4 Discussion

4.4.1 Potential changes in the oxygen isotope ratio in phosphate in operationally defined pools

Since there were no parallel samples for the initial solution isotope determination (n=1), therefore, the results of α values in Fig 4.2 are only discussed speculatively in this section. The α values of Fe3(O) P pools ($NaHCO_3$-, NaOH and CDB-P) were close to 1.00, indicating there was no fractionation. However, in other measurements of single sample or mixtures, P pools yielded α < 1.00, representing fractionation occurred. The PO_4 obtained in P pools may be isotopically lighter than that in the initial labeling solution. Based on the experimental design process, I speculate that the variation of α value in P pools could be attributed to two reasons, i) the fractionation caused by surface adsorption or co-precipitation; ii) the fractionation caused by the chemical extraction process. The variation of concentration of P in the initial labeling solution was difficult to be measured for calculating $\delta^{18}O_{PO4}$ value of total P in mineral phase, because the P concentration of initial labeling solution is way higher than the value of its variation, it is not feasible to monitor the P loss in initial labeling solution due to mineral samples only immobilize a small portion of P. In order to verify the possible fractionation that occurred during surface adsorption, alternatively, the $\delta^{18}O_{PO4}$ value of total sorbed PO_4 were calculated by the $\delta^{18}O_{PO4}$ value in each P pools and its corresponding P mass via equation (V).

The $\delta^{18}O_{PO4}$ values of all PO_4 adsorbed on Fe1(O) and Fe3(O) are calculated to be +76 ‰ and +132 ‰ with corresponding initial labeling solution $\delta^{18}O_{PO4}$ values to be +119 ‰ (Table 4.4). The result of Fe1 suggests the fractionation of oxygen isotopes in PO_4 during its interactions with ferrihydrite is due to that isotopically lighter PO_4 preferentially incorporated into sorbed phases, this observation is same as previous report (Jaisi et al., 2010). Jaisi et al. (2010) revealed this isotopic fractionation was a cumulative effect by two reasons, the fractionation during PO_4 sorption and fractionation during mineral transformation. The transformation is that ferrihydrite underwent dissolution and reprecipitation during its interaction with aqueous PO_4 and formed a more crystalline mineral phase/s (Jaisi et al., 2010; Neupane et al., 2014). The fractionation during PO_4 sorption on ferrihydrite is particularly effective in the early stages, however, concomitant with its mineral transformation, the fractionation aqueous and sorbed PO_4 becomes negligible at long reaction times (>2000 h) (Jaisi et al., 2010). In this study, the P loading experiments were conducted overnight, this may be responsible for the fractionation to isotopically lighter PO_4 was more pronounced. However, this study can not definitely

confirm the transformation fractionation the O isotope ratios of PO_4 in the more strongly bond miner phases showed a lighter value. The result of Fe3(O) yielded an isotopically heavier $\delta^{18}O_{PO4}$ value of the total PO_4 on the mineral than its initial labeling solution. This is mainly attributed to the extraction of heavier isotope values in the NaOH step. However, because of the lack of parallel samples for the initial solution isotope determination (n=1), it cannot be ruled out that the calculated $\delta^{18}O_{PO4}$ value may be close to actual $\delta^{18}O_{PO4}$ value in initial solution. And the reasons for detected high $\delta^{18}O_{PO4}$ value in NaOH-P pool will be discussed in the later paragraph regarding the variation of O isotope ratio in PO_4 in operationally defined pools. The $\delta^{18}O_{PO4}$ value of all PO_4 coprecipitated in Ca1(I) is calculated to be +78 ‰ with corresponding initial labeling solution $\delta^{18}O_{PO4}$ values to be +151 ‰, indicating an isotopically lighter fractionation after PO_4 precipitated as hydroxyapatite. Notably, Table 2.3 indicated the Ca1(I) might be subject to incomplete dissolution in HCl step, i.e., a certain amount of PO_4 might be still be retained in the undissolved mineral phase, there may be present unknown $\delta^{18}O_{PO4}$ value that was not involved in calculation. Even though the undissolved mineral phase were not measured, the observed tendency of preferential removal of isotopically lighter PO_4 from aqueous phase during precipitation of apatite is consistent with previous study (Liang and Blake, 2007). These calculation results indicates that the fractionation may have occurred already prior to the conduction of sequential extraction scheme.

In addition, since a portion of the P pools contained PO_4 that was too low in concentration to conduct Ag_3PO_4 preparation and thus has not been subjected to measure $\delta^{18}O_{PO4}$ value (for instance, 5% mass of Fe1 in Table 4.4). This unaccounted-for portion of the mass may be one of the reasons for most of the $\alpha < 1.00$. Further literature is needed to support information regarding the fractionation of PO_4 during its interaction to different type of oxides. In carrying out the above discussion, I found the fractionation that prior to the chemical extraction process, while posing a challenge to the applicability of the combined analytical method of sequential extraction and phosphorus-bound stable oxygen isotope techniques, may be due to differences in the laboratory labeling experiments versus the natural conditions (for example, contact time). However, there might be another bigger challenge to the combined analytic approach, i.e. chemical extraction process can also cause fractionation in terms of the $\delta^{18}O_{PO4}$ value in different P pools.

The fractionation caused by the chemical extraction process may be indicated by comparing $\delta^{18}O_{PO4}$ value among the extraction steps within the same sample (Table 4.3). For Fe1(O), the $\delta^{18}O_{PO4}$ value in NaOH-P pool (+109 ± 0.2 ‰) was higher than that in

CDB-P pool (+34 ‰). For Fe3(O), the $\delta^{18}O_{PO4}$ value in NaOH-P pool (+137 ± 4 ‰) was significantly higher than that in $NaHCO_3$- and CDB-P pools (+118 ± 3 ‰ and +115 ± 3 ‰, respectively). For the inside loading Fe-(hydr)oxides, the preliminary wash by NaOH step yielded higher $\delta^{18}O_{PO4}$ value than initial labeling solutions and other detectable P pool. This observation may indicate that even within same mineral sample, the O isotope ratio in PO_4 in its operationally defined pools are influenced by the chemical extraction process. Interestingly, for inside loading samples, preliminary NaOH wash steps yielded particularly high $\delta^{18}O_{PO4}$ value compared to that in initial labeling solutions. For instance, the detected $\delta^{18}O_{PO4}$ value in preliminary NaOH wash step, initial labeling solution and CDB-P of Fe1(I) were +301 ‰, +260‰ and +197‰, respectively. One reason may be attributed to the O isotope ratio in PO_4 in NaOH-P pool was influenced by chemical extraction process. Another reason may be attributed to the formation of secondary precipitation. Massive P and Fe were removed from initial synthesized inside loading samples, and due to isotopically lighter PO_4 preferentially immobilized in secondary precipitated mineral, eventually resulted in a high value in aqueous NaOH wash step. However, due to the lack of research on the isotopic value of PO_4 during its interaction with different types of Fe-(hydr)oxides, it requires further investigation to assist the explanation, for example, how does exact structure of surface complex of PO_4 on different Fe-(hydr)oxides influence $\delta^{18}O_{PO4}$ value in aqueous and sorbed phase (Acelas et al., 2013; Spicher et al., 2023). Given that for individual mineral phases, the leveling-off of adsorption is primarily due to electrostatic repulsion rather than actual saturation of the Fe-(hydr)oxides surface sites by PO_4 (Wang et al., 2013). Therefore, one possible speculation is that during the chemical reaction with extraction solutions (like NaOH or CDB), previously vacant sites that could bind to PO_4 might be reutilized, making the re-arrangement of PO_4 possible, and this series of changes may lead to an order in which PO_4 isotopes of different weights are preferentially desorbed by different chemical reagents (Ajmal et al., 2018; Daou et al., 2007; Neupane et al., 2014; Wang et al., 2013). For Ca1(I), the $\delta^{18}O_{PO4}$ in $NaHCO_3$ and CDB steps (both yield 58 ‰) showed isotopically lighter values than that in acetate buffer and HCl steps (+109 ± 8 ‰ and +77 ± 10 ‰). For hydroxyapatite, alkaline extractants produced different results compared to their application on Fe-(hydr)oxides. This may be due to the different adsorption mechanisms of PO_4 ions on Fe- and Ca-mineral surfaces, chemical precipitation may act as an important mechanism of PO_4 adsorption on Ca-mineral surface (Cheng et al., 2023; Dorozhkin, 2011; Flower et al., 2022; L. Li et al., 2023; Ren et al., 2021). Considering the alkaline extractants ($NaHCO_3$ and CDB) are less reactive to hydroxyapatite than the

acidic extractants (acetate buffer and HCl), it may further imply that relatively lighter PO_4 isotopes precipitated at the solid-liquid contact surface while relatively heavier are precipitated in the bulk where better-ordered apatite crystal structure, based on previous study that isotopically light PO_4 are preferentially incorporated into apatite (Liang and Blake, 2007). Notably, Ca1(I) might be subject to incomplete dissolution in HCl-P pool, while the mixture Fe1(O)+Fe1(I)+Fe4(I)+Ca1(I) underwent complete dissolution, considering the HCl-P was contributed only by Ca1(I), further discussion regarding hydroxyapatite HCl-P will be conducted in the following section. These results may indicate that $\delta^{18}O_{PO4}$ values of P pools are subject to change by the extraction protocols. Differences of among $\delta^{18}O_{PO4}$ value in neighboring P pools may not be necessarily due to pools were affected by the different P sources but rather to fractionation caused by the extraction schemes. I further tested mixtures of the minerals above to investigate the performances of $\delta^{18}O_{PO4}$ values in mixtures' P pools.

4.4.2 Oxygen isotope ratio in phosphate in operationally defined pools of mixture groups and natural samples

For mixture samples, the $NaHCO_3$- and NaOH-P pools were supposed to be extracted from outside loading sample, the CDB-P pool was supposed to be extracted from both outside and inside loading sample, the acetate buffer- and HCl-P pools were supposed to be extracted from inside loading sample. The variation of $\delta^{18}O_{PO4}$ values in $NaHCO_3$-P pool between single and mixture can be estimated by Fe3(O) versus Fe3(O)+Fe3(I). The results of $\delta^{18}O_{PO4}$ values in $NaHCO_3$-P pool of both samples were similar, indicating that the PO_4 extracted by $NaHCO_3$ step from the mixture comes from Fe3(O). The variation of $\delta^{18}O_{PO4}$ values in NaOH-P pool between single and mixture can be estimated by Fe1(O) versus Fe1(O)+Fe1(I), Fe3(O) versus Fe3(O)+Fe3(I), and Fe1(O) versus Fe1(O)+Fe1(I)+Fe4(I)+Ca1(I). The results of $\delta^{18}O_{PO4}$ values in NaOH-P pool of mixture samples were lower than single cases, suggesting that an isotopically heavier PO_4 pool may be present in the analyzed reaction products. Unmeasured $NaHCO_3$-P in Fe1(O)+Fe1(I) and increased extractable $NaHCO_3$-P in Fe3(O)+Fe3(I) could be possible reasons. Additionally, the results suggest that the NaOH extractable PO_4 of the mixture that consists of multi-minerals was isotopically heavier (+140 ‰) than the mixture only consists of two Fe-(hydr)oxides (+91 ‰). The possibility may be attributed to a portion of isotopically heavier PO_4 from other pools were additionally extracted by NaOH step, for example, additional contribution by Fe1(O) CDB-P (+197 ‰). This suggests that the

variation in isotopic values between different combination of mineral types might be based on the isotope-related prioritization during chemical extraction. This isotope-related prioritization during chemical extraction could be attributed to migration of PO_4 from their positions in the mineral system, or rearrangement of binding sites on different mineral surfaces (Ganta et al., 2021; Paige et al., 1997; X. Wang et al., 2013; Willett et al., 1988). Another possibility is the presence of hydroxyapatite resulted in re-adsorption and re-precipitation of PO_4 during the NaOH extraction on mixture Fe1(O)+Fe1(I)+Fe4(I)+Ca1(I), as alkaline solutions can enhance the adsorption of PO_4 on Ca-minerals rather than remove it (Claveau-Mallet et al., 2020; Ren et al., 2021; Xu et al., 2014). The results of Table 4.5 showed there were less P extracted by $NaHCO_3$ and NaOH than expected, suggesting the presence of hydroxyapatite re-immobilized a portion of PO_4 on the surface, and it implies these re-immobilized P were preferentially isotopically heavier, finally resulting higher $\delta^{18}O_{PO4}$ value in NaOH-P pool of Fe1(O)+Fe1(I)+Fe4(I)+Ca1(I). Regarding how does PO_4 on the surface of Fe-(hydr)oxides respond to the influence of hydroxyapatite calls for further investigation.

$\delta^{18}O_{PO4}$ value of natural samples were mostly restricted to HCl-P pools (Table 4.6). Except CDB-P in Tufa2, the distribution of CO peak area and sample weight indicated contamination by exogenous oxygen in rest analytes, which may be the presence of organic P (McLaughlin et al., 2006; Tamburini et al., 2018; von Sperber et al., 2023). There are limited reports on the $\delta^{18}O_{PO4}$ values of different P pools in sediments in groundwater systems. The aquifer sample Peat4 showed a higher $\delta^{18}O_{PO4}$ value in HCl-P pool than others, considering it owns 21% of organic matter by mass, the elevated O isotope ratio in PO_4 may be attributed to the microbial activities-oriented P cycling (Lei et al., 2020). In contrast, the light isotope ratio in NaOH-P is very low and differentiates it from the oxygen isotope ratio in most PO_4, suggesting the result may have been disturbed by sample preparation and/or the measurement did not work out properly, which belongs to common problems encountered with the interpretation of oxygen isotope ratios of PO_4 in the organic enriched samples, like soils and sediments (McLaughlin et al., 2006; Tamburini et al., 2018; von Sperber et al., 2023). The result of CDB-P in Tufa2 showed a light $\delta^{18}O_{PO4}$ value, which may be a response to less biological cycling (Helfenstein et al., 2018; Lei et al., 2020; Tamburini et al., 2010). This may be attributed to the CDB-P in the Ammer floodplain aquifer case represents Ca-associated P which is strongly bound on the mineral surface or within mineral structure, therefore, hardly to be bioavailable.

4.5 Conclusion

This study investigates the $\delta^{18}O_{PO4}$ values of different P pools in synthesized minerals that are representative in groundwater systems to evaluate the performance of a combined approach of sequential extraction and phosphorus-bound stable oxygen isotope technique. The conclusions have been summarized in the following:

1. The fractionation factors (α) in P pools of tested samples tended to be equal or lower than the corresponding initial labeling solution. However, this conclusion is speculative due to there were no parallel samples for the initial solution isotope determination (n=1). Therefore, I merely infer that the $\delta^{18}O_{PO4}$ values in P pools obtained by this combinatorial approach has the potential fractionation risk with original environment.
2. The oxygen isotope ratio in PO_4 in operationally defined pools of same mineral may be subject to change by the chemical extraction protocols. Therefore, the differences of among $\delta^{18}O_{PO4}$ value in neighboring P pools may be not necessarily due to pools were affected by the different P sources but rather to fractionation caused by the extraction schemes. However, due to lack of parameters regarding the properties of mineral and limited literatures, this observation calls for further research.
3. Even if a P pool in the mixture of different minerals is specifically contributed by a single mineral therein, the $\delta^{18}O_{PO4}$ value in this specific P pool of the mixture may deviate from the $\delta^{18}O_{PO4}$ value in P pool of corresponding single sample. The variation of isotopic values in mixture might be attributed to two possibilities, i) preferentially extracted P between different combination of mineral types might be based on the isotope-related prioritization during chemical extraction; ii) re-adsorption and re-precipitation of PO_4 occurred during the extraction, thus leading to changes in the isotopic ratios.

Based on the above summary, a more conservative interpretation of the $\delta^{18}O_{PO4}$ value of P pools in samples that consist of Fe-(hydr)oxides and hydroxyapatite is suggested. Fractionation of oxygen isotopes in PO_4 during its interactions with Fe-(hydr)oxides under chemical extraction protocol and the distribution of different isotopes of PO_4 in mixtures consisting of Fe-(hydr)oxides and hydroxyapatite need to be further investigated. The isotope labeling experiment with synthetic mineral samples in this study is the first investigation on the reliability of $\delta^{18}O_{PO4}$ analysis on extraction of operationally defined PO_4 pools.

5 Summary and conclusion

5.1 Key Findings

The main objectives of this thesis were to i) propose a suitable chemical sequential extraction scheme for studying P cycling in groundwater systems, ii) apply this approach to a case study of elevated P in the groundwater of the Ammer floodplain, iii) and explore the feasibility of using phosphorus-bound stable oxygen isotopic methods in conjunction with the operationally defined P pool analysis. I achieved each of these objectives through three studies in Chapter 2, 3 and 4, respectively. The key questions raised and the answers derived from this thesis are as follows.

- *Q1 How effectively P incorporated into representative minerals in groundwater systems can be selectively extracted by the two extraction schemes?*

To investigate if surface-adsorbed P could be extracted selectively by two tested extraction schemes, P (both PO_4 and phytate) outside loading experiments were conducted with five synthetic mineral samples, ferrihydrite, hematite, magnetite with goethite, pyrolusite and mica. For the above five mineral samples: Scheme A mainly classifies the incorporated PO_4 into three pools, $NaHCO_3$-, NaOH- and CDB-P pool. The expected surface-adsorbed P pools by Scheme A consist of $NaHCO_3$- and NaOH-extractable P, accounting for 57%, 78%, 89%, 49% and 85% of the total extractable PO_4, respectively. Scheme B mainly classifies the incorporated PO_4 into two pools, $MgCl_2$- and CDB-P pool. The expected labile P pool by Scheme B consists of $MgCl_2$ extractable P, accounting for 0%, 13%, 6%, 67% and 61% of the total extractable PO_4, respectively. The extraction of P_{org}, i.e. phytate, by both methods were consistent with their effect on PO_4 extraction. However, for surface-adsorbed PO_4, neither scheme was able to achieve complete extraction for all five minerals within the expected steps. This also suggests that a portion of the P immobilized by surface adsorption may become relatively stable, meaning that the amount of P that can re-enter the water is less than the total immobilized amount.

To investigate if coprecipitated P could be extracted selectively, inside loading experiment was conduct with five mineral samples, ferrihydrite, hematite, magnetite with goethite, vivianite with decayed ferrihydrite, and hydroxyapatite. In both extraction schemes, the CDB step extracted all of the inside loading P in four Fe-(hydr)oxides, indicating good selectivity for the Fe(III)-P pool, however, considering the results of the outside loading experiments, since no method can extract all of the surface-adsorbed

PO_4 without dissolving the mineral phase, it is inevitable that the CDB step also mixes in a portion of the surface-adsorbed PO_4. At the same time, the soluble Fe content detected during the preliminary NaOH wash step was much higher than the value for outside loaded P-free synthetic minerals that undergoing the NaOH step, implying that as P is coprecipitated into the mineral structure, it becomes more unstable itself, and in such cases the NaOH step could dissolve the mineral and release P from the structure. This means that the judgment that the P extracted by the NaOH step is either from surface adsorption or co-precipitation mineral dissolution should be based on combination analysis of the sequential extraction and the mineral composition of the sediment. Additionally, comparable amounts of PO_4 were extracted in the CDB step of both Scheme A and Scheme B in hydroxyapatite, with contents of 11835 and 17272 mg kg^{-1}, respectively. In contrast, the extractable PO_4 in the CDB step of the Fe-(hydr)oxides in inside loading experiments, which underwent the same sequential extraction steps, was only ranged from 696 to 1769 mg kg^{-1} in both extraction schemes. This suggests that the good selectivity of CDB for Fe(III)-(hydr)oxides is challenged in the face of the simultaneous presence of hydroxyapatite in the sample.

- *Q2 Which tested extraction scheme is more suitable for groundwater systems?*

A schematic overview of the estimated suitability of groundwater system extraction schemes is provide in Table 2.6. Compared to use $MgCl_2$ in Scheme B, using $NaHCO_3$ and NaOH in Scheme A is clearly able to extract more surface-adsorbed P (both PO_4 and phytate). From this point of view, Scheme A should therefore be applied to the study of P in groundwater systems, as it reflects the pathway of origin of the P species in the sample. For Scheme A, in cases where its NaOH step is able to completely extract surface-adsorbed PO_4, for example in hematite case, its extraction scheme can better distinguish between the PO_4 on the surface of Fe-(hydr)oxides and co-precipitation with Fe-(hydr)oxides. Whereas Scheme B would misclassify most surface-adsorbed PO_4 as co-precipitation fraction with Fe-(hydr)oxides. Therefore, Scheme A ($NaHCO_3$ – NaOH – 2,2'-bipyridine – CDB – Acetate buffer – HCl) was tested to be more suitable for groundwater systems than Scheme B ($MgCl_2$ – 2,2'-bipyridine – CDB – NaOH– Acetate buffer – HCl) by applying them to outside loading PO_4 and phytate, and inside loading PO_4 in synthetic mineral samples.

The extraction scheme was further applied to natural aquifer materials. Aquifer sediments from three different ecosystems were effectively differentiated. The samples from calcareous aquifer in the Ammer floodplain showed diverse P pools with large

amounts of surface-adsorbed P, up to around 40%. Correspondingly, the aquitard composed of silty clay exhibited a markedly different composition of P pools. This additionally demonstrates that the sequential extraction scheme can effectively differentiate the functional sink of P between various sediments within the same geological environment. The samples from Fe(III)-(hydr)oxides rich aquifer in the Red River Delta showed large CDB-P pool proportion. The samples clay aquifer in the Hetao floodplain showed predominated stable HCl-P pool. However, 2,2'-bipyridine and acetate buffer step did not perform well in practice. Considering the 2,2'-bipyridine step also showed an unstable selectivity in the synthesis sample experiments, the sequential extraction scheme was further refined as: $NaHCO_3$ – NaOH – CDB – HCl. Notably, the necessity of the NaOH and CDB steps is once again demonstrated by the extraction results of these natural samples, as they represent distinguish P fractions which might be misclassified to subsequent P pools.

- *Q3 What are the sources that are responsible for elevated P in the groundwater of the calcareous floodplain aquifers?*

To investigate the P cycling in calcareous floodplain aquifer, groundwater samples were collected from a shallow calcareous and organic matter-rich aquifer and a sediment core was collected at a location with elevated TDP concentration in groundwater. In the groundwater system, the TDP in groundwater (as represented by PO_4) was positively correlated with NH_4^+ and DOC concentrations and were observed mainly under reducing redox conditions ($p < 0.05$). This suggested that TDP concentrations were mainly influenced by microbial metabolic activities, as TDP, DOC, and NH_4^+ can all be released to groundwater through the *in-situ* mineralization of OM under anaerobic and reducing conditions. Meantime, the aquifer was characterized by a low hydraulic transmissivity, which could allow for a subsequent accumulation of TDP, NH_4^+ and DOC in the aqueous phase. The chemical-physical properties and trace element composition emphasized the impact of anoxic microbial mineralization of OM on the groundwater, which is tightly connected to the fate of P. Notably, the important role of OM as source of PO_4 in groundwater was also reflected in the composition of the aquifer sediments. A large amount of PO_4 and P_{org} were found in surface P pools ($NaHCO_3$- and NaOH extractable). Distribution coefficient (Kd values) suggested that P_{org} was preferentially adsorbed over PO_4 in the aquifer material. The large adsorption of PO_4 and P_{org} from the surface P pools suggesting that as OM can be subsequently mineralized. PO_4 and P_{org} can be (re-)released into ambient groundwater. I therefore considered the i) PO_4 was released to the groundwater *in-situ* via the mineralization of OM in the Ammer floodplain, where

consists of calcareous and OM-rich aquifer material; ii) OM present in the shallow aquifer to not only represent a sink for PO_4 and P_{org}, but also as a potential source when it is subject to microbial mineralization.

- *Q4 How can elevated PO_4 concentrations in a calcareous aquifer system prevail?*

I suggest a competition between mobilization and immobilization of P in the calcareous and OM-rich aquifer system. According to the sequential extraction outcomes, the largest P pool in the aquifer materials was represented by the HCl-extractable P fraction (tufa median: 55% of TP, peat median: 44% of TP). This fraction generally represents Ca-mineral related P in our case. However, this P pool is not the protagonist of the competitive factors, as a pronounced proportion of surface-adsorbed PO_4 and P_{org} were found as main P sinks in addition to PO_4 that was structurally incorporated into Ca-minerals. Surface adsorption is further determined as the most likely active mechanism of immobilizing PO_4 and P_{org}. Meanwhile, sedimentary OM and re-sorbed OM on sediment surface continues to be mineralized in a reducing groundwater system. However, the immobilization of PO_4 is slower as compared to its mobilization, which I attribute to slow kinetics of Ca-minerals precipitation reactions and a competition for sorption sites (including preferential adsorption of P_{org} over PO_4). I further highlight the limited and absent self-purification capabilities of calcareous groundwater systems, warning they are susceptible to anthropogenic contamination with DOC and PO_4.

- *Q5 Are the $\delta^{18}O_{PO4}$ values in each P pool of a given single mineral related to the extraction scheme under abiotic condition*

The variation of the $\delta^{18}O_{PO4}$ values in extracted P pools in mineral due to extraction scheme were observed. This variation indicates fractionation which can be manifested in two aspects. First aspect, the O ratio in all PO_4 that incorporated into minerals (surface adsorption or coprecipitation) can be different with that in initial labeling solution. The results support previous study that ferrihydrite preferentially adsorbs isotopically lighter PO_4 from the environment. However, in this study, the $\delta^{18}O_{PO4}$ value of total PO_4 in sorbed phase was obtained by calculation on $\delta^{18}O_{PO4}$ values in all detected P pools, while a portion of the P pools did not yield enough mass for $\delta^{18}O_{PO4}$ measurement, the unaccounted-for portion of the mass may be one of the reasons for the fractionation ($\alpha < 1.00$). Besides, since there were no parallel samples for the initial solution isotope determination (n=1), the potential fractionation is speculatively, it could not draw solid conclusion that this fractionation was caused by extraction scheme. Second aspect, the O ratio in PO_4 of extracted P pool may get changed by different chemical extraction steps.

This trend of fractionation of $\delta^{18}O_{PO4}$ values may be related to the certain extraction protocol in every study cases. It may interfere with the proper interpretation of isotope values in the P pools. Therefore, the differences of among $\delta^{18}O_{PO4}$ value in subsequently extracted P pools may be not necessarily due to pools were affected by the different P sources but rather to fractionation caused by the extraction schemes. However, due to lack of parameters regarding the properties of mineral and limited literatures, this observation calls for further research.

- *Q6 How is the variation of $\delta^{18}O_{PO4}$ values in P pools when these minerals are mixed?*

After the $\delta^{18}O_{PO4}$ in P pools of single mineral have been measured, I further tested the $\delta^{18}O_{PO4}$ in P pools of the mixture that consists different minerals. Interestingly, even if a P pool in mixture that is specifically contributed by a single mineral therein, the $\delta^{18}O_{PO4}$ value in this specific P pool of the mixture may vary from the $\delta^{18}O_{PO4}$ value in P pool of corresponding single sample. The variation of $\delta^{18}O_{PO4}$ value might be attributed to two possibilities, i) preferentially extracted P between different combination of mineral types, which might be based on the isotope-related prioritization during chemical extraction; ii) re-adsorption and re-precipitation of PO_4 occurred during the extraction, thus leading to changes in the isotopic ratios. It is additionally noteworthy that for the sample consists of both Fe- and Ca-minerals, the isotope value obtained in alkaline extraction step might be related to inter-pool migration of P due to adsorption-desorption processes of PO_4 among Fe- and Ca-minerals. I therefore suggest that the plausibility of inferring the P sources or P cycling by investigating $\delta^{18}O_{PO4}$ value in extractions needs further research.

5.2 Summarizing discussion

It is important to know that how the storage phase of P is correctly interpreted by chemical extraction schemes in groundwater systems. In Chapter 2, the different effect of NaOH and CDB on Fe(III)-(hydr)oxides was clearly shown in the result, NaOH does not cause obvious dissolution of Fe-mineral in outside loading group, while CDB has the ability to dissolve Fe-mineral phases. Therefore, premature use of the CDB step can lead to lose the information of surface-adsorbed P or structurally bound P due to the CDB could completely dissolved Fe(III)-(hydr)oxides before NaOH step. This extraction strategy is different with lake sediments and soils (He et al., 2024; Yuan et al., 2019). Next, I will further discuss the proper interpretation of P pools and potential interferences.

In Chapter 2, I conclude the surface-adsorbed P can be represented by $NaHCO_3$ and NaOH extractable P. In Chapter 3, a large proportion of $NaHCO_3$- and NaOH-P were detected on sediments, along with half proportion being P_{org}, indicating a significant amount of P accumulated on the sediment surface. The elevated TDP and DOC in aqueous phase could be attributed to this reason. The potential P storage phases of NaOH-P rule out firstly for calcium carbonate deposits in the Ammer floodplain aquifer, because strong alkaline extractants enhance P adsorption on calcareous sediments rather than remove it (Claveau-Mallet et al., 2020; Ren et al., 2021; Xu et al., 2014); and secondly for surface of Fe-minerals, because the data showed the distribution of Fe-mineral is limited in the aquifer. Instead, a significant amount of OM was detected in aquifer sediments. These OM were formed 8400 to 7870 years before present when the system represented a paleo-mire (Heidgen et al., 2020). Notably, the results in Chapter 2 also suggests the proper interpretation of NaOH-P should include the possibility of coprecipitated P, as coprecipitation of PO_4 alters the structure of Fe (hydr)oxides, decreases the crystallinity of the Fe-P precipitate (Kraal et al., 2019; Waychunas et al., 1993). This reason is attributed to a large mass of Fe and P were found in preliminary NaOH wash step before extraction scheme. Correspondingly, the samples with a high percentage of NaOH-P pool in the Red River floodplain aquifers may be attributed to the changes in redox conditions resulting in a portion of the P being newly precipitated with Fe, which is relatively fragile and should be alerted to its environmental risk (Neidhardt et al., 2021).

The meaning of the P pool represented by CDB-P was further explored in this research. In the case of recommended extraction scheme, the surface-adsorbed P can be extracted by $NaHCO_3$, NaOH and CDB from Fe-(hydro)oxides. And as the CDB solution was intended to release coprecipitated PO_4 in Fe(III)-(hydr)oxides (Hupfer et al., 1995; Ruttenberg et al., 2009). It implies a fraction of the surface-adsorbed PO_4 can not be extracted by strong alkaline solution (for example, by NaOH) until the complete dissolution of the mineral structure (for example, by CDB). The same phenomenon has also been observed in removing PO_4 and phytate on the surface of Fe-(hydr)oxides , such as synthetic ferrihydrite, goethite and magnetite (Ajmal et al., 2018; Chen and Arai, 2019). In Chapter 4, the results may indicate this fraction can be isotopically lighter PO_4 that incorporated into Fe-(hydr)oxides. As Fe1(O) and Fe3(O) all yielded a lighter $\delta^{18}O_{PO4}$ value in CDB-P pool than NaOH-P pool, and the preliminary NaOH wash for inside loading samples also yielded $\delta^{18}O_{PO4}$ value higher than that in CDB-P pool of Fe1(I), a key discussion point regarding the fractionation results of Fe-(hydr)oxides is whether the

lighter isotopic value observed in the CDB step may be due to the extractant's bias toward lighter PO_4, or if it had no bias toward lighter PO_4 but instead may reflect that the retained PO_4 ions were lighter due to the previous NaOH step. As previously discussed, if the NaOH step is skipped, the CDB-P pool will also include the information from the NaOH-P pool. I therefore infer that some certain chemical reagents in extraction scheme may preferentially extract isotopically heavier PO_4 from the mineral. Considering PO_4 ions are assumed to be covalently bound via oxygen to one (monodentate ligands) or two surface iron ions (bidentate ligands), the preference might be related to the isotope-related binding stability in exact structure of in surface complexation with Fe-(hydr)oxides (Acelas et al., 2013; Antelo et al., 2010; Spicher et al., 2023; Wang et al., 2013). Another speculation is that during the chemical reaction with extraction solutions (like NaOH or CDB), previously vacant sites that could bind to PO_4 might be reutilized during mineral transformation, making the re-arrangement of PO_4 possible, and this series of changes may lead to an order in which PO_4 isotopes of different weights are preferentially desorbed in different chemical reagents (Ajmal et al., 2018; Daou et al., 2007; Neupane et al., 2014; Wang et al., 2013). Consequently, a portion of the lighter isotopic PO_4 ions may be adsorbed on the surface of the Fe-minerals in a relatively stable manner under specific conditions, making them difficult to be extracted. The mechanisms behind the observed tendency of NaOH to extract heavier PO_4, isotopes still require further study.

Moreover, Chapter 2 suggests that for the interpretation of CDB-P, it is important to note that it not only represents both surface-adsorbed P and structurally bound P of Fe-minerals, but also that it represents P incorporated with Ca-minerals. In Chapter 4, the isotope results of synthetic mineral (n=3) indicate the $\delta^{18}O_{PO4}$ value in CDB-P is supposed to be lighter than that in HCl-P pool (n=3), this might reflect the characteristics of PO_4 isotopes of the Ca-associated P by these two extraction steps. For natural sample, the result of CDB-P in Tufa2 showed a relatively light $\delta^{18}O_{PO4}$ value +6.43 ‰, indicating less biological cycling. This conclusion corresponds to the conclusions of Chapter 3, that the CDB-P in the Ammer floodplain aquifer case represents Ca-associated P which is strongly bound on the mineral surface or within mineral structure, therefore, hardly to be bioavailable.

The fractionation caused by surface adsorption or co-precipitation that made isotopic difference in PO_4 between its original environments and cumulative P in sediments does not overly affect the application of the methods, as fractionation effect can diminish over time, the natural samples may not be significantly affected by this process (Jaisi et al., 2010). As indicated by labeling experiment, some chemical reagents (for example, NaOH)

in extraction scheme may preferentially extract isotopically heavier PO_4 from the sample, resulting a relatively higher $\delta^{18}O_{PO4}$ value in certain P pool/s. This tendency can also be found in previous studies on natural samples, often, these studies attribute the results of obvious different $\delta^{18}O_{PO4}$ values to equilibrium conditions, varied P sources and biological processes (Helfenstein et al., 2018; Jiang et al., 2017; Jin et al., 2023; Joshi et al., 2016, 2015; Lei et al., 2020; Yuan et al., 2019). Referencing Joshi et al. (2015), it is notable that $MgCl_2$ and CDB were used as the first and second extraction steps, respectively, and the results demonstrated that the $\delta^{18}O_{PO4}$ in CDB step were the heaviest. Of course, even though, some P pools like NaOH-P, have a tendency to extract heavy isotopes, it has still been reported with lighter isotopes result, as was the case in the Ammer floodplain aquifer in this study. However, through the above discussion, my investigation offers a different point of view that isotope fractionation in different P pool may also be due to chemical extraction schemes.

5.3 Conclusion

This thesis further explores the research gaps in the study of P cycling in groundwater systems through methodological discussions involving synthesis, labeling experiments, and their applications to groundwater and aquifer sediments. The contributions of this thesis in advancing the current state of research and outlook for future research are summarized below:

(i) Exercise greater caution with respect to the NaOH and CDB steps in chemical extraction schemes, particularly concerning the binding forms of extracted P and the interpretation of their corresponding roles in biogeochemical processes. NaOH-P represents strongly surface-adsorbed P on Fe- and Al-minerals, moderately labile P_{org}, and relatively fragile structurally bound Fe-P. CDB-P represents relatively strong structurally bound Fe-P, non-extractable surface-adsorbed P on Fe-minerals, and Ca-associated P. Therefore, it is recommended that NaOH-P should be interpreted alongside sediment mineral composition analysis, CDB-P should be interpreted alongside simultaneous measurements of Fe, Mn, and Ca.

(ii) Place more emphasis on the retention of P in groundwater of calcareous floodplain aquifers. Although calcareous sediments are capable of holding large amounts of P, its capacity to immobilize P is fall at a disadvantageous position, while OM became an important player in mobilizing and immobilizing P by *in-situ*

microbial mineralization and surface-adsorbed P_{org}. As surface-adsorbed P_{org} form is an important sink, its role in P im/mobilization needs to be further explored.

(iii) Pay closer attention to the interpretation of isotopic results in different P pools, particularly considering that the P extracted by these methods may originate from various binding substances. A more conservative interpretation of the $\delta^{18}O_{PO4}$ value of P pools in samples that consist of Fe-(hydr)oxides and hydroxyapatite is suggested. Fractionation of oxygen isotopes in PO_4 during its interactions with Fe-(hydr)oxides under chemical extraction protocol and the distribution of different isotopes of PO_4 in mixtures consisting of Fe-(hydr)oxides and hydroxyapatite need to be further investigated.

References

Acelas, N.Y., Mejia, S.M., Mondragón, F., Flórez, E., 2013. Density functional theory characterization of phosphate and sulfate adsorption on Fe-(hydr)oxide: Reactivity, pH effect, estimation of Gibbs free energies, and topological analysis of hydrogen bonds. Computational and Theoretical Chemistry 1005, 16–24. https://doi.org/10.1016/j.comptc.2012.11.002

Abdolvand, B., Mez, L., Winter, K., Mirsaeedi-Gloßner, S., Schütt, B., Rost, K. T. and Bar, J., 2015. The dimension of water in Central Asia: Security concerns and the long road of capacity building. Environmental Earth Sciences 73, 897–912. https://doi.org/10.1007/s12665-014-3579-9

Adu-Gyamf, J., Pfahler, V., 2022. Oxygen Isotopes of Inorganic Phosphate in Environmental Samples: Purification and Analysis. ISBN: 978-3-030-97496-1

Ajmal, Z., Muhmood, A., Usman, M., Kizito, S., Lu, J., Dong, R., Wu, S., 2018. Phosphate removal from aqueous solution using iron oxides: Adsorption, desorption and regeneration characteristics. Journal of Colloid and Interface Science 528, 145–155. https://doi.org/10.1016/j.jcis.2018.05.084

Alobeedallah, H., Ellis, J.L., Rohanizadeh, R., Coster, H., Dehghani, F., 2011. Preparation of nanostructured hydroxyapatite in organic solvents for clinical applications. Trends Biomater Artif Organs 25, 12–19.

Anderson, M.A., Malotky, D.T., 1979. The adsorption of protolyzable anions on hydrous oxides at the isoelectric pH. Journal of Colloid and Interface Science 72, 413–427. https://doi.org/10.1016/0021-9797(79)90343-6

Antelo, J., Fiol, S., Pérez, C., Mariño, S., Arce, F., Gondar, D., López, R., 2010. Analysis of phosphate adsorption onto ferrihydrite using the CD-MUSIC model. Journal of Colloid and Interface Science 347, 112–119. https://doi.org/10.1016/j.jcis.2010.03.020

Bai, J., Ye, X., Jia, J., Zhang, G., Zhao, Q., Cui, B., Liu, X., 2017. Phosphorus sorption-desorption and effects of temperature, pH and salinity on phosphorus sorption in marsh soils from coastal wetlands with different flooding conditions. Chemosphere 188, 677–688. https://doi.org/10.1016/j.chemosphere.2017.08.117

Bańkowska-Sobczak, A., 2021. Calcite as a candidate for non-invasive phosphorus removal from lakes. Ecohydrology & Hydrobiology 21, 683–699. https://doi.org/10.1016/j.ecohyd.2021.06.005

Barcala, V., Jansen, S., Gerritse, J., Mangold, S., Voegelin, A., Behrends, T., 2023. Phosphorus adsorption on iron-coated sand under reducing conditions. Journal of Environmental Quality 52, 74–87. https://doi.org/10.1002/jeq2.20432

Barrow, N.J., 2021. Comparing two theories about the nature of soil phosphate. European Journal of Soil Science 72, 679–685. https://doi.org/10.1111/ejss.13027

Bean, J.R., Wilcox, A.C., Woessner, W.W., Muhlfeld, C.C., 2015. Multiscale hydrogeomorphic influences on bull trout (Salvelinus confluentus) spawning habitat. Can. J. Fish. Aquat. Sci. 72, 514–526. https://doi.org/10.1139/cjfas-2013-0534

Bingham, S.T., Buss, H.L., Mouchos, E.M., Johnes, P.J., Gooddy, D.C., Bagnall, J.P., 2020. Rates of hydroxyapatite formation and dissolution in a sandstone aquifer: Implications for understanding dynamic phosphate behaviour within an agricultural catchment. Applied Geochemistry 115, 104534. https://doi.org/10.1016/j.apgeochem.2020.104534

Blake, R.E., O'Neil, J.R., Garcia, G.A., 1998. Effects of microbial activity on the δ18O of dissolved inorganic phosphate and textural features of synthetic apatites. American Mineralogist 83, 1516–1531. https://doi.org/10.2138/am-1998-1113

Blake, R.E., O'neil, J.R., Garcia, G.A., 1997. Oxygen isotope systematics of biologically mediated reactions of phosphate: I. Microbial degradation of organophosphorus compounds. Geochimica et Cosmochimica Acta 61, 4411–4422. https://doi.org/10.1016/S0016-7037(97)00272-X

Blake, R.E., O'Neil, J.R., Surkov, A.V., 2005. Biogeochemical cycling of phosphorus: insights from oxygen isotope effects of phosphoenzymes. American Journal of Science 305, 596–620.

Burkholder, J.M., Glibert, P.M., 2013. Eutrophication and Oligotrophication, in: Levin, S.A. (Ed.), Encyclopedia of Biodiversity (Second Edition). Academic Press, Waltham, pp. 347–371. https://doi.org/10.1016/B978-0-12-384719-5.00047-2

Cao, X., Han, X., Chen, Y., Li, J., Zhai, Y., 2024. Flood irrigation increases the release of phosphorus from aquifer sediments into groundwater. Journal of Contaminant Hydrology 261, 104297. https://doi.org/10.1016/j.jconhyd.2024.104297

Chang, S.J., Blake, R.E., 2015. Precise calibration of equilibrium oxygen isotope fractionations between dissolved phosphate and water from 3 to 37 °C. Geochimica et Cosmochimica Acta 150, 314–329. https://doi.org/10.1016/j.gca.2014.10.030

Chapin, F.S., 1996. Phosphorus in the global environment. Transfers, cycles and management. Geoderma 73, 257–258. https://doi.org/10.1016/0016-7061(96)00046-8

Chen, A., Arai, Y., 2019. Functional Group Specific Phytic Acid Adsorption at the Ferrihydrite–Water Interface. Environ. Sci. Technol. 53, 8205–8215. https://doi.org/10.1021/acs.est.9b01511

Chen, X., Tao, M., Zhou, Z., Holland, G., Wang, Y., 2023. Geological control on carbon isotope equilibrium and kinetic fractionation of CH4-CO2-HCO3− in microbial coalbed and shale gas systems. Chemical Geology 635, 121609. https://doi.org/10.1016/j.chemgeo.2023.121609

Cheng, P., Liu, Y., Yang, L., Ren, Q., Wang, X., Chi, Y., Yuan, H., Wang, S., Ren, Y.-X., 2023. Phosphate adsorption using calcium aluminate decahydrate to achieve low phosphate concentrations: Batch and fixed-bed column studies. Journal of Environmental Chemical Engineering 11, 109377. https://doi.org/10.1016/j.jece.2023.109377

Cheryan, M., Anderson, F.W., Grynspan., F., 1983. Magnesium-Phytate Complexes: Effect of pH and Molar Ratio on Solubility Characteristics. Cereal Chem 60, 235-237.

Childers, D.L., Corman, J., Edwards, M., Elser, J.J., 2011. Sustainability Challenges of Phosphorus and Food: Solutions from Closing the Human Phosphorus Cycle. BioScience 61, 117–124. https://doi.org/10.1525/bio.2011.61.2.6

Claveau-Mallet, D., Seltani, H., Comeau, Y., 2020. Phosphorus Removal and Carbon Dioxide Capture in a Pilot Conventional Septic System Upgraded with a Sidestream Steel Slag Filter. Water 12(1) 2073-4441. https://doi.org/10.3390/w12010275

Cohn, M., 1958. Phosphate-Water Exchange Reaction Catalyzed by Inorganic Pyrophosphatase of Yeast. Journal of Biological Chemistry 230, 369–379. https://doi.org/10.1016/S0021-9258(18)70572-3

Cordell, D., Drangert, J.-O., White, S., 2009. The story of phosphorus: Global food security and food for thought. Global Environmental Change 19, 292–305. https://doi.org/10.1016/j.gloenvcha.2008.10.009

Correa, R.E., Tait, D.R., Sanders, C.J., Conrad, S.R., Harrison, D., Tucker, J.P., Reading, M.J., Santos, I.R., 2020. Submarine groundwater discharge and associated nutrient and carbon inputs into Sydney Harbour (Australia). Journal of Hydrology 580, 124262. https://doi.org/10.1016/j.jhydrol.2019.124262

Cross, A.F., Schlesinger, W.H., 1995. A literature review and evaluation of the. Hedley fractionation: Applications to the biogeochemical cycle of soil phosphorus in natural ecosystems. Geoderma 64, 197–214. https://doi.org/10.1016/0016-7061(94)00023-4

Danert, K., Adekile, D. and Gesti Canuto, J., 2020. Striving for borehole drilling professionalism in Africa: A review of a 16-year initiative through the rural water supply network from 2004 to 2020. Water 12, 3305. https://doi.org/10.3390/w12123305

Daou, T.J., Begin-Colin, S., Grenèche, J.M., Thomas, F., Derory, A., Bernhardt, P., Legaré, P., Pourroy, G., 2007. Phosphate Adsorption Properties of Magnetite-Based Nanoparticles. Chem. Mater. 19, 4494–4505. https://doi.org/10.1021/cm071046v

Davies, C.L., Surridge, B.W.J., Gooddy, D.C., 2014. Phosphate oxygen isotopes within aquatic ecosystems: Global data synthesis and future research priorities. Science of The Total Environment 496, 563–575. https://doi.org/10.1016/j.scitotenv.2014.07.057

Dorozhkin, S.V., 2011. Calcium orthophosphates: occurrence, properties, biomineralization, pathological calcification and biomimetic applications. Biomatter 1, 121–164. https://doi.org/10.4161/biom.18790

Du, C., Ren, X., Zhang, L., Xu, M., Wang, X., Zhuang, Y., Du, Y., 2016. Adsorption Characteristics of Phosphorus onto Soils from Water Level Fluctuation Zones of the Danjiangkou Reservoir. CLEAN – Soil, Air, Water 44, 975–983. https://doi.org/10.1002/clen.201500094

Duker, A., Cambaza, C., Saveca, P., Ponguane, S., Mawoyo, T. A., Hulshof, M., Nkomo, L., Hussey, S., Van den Pol, B., Vuik, R., Stigter, T. and Van der Zaag, P., 2020. Using nature-based water storage for smallholder irrigated agriculture in African drylands: Lessons from frugal innovation pilots in Mozambique and Zimbabwe. Environmental Science and Policy 107, 1–6. https://doi.org/10.1016/j.envsci.2020.02.010

Elser, J., Bennett, E., 2011. A broken biogeochemical cycle. Nature 478, 29–31. https://doi.org/10.1038/478029a

Espindola, I.B., de Leite, M.L.T.A., Ribeiro, W.C., 2020. South-American Transboundary Waters: The Management of the Guarani Aquifer System and the La Plata Basin Towards the Future. The Palgrave Handbook of Climate Resilient Societies 978, 1-35. https://doi.org/10.1007/978-3-030-32811-5_51-1

Eynard, A., del Campillo, M.C., Barrón, V., Torrent, J., 1992. Use of vivianite (Fe3(PO4)2.8H2O) to prevent iron chlorosis in calcareous soils. Fertilizer research 31, 61–67. https://doi.org/10.1007/BF01064228

Flower, H., Rains, M., Taşcı, Y., Zhang, J.-Z., Trout, K., Lewis, D., Das, A., Dalton, R., 2022. Why is calcite a strong phosphorus sink in freshwater? Investigating the adsorption mechanism using batch experiments and surface complexation modeling. Chemosphere 286, 131596. https://doi.org/10.1016/j.chemosphere.2021.131596

Franzmeier, D. P. and Owens P. R. 2008. Soil Texture Estimates: A Tool to Compare Texture-by-Feel and Lab Data. Journal of Natural Resources & Life Sciences Education 37, 111-116. https://doi.org/10.2134/jnrlse2008.371111x

Ganta, P.B., Morshedizad, M., Kühn, O., Leinweber, P., Ahmed, A.A., 2021. The Binding of Phosphorus Species at Goethite: A Joint Experimental and Theoretical Study. Minerals 11. https://doi.org/10.3390/min11030323

Gebus-Czupyt, B., Wach, B., 2022. Application of $\delta^{18}O$-PO_4 analysis to recognize phosphate pollutions in eutrophic water. Ecohydrology & Hydrobiology 22, 21–39. https://doi.org/10.1016/j.ecohyd.2021.05.005

Geng, Y., Shang Pan, Zhang, L., Qiu, J., He, K., Gao, H., Li, Z., Tian, D., 2022. Phosphorus biogeochemistry regulated by carbonates in soil. Environmental Research 214, 113894. https://doi.org/10.1016/j.envres.2022.113894

Gilliam, J.W., 1995. Phosphorus control strategies. Ecological Engineering 5, 405–414. https://doi.org/10.1016/0925-8574(95)00035-6

Guo, H., Jia, Y., Wanty, R.B., Jiang, Y., Zhao, W., Xiu, W., Shen, J., Li, Y., Cao, Y., Wu, Y., Zhang, D., Wei, C., Zhang, Y., Cao, W., Foster, A., 2016. Contrasting distributions of groundwater arsenic and uranium in the western Hetao basin, Inner Mongolia: Implication for origins and fate controls. Science of The Total Environment 541, 1172–1190. https://doi.org/10.1016/j.scitotenv.2015.10.018

Guo, H., Stüben, D., Berner, Z., 2007. Removal of arsenic from aqueous solution by natural siderite and hematite. Applied Geochemistry 22, 1039–1051. https://doi.org/10.1016/j.apgeochem.2007.01.004

Guo, Z., Wen, Z., Bu, X., Liu, H., Yuan, S., 2023. A sand tank experimental study of distribution, migration and transformation mechanism of iron and phosphorus species under redox fluctuation in a simulated riparian zone. Journal of Hydrology 625, 130032. https://doi.org/10.1016/j.jhydrol.2023.130032

Guppy, C.N., Menzies, N.W., Moody, P.W., Blamey, F.P.C., 2005. Competitive sorption reactions between phosphorus and organic matter in soil: a review. Aust. J. Soil Res. 43, 189–202.

Hallbeck, L., Sthl, F., Pedersen, K., 1993. phytogeny and phenotypic characterization of the stalk-forming and iron-oxidizing bacterium Gallionella ferruginea. Microbiology 139, 1531-1535. https://doi.org/10.1099/00221287-139-7-1531

Hauer, F.R., Locke, H., Dreitz, V.J., Hebblewhite, M., Lowe, W.H., Muhlfeld, C.C., Nelson, C.R., Proctor, M.F., Rood, S.B., 2016. Gravel-bed river floodplains are the ecological nexus of glaciated mountain landscapes. Science Advances 2, e1600026. https://doi.org/10.1126/sciadv.1600026

He, X., Han, W., Chen, Q., Zhang, Z., Liu, C., Zhang, Y., Liu, Z., Han, C., Yao, Z., Chen, K., 2024. Internal loading regulates the phosphorus concentration in a diversion input shallow lake in the semi-humid region of North China: Differentiated processes in littoral wetland and open water areas. Water Research 257, 121680. https://doi.org/10.1016/j.watres.2024.121680

Hecky, R.E., Kilham, P., 1988. Nutrient limitation of phytoplankton in freshwater and marine environments: A review of recent evidence on the effects of enrichment. Limnology and Oceanography 33, 796–822. https://doi.org/10.4319/lo.1988.33.4part2.0796

Hedley, M.J., Stewart, J.W.B., Chauhan, B.S., 1982a. Changes in Inorganic and Organic Soil Phosphorus Fractions Induced by Cultivation Practices and by Laboratory Incubations. Soil Science Society of America Journal 46, 970–976. https://doi.org/10.2136/sssaj1982.03615995004600050017x

Hedley, M.J., WHITE, R.E., NYE, P.H., 1982b. Plant-induced changes in the rhizosphere of rape (*brassica napus var. emerald*) seedlings. New Phytologist 91, 45–56. https://doi.org/10.1111/j.1469-8137.1982.tb03291.x

Heidgen, S., Marinova, E., Krauß, R., Nelle, O., Ebner, M., Märkle, T., Miranda, T., Bofinger, J., Klingler, S., Junginger, A., 2020. Palaeoenvironment and potential resources for early Holocene subsistence in the Ammer River Valley (Germany) based on palaeoecological and bioarchaeological evidence. Quaternary International 560–561, 259–272. https://doi.org/10.1016/j.quaint.2020.05.038

Helfenstein, J., Tamburini, F., von Sperber, C., Massey, M.S., Pistocchi, C., Chadwick, O.A., Vitousek, P.M., Kretzschmar, R., Frossard, E., 2018. Combining spectroscopic and isotopic techniques gives a dynamic view of phosphorus cycling in soil. Nature Communications 9, 3226. https://doi.org/10.1038/s41467-018-05731-2

Hofmann, J., Venohr, M., Behrendt, H. and Opitz, D., 2010. Integrated water resources management in central Asia: Nutrient and heavy metal emissions and their relevance for the Kharaa River Basin, Mongolia. Water Science and Technology 62, 353–363. https://doi.org/10.2166/wst.2010.262

Holman, I.P., Whelan, M.J., Howden, N.J.K., Bellamy, P.H., Willby, N.J., Rivas-Casado, M., McConvey, P., 2008. Phosphorus in groundwater—an overlooked contributor to eutrophication? Hydrological Processes 22, 5121–5127. https://doi.org/10.1002/hyp.7198

Hooda, P.S., Truesdale, V.W., Edwards, A.C., Withers, P.J.A., Aitken, M.N., Miller, A., Rendell, A.R., 2001. Manuring and fertilization effects on phosphorus accumulation in soils and potential environmental implications. Advances in Environmental Research 5, 13–21. https://doi.org/10.1016/S1093-0191(00)00037-X

Huang, C.P., 1975. Adsorption of phosphate at the hydrous γ-Al2O3-electrolyte interface. Journal of Colloid and Interface Science 53, 178–186. https://doi.org/10.1016/0021-9797(75)90004-1

Huang, G., Liu, C., Zhang, Y., Chen, Z., 2020. Groundwater is important for the geochemical cycling of phosphorus in rapidly urbanized areas: a case study in the Pearl River Delta. Environmental Pollution 260, 114079. https://doi.org/10.1016/j.envpol.2020.114079

Hupfer, M., Gächter, R., Giovanoli, R., 1995. Transformation of phosphorus species in settling seston and during early sediment diagenesis. Aquatic Sciences 57, 305–324. https://doi.org/10.1007/BF00878395

Hupfer, M., Zak, D., Roßberg, R., Herzog, C., Pöthig, R., 2009. Evaluation of a well-established sequential phosphorus fractionation technique for use in calcite-rich lake sediments: identification and prevention of artifacts due to apatite formation. Limnology and Oceanography: Methods 7, 399–410. https://doi.org/10.4319/lom.2009.7.399

Hylén, A., van de Velde, S.J., Kononets, M., Luo, M., Almroth-Rosell, E., Hall, P.O.J., 2021. Deep-water inflow event increases sedimentary phosphorus release on a multi-year scale. Biogeosciences 18, 2981–3004. https://doi.org/10.5194/bg-18-2981-2021

Iheagwara, O.S., Ing, T.S., Kjellstrand, C.M., Lew, S.Q., 2013. Phosphorus, phosphorous, and phosphate. Hemodialysis International 17, 479–482. https://doi.org/10.1111/hdi.12010

Ishida, T., Tamura, M., Kimbi, S.B., Tomozawa, Y., Saito, M., Hirayama, Y., Nagasaka, I., Onodera, S.-I., 2024. Evaluation of Phosphorus Enrichment in Groundwater by Legacy Phosphorus in Orchard Soils with High Phosphorus Adsorption Capacity Using Phosphate

Oxygen Isotope Analysis. Environ. Sci. Technol. 58, 5372–5382. https://doi.org/10.1021/acs.est.3c07170

Jaisi, D.P., Blake, R.E., Kukkadapu, R.K., 2010. Fractionation of oxygen isotopes in phosphate during its interactions with iron oxides. Geochimica et Cosmochimica Acta 74, 1309–1319. https://doi.org/10.1016/j.gca.2009.11.010

Jiang, Z.-H., Zhang, H., Jaisi, D.P., Blake, R.E., Zheng, A.-R., Chen, M., Zhang, X.-G., Peng, A.-G., Lei, X.-T., Kang, K.-Q., Chen, Z.-G., 2017. The effect of sample treatments on the oxygen isotopic composition of phosphate pools in soils. Chemical Geology 474, 9–16. https://doi.org/10.1016/j.chemgeo.2017.10.017

Jin, Z., Wang, J., Zhang, R., Liao, P., Liu, Y., Yang, J., Chen, J., 2023. Identification of the sources of different phosphorus fractions in lake sediments by oxygen isotopic composition of phosphate. Applied Geochemistry 151, 105627. https://doi.org/10.1016/j.apgeochem.2023.105627

Joshi, S.R., Kukkadapu, R.K., Burdige, D.J., Bowden, M.E., Sparks, D.L., Jaisi, D.P., 2015. Organic Matter Remineralization Predominates Phosphorus Cycling in the Mid-Bay Sediments in the Chesapeake Bay. Environ. Sci. Technol. 49, 5887–5896. https://doi.org/10.1021/es5059617

Joshi, S.R., Li, X., Jaisi, D.P., 2016. Transformation of Phosphorus Pools in an Agricultural Soil: An Application of Oxygen-18 Labeling in Phosphate. Soil Science Society of America Journal 80, 69–78. https://doi.org/10.2136/sssaj2015.06.0219

Jutebring Sterte, E., Lidman, F., Sjöberg, Y., Ploum, S.W., Laudon, H., 2022. Groundwater travel times predict DOC in streams and riparian soils across a heterogeneous boreal landscape. Science of The Total Environment 849, 157398. https://doi.org/10.1016/j.scitotenv.2022.157398

Karl, D.M., Tien, G., 1992. MAGIC: A sensitive and precise method for measuring dissolved phosphorus in aquatic environments. Limnology and Oceanography 37, 105–116. https://doi.org/10.4319/lo.1992.37.1.0105

Kazmierczak, J., Nilsson, B., Postma, D., Sebok, E., Karan, S., Müller, S., Czekaj, J., Engesgaard, P., 2021. Transport of geogenic phosphorus to a groundwater-dominated eutrophic lake. Journal of Hydrology 598, 126175. https://doi.org/10.1016/j.jhydrol.2021.126175

Kazmierczak, J., Postma, D., Müller, S., Jessen, S., Nilsson, B., Czekaj, J., Engesgaard, P., 2020. Groundwater-controlled phosphorus release and transport from sandy aquifer into lake. Limnology and Oceanography 65, 2188–2204. https://doi.org/10.1002/lno.11447

Kimura, S., Noda, S., Minagawa, H., 2021. Experimental investigation of effects of mica content, Fe and pressure on the pore size distribution and permeability of sandy sediment using proton nuclear magnetic resonance. Engineering Geology 295, 106408. https://doi.org/10.1016/j.enggeo.2021.106408

Klingler, S., Cirpka, O.A., Werban, U., Leven, C., Dietrich, P., 2020. Direct-Push Color Logging Images Spatial Heterogeneity of Organic Carbon in Floodplain Sediments. Journal of Geophysical Research: Biogeosciences 125, e2020JG005887. https://doi.org/10.1029/2020JG005887

Klotzbücher, A., Kaiser, K., Klotzbücher, T., Wolff, M., Mikutta, R., 2019. Testing mechanisms underlying the Hedley sequential phosphorus extraction of soils. Journal of Plant Nutrition and Soil Science 182, 570–577. https://doi.org/10.1002/jpln.201800652

Kornexl, B.E., Gehre, M., Höfling, R., Werner, R.A., 1999. On-line $\delta^{18}O$ measurement of organic and inorganic substances. Rapid Communications in Mass Spectrometry 13, 1685–1693. https://doi.org/10.1002/(SICI)1097-0231(19990830)13:16<1685::AID-RCM699>3.0.CO;2-9

Kraal, P., van Genuchten, C.M., Behrends, T., 2022. Phosphate coprecipitation affects reactivity of iron (oxyhydr)oxides towards dissolved iron and sulfide. Geochimica et Cosmochimica Acta 321, 311–328. https://doi.org/10.1016/j.gca.2021.12.032

Kraal, P., van Genuchten, C.M., Behrends, T., Rose, A.L., 2019. Sorption of phosphate and silicate alters dissolution kinetics of poorly crystalline iron (oxyhydr)oxide. Chemosphere 234, 690–701. https://doi.org/10.1016/j.chemosphere.2019.06.071

Lei, X.-T., Zhang, H., Chen, M., Guo, L., Zhang, X.-G., Jiang, Z.-H., Blake, R.E., Chen, Z.-G., 2020. The efficiency of sequential extraction of phosphorus in soil and sediment: insights from the oxygen isotope ratio of phosphate. Journal of Soils and Sediments 20, 1332–1343. https://doi.org/10.1007/s11368-019-02517-x

Lewandowski, J., Meinikmann, K., Nützmann, G., Rosenberry, D.O., 2015. Groundwater – the disregarded component in lake water and nutrient budgets. Part 2: effects of groundwater on nutrients. Hydrological Processes 29, 2922–2955. https://doi.org/10.1002/hyp.10384

Li, L., Wang, W., Jiang, Z., Luo, A., 2023. Phosphate in Aqueous Solution Adsorbs on Limestone Surfaces and Promotes Dissolution. Water 15. https://doi.org/10.3390/w15183230

Li, Q., Wang, X., Bartlett, R., Pinay, G., Kan, D., Zhang, W., Sun, J., 2012. Ferrous Iron Phosphorus in Sediments: Development of a Quantification Method through 2,2′-Bipyridine Extraction. Water Environment Research 84, 2037–2044. https://doi.org/10.2175/106143012X13373575830872

Li, Y., Guo, H., Gao, Z., Ke, T., Zhu, Z., Cao, Y., Su, X., Wu, X., 2023. Phosphorus in shallow and deep groundwater: Importance of P/Fe ratio in Fe(III) oxides in aquifer sediments. Journal of Hydrology 623, 129860. https://doi.org/10.1016/j.jhydrol.2023.129860

Li, Y., Yu, C., Zhao, B., Chen, D., Ye, H., Nagel, C., Shao, W., Oelmann, Y., Neidhardt, H., Guo, H., 2022. Spatial variation in dissolved phosphorus and interactions with arsenic in response to changing redox conditions in floodplain aquifers of the Hetao Basin, Inner Mongolia. Water Research 209, 117930. https://doi.org/10.1016/j.watres.2021.117930

Liang, Y., Blake, R.E., 2007. Oxygen isotope fractionation between apatite and aqueous-phase phosphate: 20 – 45 °C. Chemical Geology 238, 121–133. https://doi.org/10.1016/j.chemgeo.2006.11.004

Liao, X., Nair, V.D., Canion, A., Dobberfuhl, D.R., Foster, D.K., Inglett, P.W., 2019. Subsurface transport and potential risk of phosphorus to groundwater across different land uses in a karst springs basin, Florida, USA. Geoderma 338, 97–106. https://doi.org/10.1016/j.geoderma.2018.11.005

Limousin, G., Gaudet, J.-P., Charlet, L., Szenknect, S., Barthès, V., Krimissa, M., 2007. Sorption isotherms: A review on physical bases, modeling and measurement. Applied Geochemistry 22, 249–275. https://doi.org/10.1016/j.apgeochem.2006.09.010

Lisboa, M.S., Schneider, R.L., Rudstam, L.G., Walter, M.T., 2024. Groundwater inputs could be a significant but often overlooked source of phosphorus in lake ecosystems. Scientific Reports 14, 16269. https://doi.org/10.1038/s41598-024-66985-z

Liu, M., Du, Y., Deng, Y., Li, Y., Tao, Y., Gan, Y., Ma, T., 2023. Effect of depositional evolution on phosphorus enrichment in aquifer sediments of alluvial-lacustrine plain. Science of The Total Environment 900, 165857. https://doi.org/10.1016/j.scitotenv.2023.165857

Liu, Z., Du, Y., Deng, Y., Huang, Y., Zhao, X., Li, Q., 2023. Enrichment of geogenic phosphorus in a coastal groundwater system: New insights from dissolved organic matter characterization. Chemosphere 322, 138214. https://doi.org/10.1016/j.chemosphere.2023.138214

Longinelli, A., Nuti, S., 1973. Revised phosphate-water isotopic temperature scale. Earth and Planetary Science Letters 19, 373–376. https://doi.org/10.1016/0012-821X(73)90088-5

M García-López, A., Delgado, A., Plassard, C., 2024. Kinetics of phytate adsorption and response of phosphorus forms initially present in alkaline soils. Geoderma 443, 116800. https://doi.org/10.1016/j.geoderma.2024.116800

Martin, S., Klingler, S., Dietrich, P., Leven, C., Cirpka, O.A., 2020. Structural controls on the hydrogeological functioning of a floodplain. Hydrogeology Journal 28, 2675–2696. https://doi.org/DOI 10.1007/s10040-020-02225-8

März, C., Riedinger, N., Sena, C., Kasten, S., 2018. Phosphorus dynamics around the sulphate-methane transition in continental margin sediments: Authigenic apatite and Fe(II) phosphates. Marine Geology 404, 84–96. https://doi.org/10.1016/j.margeo.2018.07.010

McGinley, P.M., Masarik, K.C., Gotkowitz, M.B., Mechenich, D.J., 2016. Impact of anthropogenic geochemical change and aquifer geology on groundwater phosphorus concentrations. Applied Geochemistry 72, 1–9. https://doi.org/10.1016/j.apgeochem.2016.05.020

McLaughlin, K., Silva, S., Kendall, C., Stuart-Williams, H., Paytan, A., 2004. A precise method for the analysis of $\delta^{18}O$ of dissolved inorganic phosphate in seawater. Limnology and Oceanography: Methods 2, 202–212. https://doi.org/10.4319/lom.2004.2.202

McLaughlin, K., Paytan, A., Kendall, C., Silva, S., 2006. Oxygen isotopes of phosphatic compounds—Application for marine particulate matter, sediments and soils. Marine Chemistry 98, 148–155. https://doi.org/10.1016/j.marchem.2005.09.004

Meinikmann, K., Hupfer, M., Lewandowski, J., 2015. Phosphorus in groundwater discharge – A potential source for lake eutrophication. Journal of Hydrology 524, 214–226. https://doi.org/10.1016/j.jhydrol.2015.02.031

Mellander, P.-E., Jordan, P., Melland, A.R., Murphy, P.N.C., Wall, D.P., Mechan, S., Meehan, R., Kelly, C., Shine, O., Shortle, G., 2013. Quantification of phosphorus transport from a karstic agricultural watershed to emerging spring water. Environmental Science & Technology 47, 6111–6119. https://doi.org/10.1021/es304909y

Millero, F., Huang, F., Zhu, X., Liu, X., Zhang, J.-Z., 2001. Adsorption and Desorption of Phosphate on Calcite and Aragonite in Seawater. Aquatic Geochemistry 7, 33–56. https://doi.org/10.1023/A:1011344117092

Montangero, A., Cau, L.N., Anh, N.V., Tuan, V.D., Nga, P.T., Belevi, H., 2007. Optimising water and phosphorus management in the urban environmental sanitation system of Hanoi, Vietnam. Science of The Total Environment 384, 55–66. https://doi.org/10.1016/j.scitotenv.2007.05.032

Neidhardt, H., Achten, F., Kern, S., Schwientek, M., Oelmann, Y., 2019. Phosphorus Pool Composition in Soils and Sediments of Transitional Ecotones under the Influence of Agriculture. Journal of Environmental Quality 48, 1325–1335. https://doi.org/10.2134/jeq2019.01.0012

Neidhardt, H., Rudischer, S., Eiche, E., Schneider, M., Stopelli, E., Duyen, V.T., Trang, P.T.K., Viet, P.H., Neumann, T., Berg, M., 2021. Phosphate immobilisation dynamics and interaction with arsenic sorption at redox transition zones in floodplain aquifers: Insights from the Red River Delta,

Vietnam. Journal of Hazardous Materials 411, 125128. https://doi.org/10.1016/j.jhazmat.2021.125128

Neidhardt, H., Schoeckle, D., Schleinitz, A., Eiche, E., Berner, Z., Tram, P.T.K., Lan, V.M., Viet, P.H., Biswas, A., Majumder, S., Chatterjee, D., Oelmann, Y., Berg, M., 2018. Biogeochemical phosphorus cycling in groundwater ecosystems – Insights from South and Southeast Asian floodplain and delta aquifers. Science of The Total Environment 644, 1357–1370. https://doi.org/10.1016/j.scitotenv.2018.07.056

Neidhardt, H., Shao, W., 2023. Impact of climate change-induced warming on groundwater temperatures and quality. Applied Water Science 13, 235. https://doi.org/10.1007/s13201-023-02039-5

Németh, Z., Gáncs, L., Gémes, G., Kolics, A., 1998. pH dependence of phosphate sorption on aluminum. Corrosion Science 40, 2023–2027. https://doi.org/10.1016/S0010-938X(98)00089-4

Neupane, G., Donahoe, R.J., Arai, Y., 2014. Kinetics of competitive adsorption/desorption of arsenate and phosphate at the ferrihydrite–water interface. Chemical Geology 368, 31–38. https://doi.org/10.1016/j.chemgeo.2013.12.020

Nisbeth, C.S., Kidmose, J., Weckström, K., Reitzel, K., Odgaard, B.V., Bennike, O., Thorling, L., McGowan, S., Schomacker, A., Kristensen, D.L., Jessen, S., 2019. Dissolved Inorganic Geogenic Phosphorus Load to a Groundwater-Fed Lake: Implications of Terrestrial Phosphorus Cycling by Groundwater. Water 11. https://doi.org/10.3390/w11112213

O'Neil, J.R., Vennemann, T.W., McKenzie, W.F., 2003. Effects of speciation on equilibrium fractionations and rates of oxygen isotope exchange between (PO_4)aq and H_2O. Geochimica et Cosmochimica Acta 67, 3135–3144. https://doi.org/10.1016/S0016-7037(02)00970-5

Paige, C.R., Snodgrass, W.J., Nicholson, R.V., Scharer, J.M., He, Q.H., 1997. The effect of phosphate on the transformation of ferrihydrite into crystalline products in alkaline media. Water, Air, and Soil Pollution 97, 397–412. https://doi.org/10.1007/BF02407475

Pastero, L., Bruno, M., Aquilano, D., 2017. About the Genetic Mechanisms of Apatites: A Survey on the Methodological Approaches. Minerals 7. https://doi.org/10.3390/min7080139

Ren, C., Li, Y., Zhou, Q., Li, W., 2021. Phosphate uptake by calcite: Constraints of concentration and pH on the formation of calcium phosphate precipitates. Chemical Geology 579, 120365. https://doi.org/10.1016/j.chemgeo.2021.120365

Richardson, A.E., Simpson, R.J., 2011. Soil Microorganisms Mediating Phosphorus Availability Update on Microbial Phosphorus. Plant Physiology 156, 989–996. https://doi.org/10.1104/pp.111.175448

Robertson, W.D., Van Stempvoort, D.R., Schiff, S.L., 2019. Review of phosphorus attenuation in groundwater plumes from 24 septic systems. Science of The Total Environment 692, 640–652. https://doi.org/10.1016/j.scitotenv.2019.07.198

Rothe, M., Kleeberg, A., Hupfer, M., 2016. The occurrence, identification and environmental relevance of vivianite in waterlogged soils and aquatic sediments. Earth-Science Reviews 158, 51–64. https://doi.org/10.1016/j.earscirev.2016.04.008

Roy, J.W., Bickerton, G., 2014. Elevated Dissolved Phosphorus in Riparian Groundwater along Gaining Urban Streams. Environ. Sci. Technol. 48, 1492–1498. https://doi.org/10.1021/es404801y

Ruttenberg, K.C., 1992. Development of a sequential extraction method for different forms of phosphorus in marine sediments. Limnology and Oceanography 37, 1460–1482. https://doi.org/10.4319/lo.1992.37.7.1460

Ruttenberg, K.C., Ogawa, N.O., Tamburini, F., Briggs, R.A., Colasacco, N.D., Joyce, E., 2009. Improved, high-throughput approach for phosphorus speciation in natural sediments via the SEDEX sequential extraction method. Limnology and Oceanography: Methods 7, 319–333. https://doi.org/10.4319/lom.2009.7.319

Sawada, K., Abdel-Aal, N., Sekino, H., Satoh, K., 2003. Adsorption of inorganic phosphates and organic polyphosphonate on calcite. Dalton Transactions 342, 342–347. https://doi.org/DOI: 10.1039/B209758N

Schilling, K.E., Streeter, M.T., Isenhart, T.M., Beck, W.J., Tomer, M.D., Cole, K.J., Kovar, J.L., 2018. Distribution and mass of groundwater orthophosphorus in an agricultural watershed. Science of The Total Environment 625, 1330–1340. https://doi.org/10.1016/j.scitotenv.2018.01.035

Schütze, E., Gypser, S., Freese, D., 2020. Kinetics of Phosphorus Release from Vivianite, Hydroxyapatite, and Bone Char Influenced by Organic and Inorganic Compounds. Soil Systems 4. https://doi.org/10.3390/soilsystems4010015

Schwertmann, U., Cornell, R.M., 2008. Iron Oxides in the Laboratory: preparation and characterization. https://doi.org/10.1002/9783527613229.ch01

Seo, D.-I., Canale, R.P., 1996. Performance, reliability and uncertainty of total phosphorus models for lakes—I. Deterministic analyses. Water Research 30, 83–94. https://doi.org/10.1016/0043-1354(95)00114-Z

Sharpley, A., Jarvie, H.P., Buda, A., May, L., Spears, B., Kleinman, P., 2013. Phosphorus Legacy: Overcoming the Effects of Past Management Practices to Mitigate Future Water Quality Impairment. Journal of Environmental Quality 42, 1308–1326. https://doi.org/10.2134/jeq2013.03.0098

Sheppard, S., Long, J., Sanipelli, B., Sohlenius, G., 2009. Solid/liquid partition coefficients (Kd) for selected soils and sediments at Forsmark and Laxemar-Simpevarp (No. 1402–3091). Sweden.

Siegenthaler, M.B., Ramoneda, J., Frossard, E., Mészáros, É., 2022. Microbial community responses to phosphorus and nitrogen inputs in the organic soil horizons of two contrasting temperate beech forests. Applied Soil Ecology 172, 104357. https://doi.org/10.1016/j.apsoil.2021.104357

Sondergaard, M., Jensen, P.J., Jeppesen, E., 2001. Retention and internal loading of phosphorus in shallow, eutrophic lakes. Scientific World Journal 1, 427–442. https://doi.org/10.1100/tsw.2001.72

Song, J., Yang, W., Han, X., Jiang, S., Zhang, C., Pan, W., Jian, S., Hu, J., 2023. Performance of Rod-Shaped Ce Metal–Organic Frameworks for Defluoridation. Molecules 28. https://doi.org/10.3390/molecules28083492

Spicher, M.T., Schwaminger, S.P., von der Haar-Leistl, D., Reindl, M., Wagner, F.E., Berensmeier, S., 2023. Interaction and mechanisms in the phosphate–binding of iron(oxyhydr)oxide core–shell nanoparticles. Journal of Colloid and Interface Science 634, 418–430. https://doi.org/10.1016/j.jcis.2022.12.035

Spiteri, C., Slomp, C.P., Regnier, P., Meile, C., Van Cappellen, P., 2007. Modelling the geochemical fate and transport of wastewater-derived phosphorus in contrasting groundwater systems. Journal of Contaminant Hydrology 92, 87–108. https://doi.org/10.1016/j.jconhyd.2007.01.002

Spohn, M., 2024. Preferential adsorption of nitrogen- and phosphorus-containing organic compounds to minerals in soils: A review. Soil Biology and Biochemistry 194, 109428. https://doi.org/10.1016/j.soilbio.2024.109428

Spohn, M., 2020. Increasing the organic carbon stocks in mineral soils sequesters large amounts of phosphorus. Global Change Biology 26, 4169–4177. https://doi.org/10.1111/gcb.15154

Sprenger, C., Hartog, N., Hernández, M., Vilanova, E., Grützmacher, G., Scheibler, F. and Hannappel, S., 2017. Inventory of managed aquifer recharge sites in Europe: Historical development, current situation and perspectives. Hydrogeology Journal 25, 1909–1922. https://doi.org/10.1007/s10040-017-1554-8

Stober, I., Grimmer, J., Kraml, M., 2023. The Muschelkalk aquifer of the Molasse basin in SW-Germany: implications on the origin and development of highly saline lithium-rich brines in calcareous hydrothermal reservoirs. Geothermal Energy 11, 27. https://doi.org/10.1186/s40517-023-00270-6

Stolze, L., Zhang, D., Guo, H., Rolle, M., 2019. Surface complexation modeling of arsenic mobilization from goethite: Interpretation of an in-situ experiment. Geochimica et Cosmochimica Acta 248, 274–288. https://doi.org/10.1016/j.gca.2019.01.008

Tamburini, F., Bernasconi, S.M., Angert, A., Weiner, T., Frossard, E., 2010. A method for the analysis of the $\delta^{18}O$ of inorganic phosphate extracted from soils with HCl. European Journal of Soil Science 61, 1025–1032. https://doi.org/10.1111/j.1365-2389.2010.01290.x

Tamburini, F., Pistocchi, C., Helfenstein, J., Frossard, E., 2018. A method to analyse the isotopic composition of oxygen associated with organic phosphorus in soil and plant material. European Journal of Soil Science 69, 816–826. https://doi.org/10.1111/ejss.12693

Tao, Y., Deng, Y., Du, Y., Xu, Y., Leng, Z., Ma, T., Wang, Y., 2020. Sources and enrichment of phosphorus in groundwater of the Central Yangtze River Basin. Science of The Total Environment 737, 139837. https://doi.org/10.1016/j.scitotenv.2020.139837

Tao, Y., Du, Y., Deng, Y., Ma, T., Wang, Y., 2023. Degradation of phosphorus-containing natural organic matter facilitates enrichment of geogenic phosphorus in Quaternary aquifer systems: A molecular perspective. Journal of Hydrology 620, 129513. https://doi.org/10.1016/j.jhydrol.2023.129513

Tiessen, H., Stewart, J.W.B., Cole, C.V., 1984. Pathways of Phosphorus Transformations in Soils of Differing Pedogenesis. Soil Science Society of America Journal 48, 853–858. https://doi.org/10.2136/sssaj1984.03615995004800040031x

Trentman, M.T., Tank, J.L., Jones, S.E., McMillan, S.K., Royer, T.V., 2020. Seasonal evaluation of biotic and abiotic factors suggests phosphorus retention in constructed floodplains in three agricultural streams. Science of The Total Environment 729, 138744. https://doi.org/10.1016/j.scitotenv.2020.138744

Urdiales, C., Gacitua, M., Villacura, L., Pizarro, C., Escudey, M., Canales, C., Antilén, M., 2020. Variable surface charge of humic acid-ferrihydrite composite: Influence of electrolytes on

ciprofloxacin adsorption. Journal of Hazardous Materials 385, 121520. https://doi.org/10.1016/j.jhazmat.2019.121520

Vennemann, T.W., Fricke, H.C., Blake, R.E., O'Neil, J.R., Colman, A., 2002. Oxygen isotope analysis of phosphates: a comparison of techniques for analysis of Ag_3PO_4. Chemical Geology 185, 321–336. https://doi.org/10.1016/S0009-2541(01)00413-2

von Sperber, C. Pistocchi, C. Weiler, M. Tamburini, F., 2023. Oxygen isotope ratios of phosphates in the soil-plant system: Limitations and future developments. European Journal of Soil Science 74, e13434. https://doi.org/10.1111/ejss.13434

Walker, T.W., Syers, J.K., 1976. The fate of phosphorus during pedogenesis. Geoderma 15, 1–19. https://doi.org/10.1016/0016-7061(76)90066-5

Wang, C., Zhang, Y., Li, H., Morrison, R.J., 2013. Sequential extraction procedures for the determination of phosphorus forms in sediment. Limnology 14, 147–157. https://doi.org/10.1007/s10201-012-0397-1

Wang, H., ZHU, J., FU, Q.-L., XIONG, J.-W., HONG, C., HU, H.-Q., VIOLANTE, A., 2015. Adsorption of Phosphate onto Ferrihydrite and Ferrihydrite-Humic Acid Complexes. Pedosphere 25, 405–414. https://doi.org/10.1016/S1002-0160(15)30008-4

Wang, Q., Kim, T.-H., Reitzel, K., Almind-Jørgensen, N., Nielsen, U.G., 2021. Quantitative determination of vivianite in sewage sludge by a phosphate extraction protocol validated by PXRD, SEM-EDS, and 31P NMR spectroscopy towards efficient vivianite recovery. Water Research 202, 117411. https://doi.org/10.1016/j.watres.2021.117411

Wang, S., Jin, X., Zhao, H., Zhou, X., Wu, F., 2007. Effect of organic matter on the sorption of dissolved organic and inorganic phosphorus in lake sediments. Colloids and Surfaces A: Physicochemical and Engineering Aspects 297, 154–162. https://doi.org/10.1016/j.colsurfa.2006.10.040

Wang, X., Li, W., Harrington, R., Liu, F., Parise, J.B., Feng, X., Sparks, D.L., 2013. Effect of Ferrihydrite Crystallite Size on Phosphate Adsorption Reactivity. Environ. Sci. Technol. 47, 10322–10331. https://doi.org/10.1021/es401301z

Waychunas, G.A., Rea, B.A., Fuller, C.C., Davis, J.A., 1993. Surface chemistry of ferrihydrite: Part 1. EXAFS studies of the geometry of coprecipitated and adsorbed arsenate. Geochimica et Cosmochimica Acta 57, 2251–2269. https://doi.org/10.1016/0016-7037(93)90567-G

Weihrauch, C., Weber, C.J., 2020. Phosphorus enrichment in floodplain subsoils as a potential source of freshwater eutrophication. Science of The Total Environment 747, 141213. https://doi.org/10.1016/j.scitotenv.2020.141213

Willett, I.R., CHARTRES, C.J., NGUYEN, T.T., 1988. Migration of phosphate into aggregated particles of ferrihydrite. Journal of Soil Science 39, 275–282. https://doi.org/10.1111/j.1365-2389.1988.tb01214.x

Williams, J.D.H., Jaquet, J.-M., Thomas, R.L., 1976. Forms of Phosphorus in the Surficial Sediments of Lake Erie. Journal of the Fisheries Research Board of Canada 33, 413–429. https://doi.org/10.1139/f76-063

Williams, J.D.H., Syers, J.K., Harris, R.F., Armstrong, D.E., 1971. Fractionation of Inorganic Phosphate in Calcareous Lake Sediments. Soil Science Society of America Journal 35, 250–255. https://doi.org/10.2136/sssaj1971.03615995003500020023x

Williams, J.D.H., Syers, J.K., Walker, T.W., 1967. Fractionation of Soil Inorganic Phosphate by a Modification of Chang and Jackson's Procedure. Soil Science Society of America Journal 31, 736–739. https://doi.org/10.2136/sssaj1967.03615995003100060012x

Xu, J., Liu, S., Song, S., Guo, H., Tang, J., Yong, J.W.H., Ma, Y., Chen, X., 2018. Arbuscular mycorrhizal fungi influence decomposition and the associated soil microbial community under different soil phosphorus availability. Soil Biology and Biochemistry 120, 181–190. https://doi.org/10.1016/j.soilbio.2018.02.010

Xu, N., Yin, H., Chen, Z., Liu, S., Chen, M., Zhang, J., 2014. Mechanisms of phosphate retention by calcite: effects of magnesium and pH. Journal of Soils and Sediments 14, 495–503. https://doi.org/10.1007/s11368-013-0807-y

Xu, Z., Huang, T., Yin, X., 2018. Improvements in the preparation of phosphate for oxygen isotope analysis from soils and sediments. PLoS One 13, e0204203. https://doi.org/10.1371/journal.pone.0204203

Yang, Xiaoyan, Chen, X., Yang, Xitian, 2019. Effect of organic matter on phosphorus adsorption and desorption in a black soil from Northeast China. Soil and Tillage Research 187, 85–91. https://doi.org/10.1016/j.still.2018.11.016

Yu, L., Rozemeijer, J., van Breukelen, B.M., Ouboter, M., van der Vlugt, C., Broers, H.P., 2018. Groundwater impacts on surface water quality and nutrient loads in lowland polder catchments: monitoring the greater Amsterdam area. Hydrol. Earth Syst. Sci. 22, 487–508. https://doi.org/10.5194/hess-22-487-2018

Yuan, H., Li, Q., Kukkadapu, R.K., Liu, E., Yu, J., Fang, H., Li, H., Jaisi, D.P., 2019. Identifying sources and cycling of phosphorus in the sediment of a shallow freshwater lake in China using phosphate oxygen isotopes. Science of The Total Environment 676, 823–833. https://doi.org/10.1016/j.scitotenv.2019.04.322

Zaccheo, P., Genevini, P., Ambrosini, D., 1997. The role of manure in the management of phosphorus resources at an Italian crop-livestock production farm. Agriculture, Ecosystems & Environment 66, 231–239. https://doi.org/10.1016/S0167-8809(97)00106-0

Zhang, L., Zhu, Y., Wang, D., Li, W., Cheng, D., Chen, X., Liang, M., 2022. Morphological characteristics and chemical behaviour of phosphorus at the sediment–water interface in wetland. Water and Environment Journal 36, 590–597. https://doi.org/10.1111/wej.12789

Zhang, X., Ke, X., Du, Y., Tao, Y., Xue, J., Li, Q., Xie, X., Deng, Y., 2023. Coupled effects of sedimentary iron oxides and organic matter on geogenic phosphorus mobilization in alluvial-lacustrine aquifers. Science of The Total Environment 878, 163216. https://doi.org/10.1016/j.scitotenv.2023.163216

Zheng, J., Scheibe, T.D., Boye, K., Song, H.-S., 2024. Thermodynamic control on the decomposition of organic matter across different electron acceptors. Soil Biology and Biochemistry 193, 109364. https://doi.org/10.1016/j.soilbio.2024.109364

Zhou, A., Tang, H., Wang, D., 2005. Phosphorus adsorption on natural sediments: Modeling and effects of pH and sediment composition. Water Research 39, 1245–1254. https://doi.org/10.1016/j.watres.2005.01.026

Appendix

Table S3.1 The proportion of PO_4-P to TDP in groundwater. March 2020 sampling campaign ($n_{shallow}$=8, n_{deep}=12)

shallow	TDP (mg L^{-1})	PO_4-P (mg L^{-1})	PO_4-P/TDP (%)
10a	0.28	0.26	92
11a	0.03	0.02	81
12a	0.02	0.01	64
13a	0.28	0.24	84
14a	0.18	0.15	85
15a	0.03	0.03	84
16a	0.07	0.07	94
17a	0.12	0.16	133
19a	0.29	0.08	27
20a	0.19	0.20	106
21a	0.06	0.06	99
22a	0.02	0.03	167
23a	0.02	0.03	125
24a	0.04	0.04	95
30a	0.09	0.08	90
37a	0.19	0.19	96
39a	0.30	0.27	89
47a	0.10	0.05	54
49a	0.19	0.18	93
57a	0.54	0.52	96
61a	0.49	0.51	102
65a	0.49	0.46	93
72a	0.08	0.08	94
73a	0.17	0.17	99
P2.1	0.20	0.30	151
P2.2	0.02	0.06	268
P2.3	0.26	0.28	108
P2.4	0.12	0.15	120
Average			103
deep	TDP (mg L^{-1})	PO_4-P (mg L^{-1})	PO_4-P/TDP (%)

continue with Table S3.1. The proportion of PO_4-P to TDP in groundwater. March 2020 sampling campaign ($n_{shallow}$=8, n_{deep}=12)

deep	TDP (mg L^{-1})	PO_4-P (mg L^{-1})	PO_4-P/TDP (%)
11b	0.01	0.02	121
12b	0.19	0.17	86
13b	0.23	0.22	93
15b	0.27	0.25	92
17b	0.35	0.34	96
20b	0.27	0.27	98
22b	0.17	0.16	97
24b	0.18	0.17	97
30b	0.29	0.28	94
47b	0.43	0.31	73
57b	0.36	0.36	99
72b	0.02	0.03	126
Average			98

Table S3.2 Overview of individual groundwater samples, which consists of two sampling campaigns (November 2019, March 2020). Complementary data derived from March 2020 is marked with *. For major and minor elements by ICP-OES analysis, only key elements are presented here to narrow the width of the table. The sampling time of remaining elements not shown are the same as those listed in Table.

Sample Name	Group	pH	Temp (°C)	EC (µScm)	Eh (mV)	DO (mg L^{-1})	DOC (mg L^{-1})	F^- (mg L^{-1})	Cl^- (mg L^{-1})	SO_4^{2-} (mg L^{-1})	HCO_3^- (mg L^{-1})	NH_4^+ (mg L^{-1})	NO_3^- (mg L^{-1})	Ca (mg L^{-1})	Mg (mg L^{-1})	Mn (mg L^{-1})	Fe (mg L^{-1})	TDP (mg L^{-1})
10a	shallow	6.88	12.2	2801	-82	0.53	5.49	0.25	28.2	1124	766	14.45		483 *	86 *	0.22 *	0.00 *	0.28 *
11a	shallow	7.06	12.7	846	335	1.56	1.84	0.25	6.7	27	526	0.06	14.1	115	34	0.03	0.01	0.00
12a	shallow	7.18	13.0	839	-32	0.37	3.79	0.30	3.6	13	545	1.26	0.12	123 *	28 *	0.05 *	0.00 *	0.02 *
13a	shallow	7.10	13.8	769	-34	0.14	4.43	0.27	2.3	13	532	3.07	0.17	118	24	0.13	0.12	0.32
14a	shallow	7.17	13.1	924	-17	0.40	3.49	0.30	14.6	17	588	1.80	0.08	135	28	0.16	0.04	0.14
15a	shallow	7.02	14.3	675	-8	0.40	4.53	0.28	2.0	13	550	1.75	0.15	117	32	0.09	0.05	0.05
16a	shallow	7.12	12.5	1008	248	2.06	4.49	0.35	8.0	3	671	1.66	1.25	135	46	2.66	0.01	0.00
17a	shallow	6.89	12.6	1630	-36	0.54	7.80	0.24	25.8	314	735	8.09	0.06	238	53	0.05	0.01	0.21
18a	shallow	7.24	10.1	1010	176	3.01	2.81	0.37	4.8	39	624	0.14	1.06	133	40	0.12	0.00	0.00
19a	shallow	7.03	12.9	1015	-30	0.74	5.81	0.31	11.5	62	631	3.07	0.46	147	35	0.15	0.04	0.40
20a	shallow	6.95	12.7	963	-12	0.37	4.06	0.26	4.0	11	658	3.91	0.09	122	39	0.05	0.03	0.20
21a	shallow	6.99	12.5	897	-80	0.04	3.43	0.31	5.6	58	651	8.26	0.06	133	39	0.07	0.14	0.00
22a	shallow	6.89	13.2	976	-2	0.46	3.72	0.32	4.8	9	689	2.60	0.12	136	42	0.06	0.06	0.00
23a	shallow	6.89	12.7	997	-5	0.37	3.60	0.30	6.0	5	668	2.48	0.08	135	44	0.08	0.03	0.00
24a	shallow	6.97	12.8	909	-28	0.39	2.74	0.30	11.2	27	581	2.04	0.03	120	37	0.05	0.03	0.00
30a	shallow	7.02	12.8	969	-33	0.74	5.85	0.24	5.1	109	556	5.86	0.13	138	30	0.03	0.03	0.10
31a	shallow	6.99	10.8	1274	-41	1.10	8.65	0.27	6.3	131	699							
32a	shallow	7.12	12.4	919	61	3.88	4.47	0.37	12.6	5	608							
33a	shallow	6.97	10.7	1281	-37	1.20	8.02	0.29	14.3	136	863							
34a	shallow	6.94	12.2	919	-33	0.58	4.77	0.27	5.5	6	610							
37a	shallow	7.11	12.5	1212	25	0.47	4.93	0.20	6.8	221	555	1.21	0.12	185	34	0.05	0.09	0.20
38a	shallow	6.96	12.6	1119	381	3.30	1.25	0.19	6.7	185	504	0.10	20.8	175	35	0.00	0.01	0.00
39a	shallow	6.96	11.7	1751	-46	0.48	2.40	0.24	24.2	1063	484	2.09	0.14	407	74	0.05	0.04	0.23
47a	shallow	7.00	15.9	848	36	0.81	3.49	0.28	4.9	5	533	2.09	0.14	107	30	0.14	0.32	0.09
49a	shallow	7.39	10.6	811	284	4.34	5.51	0.25	6.9	79	412	0.15	18.4	98	36	0.00	0.01	0.13

52a	shallow	6.94	11.7	1066	369	0.62	1.82	0.18	2.7	18	742	0.13	2.08	137	51	0.01	0.01	0.00
57a	shallow	6.84	12.2	1266	-39	0.42	12.95	0.25	5.8	29	835	19.94	2.05	162	41	0.02	0.03	0.61
61a	shallow	7.06	13.5	1252	-64	0.68	7.48	0.24	22.3	79	740	6.06	0.35	185	39	0.43	0.06	0.51
65a	shallow	6.93	12.9	1256	-52	0.48	6.05	0.28	24.8	110	670	7.87	0.03	109 *	19 *	0.21 *	0.25 *	0.49 *
71a	shallow	6.84	13.6	2919	23	1.07	1.11	0.24	65.2	1428	391	0.43	31.9	530 *	91 *	0.03 *	0.00 *	0.01 *
72a	shallow	7.07	12.2	1008	-58	0.20	5.25	0.25	3.3	171	602	6.54		151	49	0.02	0.01	0.13
73a	shallow	7.06	12.0	913	44	2.43	2.96	0.32	6.2	4	607	1.16	0.09	127	39	0.13	0.01	0.16
P2.1	shallow	6.99	10.8	1274	-39	1.10	8.65							171	53	0.03	0.02	0.16
P2.2	shallow	7.12	12.4	919	61	3.88	4.47							125 *	38 *	0.13 *	0.40 *	0.02 *
P2.3	shallow	6.97	10.7	1281	-35	1.20	8.02							167	52	0.03	0.02	0.17
P2.4	shallow	6.94	12.2	919	-33	0.58	4.77							147 *	39 *	0.03 *	0.01 *	0.12 *
11b	deep	7.16	12.3	834	342	5.33	1.38	0.31	9.8	45	475	0.12	28.3	104	39	0.00	0.01	0.00
12b	deep	7.18	11.4	1185	-25	0.33	2.04	0.33	3.6	237	526	3.49	0.10	154 *	50 *	0.02 *	0.09 *	0.19 *
12c	deep	7.23	11.5	1150	-20	0.17	2.84	0.34	7.0	222	505	3.23	0.34	134 *	25 *	0.12 *	0.14 *	0.28 *
13b	deep	7.08	11.9	1077	-43	0.12	5.55	0.29	7.6	20	785	8.01	0.12	156	48	0.04	0.01	0.23
15b	deep	7.10	11.8	1160	-19	0.38	2.17	0.41	13.8	250	527	5.47	0.16	169	51	0.18	0.01	0.26
16b	deep	7.03	11.2	975	320	1.97	1.08	0.29	20.0	65	520	0.12	25.2	125	40	0.04	0.00	0.00
17b	deep	7.15	11.3	1622	-72	0.34	6.11	0.27	2.3	210	881	12.09	0.03	221	68	0.03	0.11	0.34
19b	deep	6.96	11.5	1185	73	0.91	1.21	0.30	14.5	253	528	0.10	22.2	185	47	0.03	0.10	0.00
20b	deep	7.07	11.4	881	-63	0.13	1.84	0.34	7.9	58	544	3.69	0.05	118	41	0.10	0.01	0.18
22b	deep	7.01	11.6	873	-30	0.33	1.29	0.31	16.1	63	524	2.14	0.12	117	41	0.19	0.01	0.17
24b	deep	7.14	11.6	924	-47	0.38	2.32	0.29	7.0	10	620	5.19		112	41	0.02	0.01	0.18
30b	deep	7.07	11.7	1496	-35	0.35	5.07	0.34	2.8	446	569	18.73	0.16	210	60	0.05	0.02	0.30
37b	deep	7.02	12.0	2495	79	0.40	1.65	0.25	22.3	1085	435	1.90	0.15	459	80	0.36	0.29	0.00
39b	deep	6.86	11.6	2413	53	2.39	0.96	0.21	32.5	1153	397	0.13	17.7	427	75	0.00	0.00	0.00
47b	deep	6.95	12.9	1249	-3	0.86	7.23	0.23	4.5	3	863	12.59	0.13	169	49	0.30	0.13	0.51
57b	deep	7.17	11.6	998	-18	0.30	2.85	0.44	18.4	65	549	5.05	0.18	130	36	0.05	0.10	0.30
61b	deep	7.07	12.2	1223	23	0.38	1.04	0.28	12.4	357	495	1.81	0.22	189	52	0.30	1.63	0.00
65b	deep	7.10	12.4	1147	37	0.51	2.48	0.36	11.9	130	608	1.89	0.22	155 *	42 *	0.25 *	0.00 *	0.01 *
71b	deep	6.85	12.7	2926	96	2.06	0.83	0.25	68.5	1482	378	0.09	38.1	539 *	88 *	0.01 *	0.00 *	0.01 *
72b	deep	7.05	11.6	1114	16	0.17	1.14	0.37	6.6	290	469	0.38	0.08	167	60	0.48	0.00	0.00

Table S3.3 Saturation indices computed with PHREEQC for mineral phases that might serve as sink or source for PO_4. Respective SI values were calculated for water samples taken in November 2019. Values < -0.25 indicate undersaturation, which means dissolution is thermodynamically possible (i.e. amorphous Fe-hydroxides). Values > +0.25 indicate supersaturation, indicating that these minerals remain stable under the prevailing conditions if already present, or might freshly precipitate. Values between -0.25 and +0.25 are considered close to equilibrium, meaning that both, dissolution and precipitation, are considered unlikely. Well name with its location could be found in previous study (Martin et al., 2020).

Well Name	amorph. Fe-hydroxide	Goethite	Hematite	Magnetite	Vivianite	Siderite	Hydroxyapatite	Calcite	Percent error, 100*(Cat-|An|)/(Cat+|An|)	TDP concentration (mg L^{-1})
	$Fe_3(OH)_8$	FeO(OH)	Fe_2O_3	Fe_3O_4	$Fe_3(PO_4)_2$	$FeCO_3$	$Ca_5(PO_4)_3OH$	$CaCO_3$		
13a	-3.53	1.94	5.84	5.66	None	-0.71	0.16	0.22	-4.33	0.32
14a	-3.53	1.92	5.79	5.25	-6.17	-1.09	-0.42	0.37	-4.87	0.14
17a	-5.26	0.17	2.3	0.6	None	-1.86	-0.81	0.31	-5.67	0.21
19a	-4.23	1.21	4.37	3.48	-5.8	-1.26	0.24	0.26	-4.54	0.40
20a	-4.35	1.08	4.11	2.87	-7.17	-1.5	-1.41	0.13	-7.03	0.20
30a	-4.45	0.99	3.93	2.87	-7.45	-1.46	-1.76	0.17	-7.52	0.10
37a	-2.68	2.75	7.44	7.08	-5.08	-0.87	0	0.34	-4.91	0.20
39a	-4.79	0.6	3.15	2	-6.89	-1.55	0.03	0.29	-8.15	0.23
47a	-2.15	3.4	8.77	8.95	-4.17	-0.34	-1.95	0.11	-3.99	0.09
49a	1.42	6.77	15.5	14.5	-7.86	-1.81	-0.3	0.26	-3.23	0.13
57a	-5.15	0.26	2.47	0.97	-6.62	-1.54	-0.16	0.21	-3.99	0.62
61a	-4.54	0.92	3.79	3.15	-5.13	-1.01	1.09	0.45	-4.61	0.51
72a	-5.26	0.15	2.25	0.72	-8.76	-1.94	-1.2	0.25	-5.56	0.13
73a	-3.48	1.92	5.79	4.35	None	-1.82	-1.04	0.22	-1.48	0.17
13b	-4.87	0.54	3.02	1.62	-7.85	-1.68	-0.27	0.41	-3.74	0.23
15b	-4.3	1.1	4.15	2.91	-7.38	-1.74	-0.02	0.25	-4.38	0.26
17b	-4.27	1.11	4.17	3.78	-4.77	-0.69	0.82	0.6	-3.59	0.34
20b	-5.36	0.03	1.99	0.44	-8.4	-1.97	-1.07	0.14	-3.54	0.18
22b	-4.77	0.63	3.19	1.74	-7.98	-1.83	-1.52	0.06	-4.33	0.17
24b	-4.81	0.58	3.11	1.77	-8	-1.77	-0.8	0.25	-5.77	0.18
30b	-4.54	0.86	3.66	2.47	-7.01	-1.61	0.15	0.29	-6.2	0.30
47b	-3.55	1.89	5.74	5.15	-4.47	-0.74	0.27	0.36	-3.43	0.51
57b	-3.22	2.18	6.29	6.04	-4.42	-0.78	0.29	0.28	-4.56	0.30
$Median_{shallow}$	-4.29	1.15	4.24	3.32	-6.62	-1.48	-0.36	0.26	-4.74	0.20
$Median_{deep}$	-4.54	0.86	3.66	2.47	-7.38	-1.68	-0.02	0.28	-4.33	0.26

Table S3.4 Median values of all measured parameters in shallow and deep groundwater. Shallow aquifer (n=36), Deep aquifer (n=20).

Parameter	pH	Temp (°C)	EC (µS/cm)	ORP (mV)	Eh (mV)	DO (mg L^{-1})	DOC (mg L^{-1})	F^- (mg L^{-1})	Cl^- (mg L^{-1})	SO_4^{2-} (mg L^{-1})	SO_4^{2-}/ Cl^-
Shallow aquifer	6.99	12.5	1002	-226	-29	0.60	4.48	0.27	6.6	29.0	3.9
Deep aquifer	7.07	11.6	1155	-208	-11	0.38	1.94	0.30	10.8	216	13.0
p		**					**	*			

Parameter	HCO_3^- (mg L^{-1})	NH_4^+ (mg L^{-1})	NO_3^- (mg L^{-1})	Al (mg L^{-1})	Ca (mg L^{-1})	Fe (mg L^{-1})	K (mg L^{-1})	Mg (mg L^{-1})	Mn (mg L^{-1})	Na (mg L^{-1})	TDP (mg L^{-1})
Shallow aquifer	609	2.09	0.14	0.00	136	0.03	0.87	39.0	0.05	6.32	0.13
Deep aquifer	527	2.69	0.16	0.00	162	0.01	2.19	48.4	0.05	4.18	0.17
p				*				**			

Table S3.5 Spearman rank correlation matrix for groundwater samples collected in November 2019 in both aquifers. Correlation ® significant at *p <0.05, **p <0.01 (two-tailed)

Shallow aquifer n=26	pH	Temp (°C)	EC (µScm)	Eh (mV)	DO (mg L^{-1})	DOC (mg L^{-1})	Cl^- (mg L^{-1})	SO_4^{2-} (mg L^{-1})	HCO_3^- (mg L^{-1})	NH_4^+ (mg L^{-1})	NO_3^- (mg L^{-1})	Al (mg L^{-1})	Ca (mg L^{-1})	Fe (mg L^{-1})	P (mg L^{-1})
pH	1.000														
Temp (°C)	-0.024	1.000													
EC (µScm)	-0.502**	-0.325	1.000												
Eh (mV)	0.275	-0.030	-0.325	1.000											
DO (mg L^{-1})	0.257	-0.429**	0.150	0.529**	1.000										
DOC (mg L^{-1})	-0.057	-0.242	0337*	-0.548**	0.042	1.000									
Cl^- (mg L^{-1})	-0.182	-0.075	0.598**	-0.198	0.334	0.157	1.000								
SO_4^{2-} (mg L^{-1})	-0.243	-0.239	0.673**	-0.404*	0.050	0.216	0.499**	1.000							
HCO_3^- (mg L^{-1})	-0.388*	-0.265	0.457**	-0.381*	-0.089	0.521**	0.103	-0.037	1.000						
NH_4^+ (mg L^{-1})	-0.401*	0.159	0.255	-0.874**	-0.530**	0.679**	0.123	0.183	0.563**	1.000					
NO_3^- (mg L^{-1})	0.152	-0.163	0.097	0.514**	0.604**	-0.223	-0.073	0.156	-0.320	-0.531**	1.000				
Al (mg L^{-1})	-0.140	0.264	-0.564**	0.291	-0.228	-0.497**	-0.164	-0.537**	-0.096	-0.230	-0.313	1.000			
Ca (mg L^{-1})	-0.311	-0.253	0.921**	-0.387	0.025	0.338	0.422*	0.626**	0.350	0.327	-0.037	-0.572**	1.000		
Fe (mg L^{-1})	-0.085	0.624**	-0.211	-0.459*	-0.561**	0.122	-0.017	-0.093	-0.036	0.406*	-0.414*	0.132	-0.055	1.000	
P (mg L^{-1})	0.028	0.045	0.378	-0.548**	-0.127	0.611**	0.295	0.324	0.054	0.483*	-0.019	-0.362	0.424*	0.286	1.000

continue with Table S3.5 Spearman rank correlation matrix for groundwater samples collected in November 2019 in both aquifers. Correlation ® significant at *p <0.05, **p <0.01 (two-tailed)

Deep aquifer n=16	pH	Temp (°C)	EC (µScm)	Eh (mV)	DO (mg L^{-1})	DOC (mg L^{-1})	Cl^- (mg L^{-1})	SO_4^{2-} (mg L^{-1})	HCO_3^- (mg L^{-1})	NH_4^+ (mg L^{-1})	NO_3^- (mg L^{-1})	Al (mg L^{-1})	Ca (mg L^{-1})	Fe (mg L^{-1})	P (mg L^{-1})
pH	1.000														
Temp (°C)	-0.256	1.000													
EC (µScm)	-0.409	0.271	1.000												
Eh (mV)	-0.414	0.392	0.177	1.000											
DO (mg L^{-1})	-0.435	0.382	0.305	0.749**	1.000										
DOC (mg L^{-1})	0.523*	0.039	-0.056	-0.624**	-0.430	1.000									
Cl^- (mg L^{-1})	-0.496*	0.198	0.081	0.647**	0.447*	-0.659**	1.000								
SO_4^{2-} (mg L^{-1})	-0.364	0.065	0.725**	0.368	0.227	-0.529*	0.347	1.000							
HCO_3^- (mg L^{-1})	0.343	-0.092	-0.180	-0.662**	-0.331	0.838**	-0.603**	-0.635**	1.000						
NH_4^+ (mg L^{-1})	0.368	-0.041	0.009	-0.803**	-0.538*	0.869**	-0.644**	-0.400	0.764**	1.000					
NO_3^- (mg L^{-1})	-0.216	0.317	0.080	0.788**	0.739**	-0.486*	0.598**	0.268	-0.464*	-0.673**	1.000				
Al (mg L^{-1})	0.128	-0.207	-0.560*	-0.578*	-0.440	0.182	-0.124	-0.568*	0.313	0.218	-0.486	1.000			
Ca (mg L^{-1})	-0.379	0.126	0.974**	0.094	0.126	-0.032	0.071	0.774**	-0.135	0.141	-0.045	-0.576*	1.000		
Fe (mg L^{-1})	-0.041	0.388	0.524*	-0.088	-0.006	0.368	-0.094	0.132	0.321	0.365	-0.086	-0.240	0.512*	1.000	
P (mg L^{-1})	0.372	0.083	0.092	-0.715**	-0.448	0.900**	-0.553*	-0.430	0.850**	0.903**	-0.496	0.117	0.006	0.344	1.000

Table S3.6 Soil porewater samples were collected at 50 cm and 100 cm bls in February 2020. PO_4-P were measured by UV-vis (n=17), TDP were measured by ICP-OES (n=5). Nm= not measured.

Soil porewater samples	PO_4-P (mg L^{-1})		TDP (mg L^{-1})	
(n=17)	average	n	average	n
SM2 50 cm bls	0.008	6	0.003	2
SM2 100 cm bls	0.004	1	nm	0
SM3 50 cm bls	0.004	2	nm	0
SM3 100 cm bls	0.027	2	nm	0
SM4 50 cm bls	<0.003	1	<0.002	1
SM4 100 cm bls	0.003	5	<0.002	2
In total	0.008	17	0.002	5

Table S3.7 Max, Min and Median value of Ca, P and Fe in different extraction pools in tufa (n=9) and peat (n=8). Bdl = below detection limit.

Tufa		$NaHCO_3$-extractable	NaOH-extractable	CDB-extractable	HCl-extractable	H_2SO_4-extractable
Ca g kg^{-1}	Max	1	3	19	338	bdl
	Min	bdl	bdl	10	126	bdl
	Median	bdl	1	13	286	bdl
P mg kg^{-1}	Max	112	115	122	334	71
	Min	40	11	31	181	2
	Median	83	21	90	214	12
Fe mg kg^{-1}	Max	13	365	7707	1147	582
	Min	bdl	bdl	bdl	bdl	5
	Median	4	12	225	204	41
peat		$NaHCO_3$-extractable	NaOH-extractable	CDB-extractable	HCl-extractable	H_2SO_4-extractable
Ca g kg^{-1}	Max	bdl	2	33	257	bdl
	Min	bdl	1	14	130	bdl
	Median	bdl	2	19	210	bdl
P mg kg^{-1}	Max	123	180	139	483	184
	Min	64	50	56	192	23
	Median	80	89	67	237	59
Fe mg kg^{-1}	Max	24	1006	1630	1245	757
	Min	bdl	11	26	bdl	25
	Median	bdl	50	34	bdl	57

Table S3.8 Spearman rank correlation matrix for aquifer sediments, comprising tufa and peat (n =17). Correlation ® significant at *p <0.05, **p <0.01 (two-tailed). Abbreviations: inorganic carbon (IC), organic carbon (OC), total carbon (TC), total nitrogen (TN), total sulfur (TS), total phosphorus (TP).

Spearman's rho	IC	OC	TC	TN	TS	$NaHCO_3$-PO_4	$NaHCO_3$-P_{org}	NaOH-PO_4	NaOH-P_{org}	CDB-P	HCl-P	H_2SO_4-P	TP
IC	1.000												
OC	-0.782**	1.000											
TC	-0.662**	0.974**	1.000										
TN	-0.740**	0.929**	0.924**	1.000									
TS	-0.771**	0.924**	0.885**	0.906**	1.000								
$NaHCO_3$-PO_4	-0.184	0.341	0.344	0.161	0.288	1.000							
$NaHCO_3$-P_{org}	-0.113	0.150	0.062	0.169	0.276	-0.086	1.000						
NaOH-PO_4	-0.632**	0.562*	0.591*	0.595*	0.585*	0.137	0.135	1.000					
NaOH-P_{org}	-0.591*	0.688**	0.703**	0.790**	0.788**	-0.262	0.203	0.750**	1.000				
CDB-P	-0.020	-0.185	-0.259	-0.153	-0.112	0.208	0.061	-0.333	-0.360	1.000			
HCl-P	-0.233	0.129	0.074	0.189	0.168	0.336	-0.176	0.015	-0.037	0.605*	1.000		
H_2SO_4-P	-0.554*	0.385	0.368	0.520*	0.412	-0.336	0.105	0.640**	0.772**	-0.110	0.304	1.000	
TP	-0.505*	0.347	0.259	0.371	0.400	0.118	0.240	0.321	0.377	0.333	0.757**	0.689**	1.000

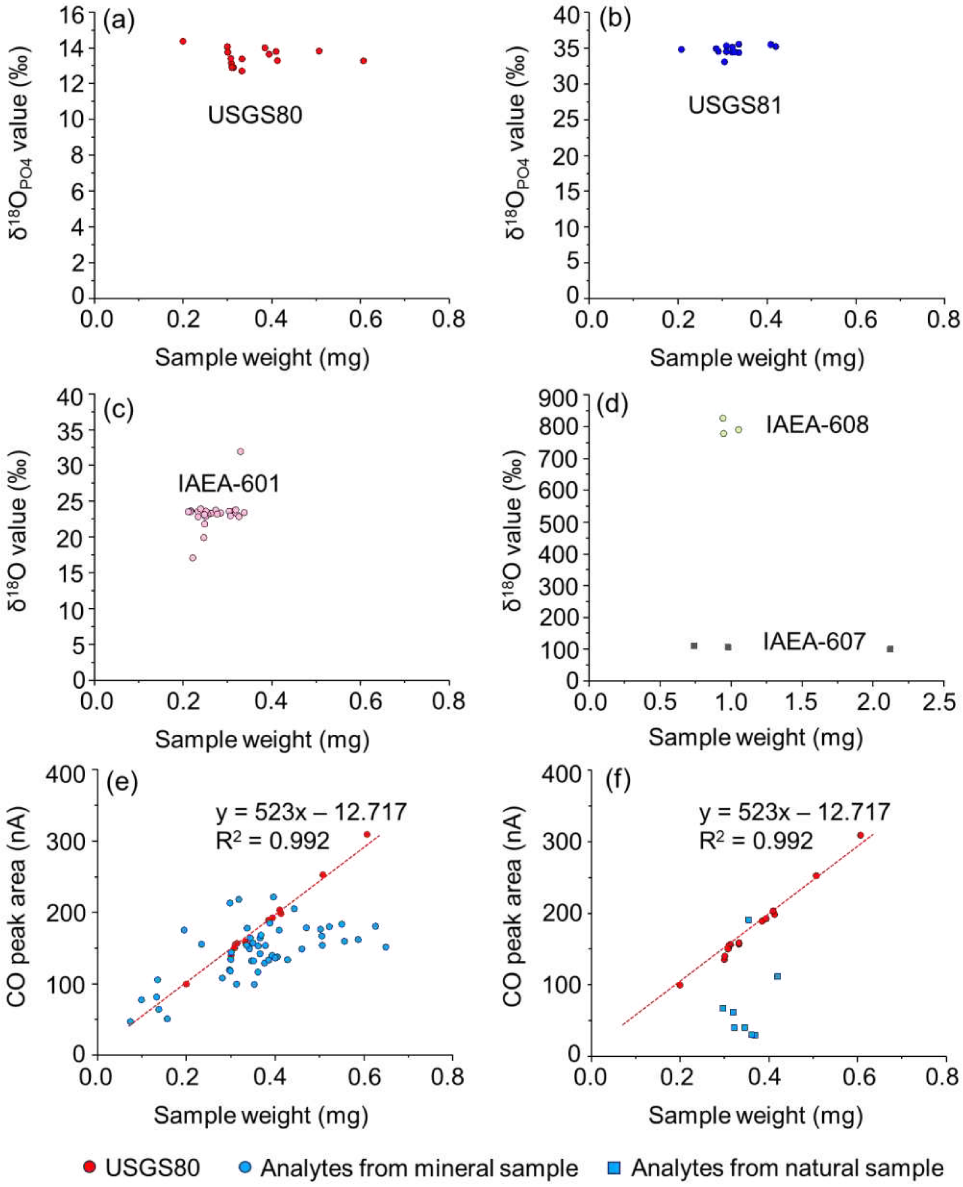

Fig. S4.1 The $\delta^{18}O$ values (vs. VSMOW) of the international certified reference standards: USGS80 ($\delta^{18}O$ = ~ +13.1 ‰) (a), USGS81 ($\delta^{18}O$ = ~ +35.4 ‰) (b), IAEA-601 ($\delta^{18}O$ = +23.14 ‰) (c), IAEA-607 ($\delta^{18}O$ = +99.02 ‰) and IAEA-608 ($\delta^{18}O$ = +736.4 ‰) (d). Pattern of analytes (Ag_3PO_4) weight and CO peak area of P pools from mineral samples(e) and natural samples (f). The equation represents the weight of USGS80 is linearly correlated with CO peak area.

Afterword

I've been away from hometown for over ten years to explore the journey of study. I'm glad I could make a little break now. So, I made a little poem as a record of my past years of life.

无题

邵敏问

十载辞乡剑，明月照两乡

走马千山绿，花似去年红

漠视思贫贱，才尽回肠中

岁月不翻书，勿恣乱回头

润物声自远，海天本澄清

功成亦未竟，千里云同风

Poem title: Untitled. General idea of the poem (translated by myself):

This sword called 'Farewell' has been along with me for ten years, the moonlight never stints to shine the place where I travel and where I come from.

Green mountains flashing by me, flowers blooming like before.

Indifference doesn't mean stop thinking, ambition consumed in stomach.

If time does not flip through books, then there is no need to browse through the past.

The sound of tiny raindrops can travel a long way, the sea and sky are clear.

Achievement has been made while the journey goes on, cloud or wind, either can over thousand miles journey.